AN ABSTRACT OF THE THESIS OF

Michael J. Edwards for the degree of Master of Science in Mechanical Engineering presented on January 7, 2005.

Title: Design, Modeling, and Performance of Miniature Reciprocating Thermocompressor

Signature redacted for privacy.

Abstract approved: _____
Richard B. Peterson

Research in the miniaturization of thermomechanical systems in recent years has proven to be both rewarding and challenging. Micro-scale devices have tremendous technological potential but come with a new set of design problems. One such problem is energy storage. Heat actuated systems, driven primarily by thermal energy, take advantage of the high stored energy density of hydrocarbon fuels, and are therefore desirable for small-scale applications. One concept for a heat-actuated compressor is called a thermocompressor, which is a variation of a traditional Stirling engine. Thermocompressors use constant volume heat addition to pressurize their working fluid without applying any mechanical work to the gas. Such devices would be well suited for numerous applications such as power cycles, heat pumps, refrigeration, and liquid pumps.

This thesis develops a detailed thermodynamic analysis of the thermocompressor cycle providing insight into the operation of the cycle and the sensitivity of the cycle's performance to various design parameters including regenerator effectiveness, regenerator dead volume, hot side dead volume, and cold side dead volume. The developed model shows that the thermal efficiency is highly sensitive to regenerator effectiveness, which motivates a regenerator optimization study. As the regenerator surface area increases, its effectiveness increases, however, so does its dead volume. The regenerator model shows that there is an optimum balance between regenerator effectiveness and regenerator dead volume, which gives a predicted maximum thermal efficiency. The optimum regenerator effectiveness is

approximately 96% with regenerator dead volume of approximately 26%, which corresponds to a maximum predicted thermal efficiency of 45-50% of Carnot efficiency. This raises questions about the practicality of the device particularly in achieving regeneration high enough to make the concept practical. More detailed modeling work would be beneficial to further understanding of this cycle.

The experimental work of this thesis includes the development and testing of a first-order, miniature thermocompressor. Its intention is to explore the pertinent issues relating to the design, operation, and performance of thermocompressors. The thermocompressor's cylinder diameter is 0.945 inches, and its cylinder length is 1 inch with a displacement volume of 0.175 cubic inches. The reciprocating motion of the regenerator/displacer is driven by an electric motor to which it is magnetically coupled.

Several tests were performed with the experimental apparatus. The primary interest was to measure pressure verses time using both nitrogen and helium as working fluids, over a range of temperature ratios from 1.2 to 2.0, operating at both 10 and 13 Hz. The pressure variation inside the cylinder is plotted as a function of time and compared to the regenerator/displacer position. In addition, some dynamic temperature measurements were made inside the cylinder during operation to indicate how much temperature variation exists in the hot space. The experimental results show that the thermocompressor produces pressure ratios of approximately 75% of the temperature ratios. Nitrogen and helium both appear to perform almost equally and operating speed does not appear to significantly affect the pressure ratio. As expected there is a linear relationship between temperature ratio and pressure ratio. Also, the temperature variation near the top of the hot side does not appear to fluctuate more than approximately 3 °C with N_2 or 13.7 °C with He during operation.

Design, Modeling, and Performance of Miniature Reciprocating Thermocompressor

by
Michael J. Edwards

A THESIS

submitted to

Oregon State University

in partial fulfillment of
the requirements for the
degree of

Master of Science

Presented January 7, 2005
Commencement June 2005

Master of Science thesis of Michael J. Edwards presented on January 7, 2005.

APPROVED:

Signature redacted for privacy.

Major Professor, representing Mechanical Engineering

Signature redacted for privacy.

Head of the Department of Mechanical Engineering

Signature redacted for privacy.

Dean of the Graduate School

I understand that my thesis will become part of the permanent collection of Oregon State University libraries. My signature below authorizes release of my thesis to any reader upon request.

Signature redacted for privacy.

Michael J. Edwards, Author

ACKNOWLEDGEMENTS

Over the past five and a half years that I have been at Oregon State, I have had a number of friendships that have tremendously impacted and influenced my life. I would like to take this opportunity to acknowledge a few of them. David Sanders, Russell Criss, Renjy Abraham, Chad Warren, Shannon Steiner, Duane Morris, Naomi Tinker, Adena Mickelson, Tammy Jennrich, Erik and Maureen York, Francis and Jenn Floth, Tammy Blumhardt, Matt Ryan, and Faris Tanyos. Thank you.

Both of my parents have been supportive, encouraging, and loving. I am so thankful for the relationship that I have with them both.

Joe, Tracy, and Luke have been a huge blessing to me these last few of years, and I look forward to many more. Thank you.

I would like to thank Barry Reeves and Xerox for the use of a computer and office space during the writing process without which this project would have been nearly impossible.

Several people have contributed to this project. Matt J. Beck worked during the early stages. David Yarger was a huge help in the design and fabrication of the experimental device. Tom Herron often offered his expertise and was incredibly helpful, particularly with the instrumentation setup. Hailei Wang was also readily available and supportive.

I would like to thank my committee members Kevin Drost, Robert Paasch, and Goran Jovanovic. I would like to particularly acknowledge my major professor, Richard Peterson. He has positively influenced me academically and professionally, but also personally. I have learned from him through his instruction and, more importantly, his example.

Soli Deo Gloria: To God alone be the all glory.

TABLE OF CONTENTS

TABLE OF CONTENTS (Continued)

TABLE OF CONTENTS (Continued)

LIST OF FIGURES

LIST OF FIGURES (Continued)

LIST OF FIGURES (Continued)

LIST OF FIGURES (Continued)

LIST OF TABLES

LIST OF NOMENCLATURE

AR	Cylinder Aspect Ratio
a	Area [m^2]
c_p	Specific Heat (constant pressure) [J/kg-K]
c_v	Specific Heat (constant volume) [J/kg-K]
D	Cylinder Diameter [m]
d	Regenerator Hole Diameter [m]
F	Friction Factor
f	Frequency [Hz]
h	Specific Enthalpy [J/kg] / Film Coefficient [W/m^2-K]
L	Cylinder Length [m]
ℓ	Regenerator Length [m]
m	Mass [kg]
NTU	Number of Transfer Units
Nu	Nusselt Number
n	Number of Regenerator Holes
P	Pressure [N/m^2]
p	Perimeter [m]
Q	Heat Transfer [J]
R	Universal Gas Constant [J/kg-K]
S	Stroke Length [m]
T	Temperature [K]
U	Internal Energy [J]
u	Specific Internal Energy [J/kg]
V	Volume [m^3]
v	Velocity [m/s]
W	Work [J]

LIST OF NOMENCLATURE (Continued)

Greek:

γ	Specific Heat Ratio (c_p/c_v)
Δ	Change of Variable
ε	Regenerator Effectiveness
λ	Regenerator Aspect Ratio
μ	Viscosity [N-s/m^2]
π	Pi (~3.1415)
ρ	Density [kg/m^3]
η_{TH}	Thermal Efficiency
η_{VOL}	Volumetric Efficiency

Superscripts:

*	Non-Dimensional

Subscripts:

1	State 1
2	State 2
3	State 3
4	State 4
atm	Atmospheric
DS	Dead Space
H	High Temperature
HHX	High Temperature Heat Exchanger
HX	High Regenerator Exit Temperature
in	Input
L	Low Temperature
LHX	Low Temperature Heat Exchanger
LX	Low Regenerator Exit Temperature
out	Output

LIST OF NOMENCLATURE (Continued)

R	Ratio
REG	Regenerator
T	Total
X	State X
Y	State Y

Design, Modeling, and Performance of Miniature Reciprocating Thermocompressor

1 INTRODUCTION

In recent years, a tremendous amount of research has been focused on the miniaturization of mechanical systems. It is believed that breakthroughs in the micro-scale and even the nano-scale area could result in a technological revolution similar to that experienced by the electronics industry over the last several decades. Thermomechanical systems, which convert thermal energy to mechanical energy or transfer thermal energy at very small scales, appear to have comparable potential.

As mechanical systems are reduced in size, a number of new design problems arise, which are not prevalent at larger scales. The heat transfer characteristics at small dimensions can change dramatically. For example, many of the above mentioned themomechanical systems require a large temperature gradient over a very small distance. This creates a new set of constraints on design and materials selection. In addition, as the size of a device is reduced, its surface area changes with the square of its characteristic dimension while its volume changes with the cube. Therefore, the surface area-to-volume ratio increases linearly with the decrease in the size of the device. With a large surface area-to-volume ratio, frictional effects become a much bigger problem. In addition, heat transfer rates increase rapidly, which can have a significant influence on thermodynamic performance. These and other design considerations make small-scale device development interesting, but also challenging.

One of the primary issues associated with any mechanical system is its power source. Small scale systems are typically intended to be portable and therefore require a portable power source. Batteries pose one possible solution; however, for moderate-to-high power applications they tend to be large, costly, and heavy. The most viable immediate alternative is hydrocarbon fuel, which can be burned to produce thermal energy. One advantage of hydrocarbon fuel over batteries is a much higher stored energy density. For example, hydrocarbon fuel has approximately 42 kJ/gm, while zinc/air batteries have approximately 1.2 kJ/gm. Although the difference in stored energy density is dramatic, these numbers do not give a perfect

comparison. This is because the energy is stored in different forms. The electrochemical energy stored in batteries can be converted directly into electricity (work), while, the energy stored in hydrocarbon fuel must first be converted to thermal energy and then into work. Therefore, in order to take advantage of hydrocarbon fuel as a power source, small-scale, highly efficient, heat-actuated systems must be developed. These systems would be driven primarily by thermal energy with as little electrical energy as possible.

Heat-actuated systems often utilize a power cycle for their operation, and power cycles require gas compression for a part of the cycle. Traditional mechanical gas compressors have a number of disadvantages at small scales. For reasons previously mentioned, they suffer from large irreversibilities due to frictional effects and heat transfer. They also require mechanical work to achieve gas compression, which must either be generated in another part of the power cycle or be supplied by an electrical input. An ideal alternative would be small-scale, heat-actuated compressors. Such devices would be well suited for power cycles but would also have other numerous applications such as heat pumps, refrigeration, and liquid pumps.

One concept, which has been proposed for a heat-actuated compressor, is called a thermocompressor, which is a variation of a traditional Stirling engine. Put simplistically, if the power piston in a gamma type Stirling engine is replaced with check valves, the result is a thermocompressor as illustrated in Fig. 1.

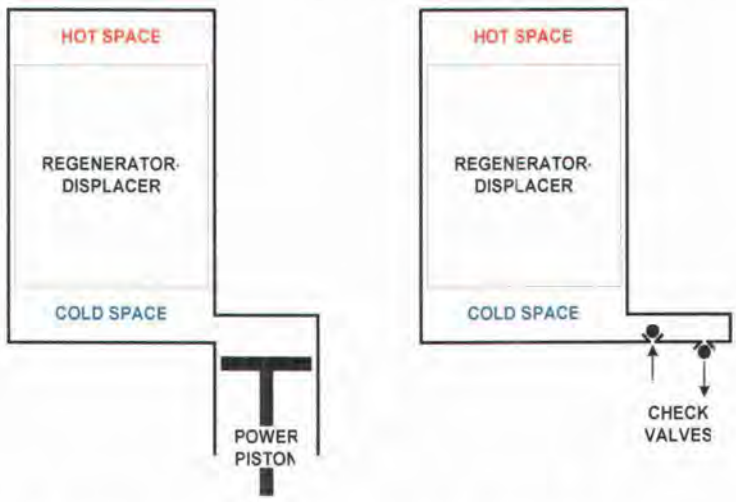

Figure 1 – Left: Gamma Type Stirling Engine, Right: Thermocompressor.

Like a Stirling engine, the thermocompressor consists of a hot region and a cold region connected by a regenerator. The working fluid is transferred from the cold to hot region through the regenerator by a displacer. As the gas is shuttled from the cold side to the hot side, its temperature is increased, but its volume is held constant. The constant volume heat addition causes the pressure of the gas to increase. It must be emphasized that ideally there is no pressure drop across the displacer piston; therefore it does not apply mechanical work to the gas. The compression is accomplished only by heat addition.

The thermocompressor has a number of appealing features. Its simple design makes the device potentially scalable to small dimensions. The system requires very little, if any, electrical input, which is used only to drive the reciprocating motion of the displacer. Finally, the device is capable of high thermal efficiency. As with a Stirling engine, in an ideal thermocompressor cycle with perfect regeneration, the hot and cold regions are isothermal. Therefore, the theoretical limit of the thermal efficiency of the device is Carnot efficiency.

In this work, thermocompressors are investigated from two perspectives; first by a theoretical analysis, and second from an experimental standpoint.

The theoretical analysis consists of an analytical model, which includes expressions derived for each part of the thermodynamic cycle describing the thermocompressor's operation and performance based upon an ideal gas assumption for the working fluid. In addition an optimization of the regenerator is presented. This model provides insight into the thermodynamics of the thermocompressor cycle and presents a predicted maximum thermal efficiency for the device. The model includes regenerator effectiveness, regenerator volume, and dead space as parameters. Several plots are presented which represent a parametric study of the effect of the various parameters on system performance.

The experimental work of this thesis includes the development and testing of a first-order, miniature thermocompressor. The device is operated using both nitrogen and helium as working fluids over a range of temperature differences and at various speeds. The pressure variation inside the cylinder is measured as a function of time

and compared to the displacer position. The displacer is driven by an electric motor and is coupled magnetically. An electric heater supplies heat to the hot side of the cylinder.

It is the intention of this work to present a foundational understanding of the pertinent issues relating to the thermodynamics, performance, design and operation of thermocompressors. Special emphasis is given to the critical design considerations of such a device, particularly the regenerator, and suggestions are given for future experimental work.

2 LITERATURE REVIEW

While Stirling engines have been the focus of a tremendous amount of research over the last one hundred years, thermocompressors have received comparatively little attention. Because thermocompressors are based upon a modified Stirling cycle, it can be argued that thermocompressors are a subset of Stirling engines.

The concept behind the thermocompressor was first proposed by Bush [1] in a patent filed in 1939. Consequently, thermocompressors are sometimes called Bush engines. Since that time, the vast majority of the experimental work done on thermocompressors has been related to artificial heart development from the late 1960's to early 1980's. White [2] gives a detailed summary of the research. In 1967 and 1968 the National Heart, Lung, and Blood Institute gave contracts to seven different groups to pursue artificial heart programs. Three of the seven groups studied device concepts based on thermocompressors.

Air Products and Chemicals was a group that pursued a thermocompressor as an artificial heart. Gibson et al. [3] give the results of that work. At the end of the program, in 1971, a bench top device was demonstrated using Helium as a working fluid. Its cylinder bore diameter was 2.25 cm with a stroke length of 0.46 cm. Running at 13 Hz with high and low of temperatures of 325 K and 830 K respectively, it produced 4.1 W of power with high and low pressures of 6.9 MPa and 8.3 MPa respectively. Its thermal efficiency was 5.4%.

McDonald Douglas Corporation was another group that studied thermocompressors for the artificial heart program. Martini et al. [4-5] report the results of the experimental work. Three engines were built and tested. An engine with an externally driven regenerator demonstrated the best performance of the three. It had a cylinder bore diameter of 8.6 cm and a stroke length of 4.5 cm. Using Argon as a working fluid and operating at 10.5 Hz with high and low temperatures of 924 K and 294 K respectively, its high and low pressures were 0.18 MPa and 0.147 MPa, respectively. Its highest thermal efficiency was measured at 14.4%. After exploring

thermocompressors until 1972, the program shifted to a different concept based upon a hydraulic Stirling engine. That move was made to eliminate sealing problems and take advantage of power piston inertia to increase cycle power.

Aerojet, which was later moved to Nimbus in 1982, was the other group researching thermocompressors for artificial hearts. Buck et al. [6], Moise et al. [7-11], and Schneider et al. [12] have reported on the thermocompressor development work. One of the later devices in the program is referred to as the MK-VII. Its cylinder diameter was 3.3 cm, and its engine volume was 680 cm^3. Using Helium as a working fluid with high and low temperatures of 900 K and 320 K respectively, its high and low pressures were 1.53 MPa and 1.27 MPa respectively. It produced a power output of 6 W with a thermal efficiency of 18%.

Table 1 gives a side by side comparison of these three thermocompressors.

Table 1: Comparison of Existing Experimental Thermocompressors

	Air Products and Chemicals (1971)	McDonald Douglas Corporation (1969)	Aerojet/Nimbus (1977)
Working Fluid	Helium	Argon	Helium
Cylinder Bore [cm]	2.25	8.6	3.3
Stroke Length [cm]	0.46	4.5	N/A
Frequency [Hz]	13	10.5	N/A
Low Temperature [K]	325	294	320
High Temperature [K]	830	924	900
T_{RATIO}	**2.55**	**3.14**	**2.81**
Low Pressure [MPa]	8.3	0.147	1.27
High Pressure [MPa]	9.6	0.18	1.53
P_{RATIO}	**1.16**	**1.22**	**1.2**
Work Output [W]	4.1	30	6
Thermal Efficiency [%]	**5.4**	**14.4**	**18**

In addition to the experimental work that has been done on thermocompressors, a few papers have been published which present theoretical analysis of the thermocompressor cycle. Arquès [13] presents a thermocompressor model which includes an analysis of piston motion. Karabulut [14] does a detailed

thermodynamic analysis of the thermocompressor cycle, which includes an examination of the optimum tank pressure. Kornhauser [15] also models the thermocompressor cycle, and compares it to the Otto cycle. Kornhauser demonstrates that for a device operating with a temperature ratio greater than two, the ideal thermocompressor cycle often requires less heat input than the Otto cycle. Both Karabulut and Kornhauser show that the ideal efficiency of the cycle is Carnot efficiency. Finally, Peterson [16] develops a thermal model for an engine with themocompression and isothermal expansion. Peterson explores the idea of including a heat exchanger outside the working volume of the engine, which would increase the heat transfer area without increasing dead space.

While there is not a large amount of existing research on thermocompressors, much of what has been done has proven invaluable to the current work. However, shortcomings in the literature include a detailed examination of a non-ideal thermocompressor cycle with imperfect regeneration. In addition, more experimental work on thermocompressors is needed to further explore the merits of the concept. This thesis rectifies these shortcomings by modeling a non-ideal cycle with imperfect regeneration and a first-order experimental device is presented which incorporates unique design features.

3 BACKGROUND

3.1 CYCLE OVERVIEW

Before presenting a detailed thermodynamic analysis of the thermocompressor cycle, a qualitative description of the cycle will provide an appropriate background. The thermocompressor cycle consists of four thermodynamic processes: two constant volume processes and two isobaric processes. The cycle is illustrated in Fig. 2. The P-V curves for the hot and cold volumes are shown in Fig. 3.

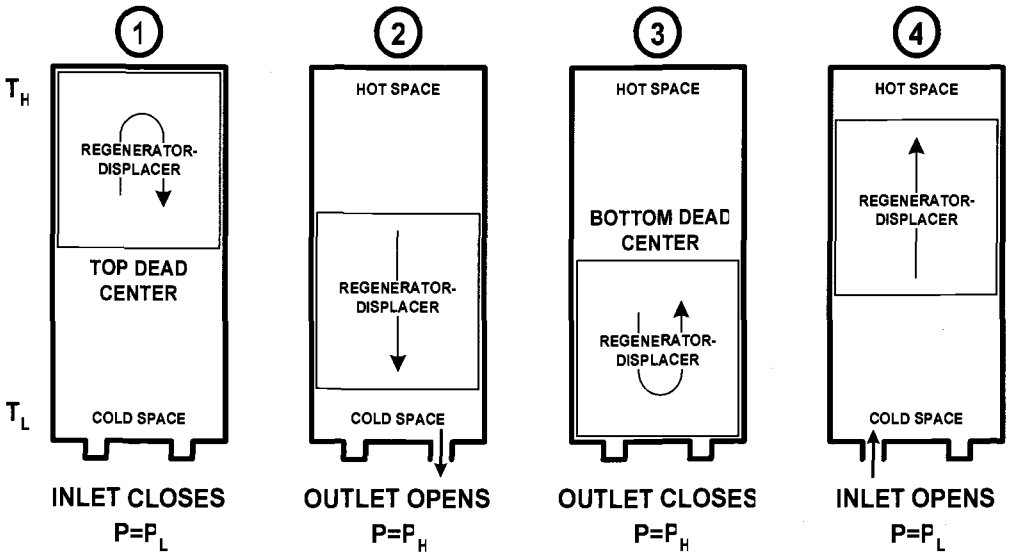

Figure 2 - Thermocompressor Cycle Diagram

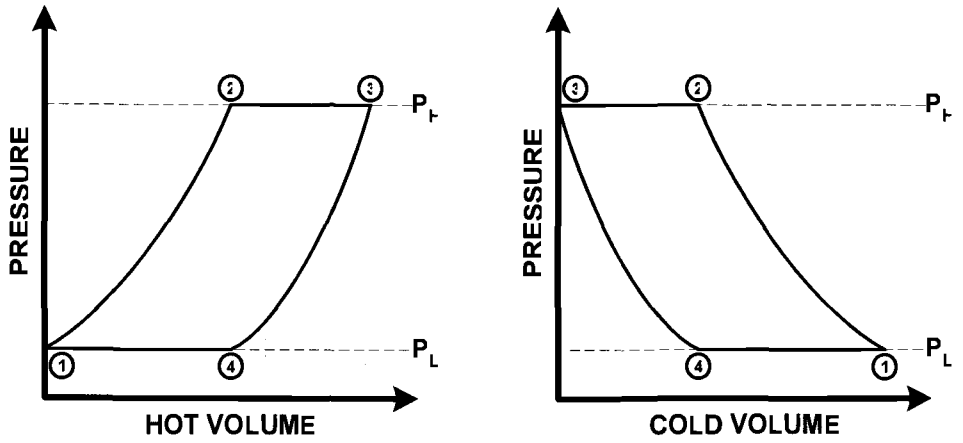

Figure 3 - P-V Diagrams

3.2 PROCESS 1-2

At State 1, the regenerator/displacer is at top dead center. Most of the gas is in the cold region, at low temperature, and consequently at low pressure. The rest of the gas is in the regenerator volume and the dead space on the hot side. Because the pressure drop across the regenerator/displacer is assumed negligible, the gas is also at the lowest pressure point. As the regenerator/displacer begins to move down the cylinder some of the gas is heated as it moves through the regenerator to the hot side. When the gas leaves the regenerator it is at an intermediate temperature, which is limited by the effectiveness of the regenerator. The greater the regenerator effectiveness, the closer the gas temperature will be to T_H. After the gas enters the hot side, additional heating in the hot space brings it up to T_H. As some of the gas inside the cylinder passes through the regenerator and increases temperature, the pressure inside the cylinder rises. At some point the pressure reaches the high pressure point, and the outlet valve is forced open. This defines State 2 and ends the first part of the cycle.

3.3 PROCESS 2-3

At State 2, some gas remains in the cold region. Some of this remaining gas will be moved to the hot region, and some of it will exit the cylinder through the outlet valve. The regenerator/displacer continues to move down the cylinder toward State 3 at bottom dead center. As it moves, the outlet valve remains open and keeps the pressure inside the cylinder constant at P_H by allowing some of the gas to leave the cylinder. Once the regenerator/displacer reaches bottom dead center most of the gas remaining in the cylinder has been moved to the hot region where it is at T_H and P_H. The rest of the gas is in the regenerator volume and the dead space on the cold side where it is also at P_H. Just as in the first process, the gas that is moved through the regenerator to the hot side is heated in the regenerator and additionally in the hot space.

3.4 PROCESS 3-4

The third process is the reverse of the first process. The regenerator/displacer begins to move up the cylinder from bottom dead center. Some of the gas loses heat as it moves through the regenerator to the cold region, and the pressure in the cylinder decreases. As soon of the regenerator/displacer begins to move up, the outlet valve closes due to the drop in pressure. When the gas leaves the regenerator it is at an intermediate temperature. The greater the regenerator effectiveness, the closer the gas temperature will be to T_L. After the gas enters the cold side, additional heat is lost from the gas in the cold space to bring it down to T_L. At some point the pressure reaches P_L, and the inlet valve opens. This defines State 4 and ends the third part of the cycle.

3.5 PROCESS 4-1

The fourth process is the reverse of the second process. At State 4, some of the gas remains in the hot region of the cylinder. That remaining gas will be moved to the cold region, and additional gas will enter the cold side through the inlet valve. The regenerator/displacer continues to move up the cylinder toward State 1 at top dead center. As it moves the inlet valve keeps the pressure inside the cylinder constant at the low pressure point by allowing gas to enter the cylinder. Once the regenerator/displacer reaches top dead center most of the gas in the cylinder has been moved to the cold region where it is at T_L. The rest of the gas is in the regenerator volume and the dead space on the hot side where it is also at the low pressure point. Just as in the third process, the gas that moves through the regenerator to the cold side loses heat in the regenerator and also in the cold space. The inlet valve closes due to the pressure increase the instant that the fourth process in the cycle ends and the first process begins.

4 ANALYTICAL ANALYSIS

4.1 ANALYSIS OVERVIEW

A detailed thermodynamic analysis of the thermocompressor cycle will provide insight into the operation of the cycle and the sensitivity of the cycle's performance to various design parameters. Kornhauser [15] presents an excellent thermodynamic model, which will be built upon in this work by the inclusion of additional factors such as regenerator effectiveness, regenerator volume, and dead volume. The end of this development are the performance curves for the thermocompressor based upon thermal efficiency (sometimes called first law efficiency), volumetric efficiency, heat input, and work output.

It is assumed that the outlet pressure of the thermocompressor is constant during operation. The pressure ratio of the device must be some value between unity and the temperature ratio. In a practical system the high pressure could be set by a pressure regulator as shown in Fig. 4. Theoretically, the model only assumes constant outlet pressure P_H.

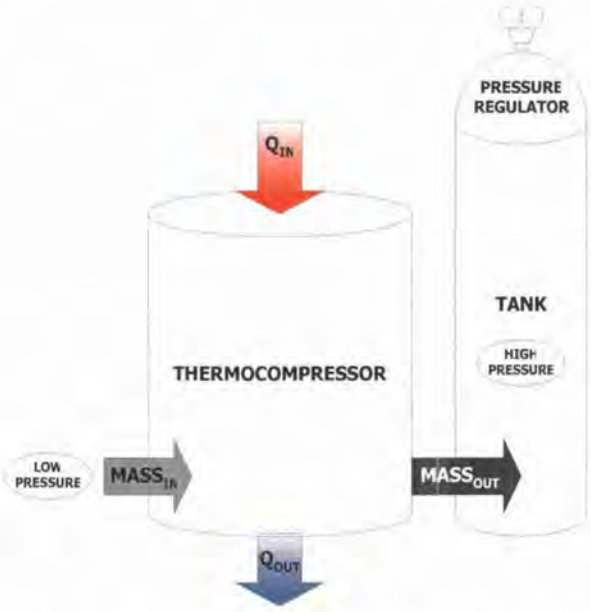

Figure 4 - Thermocompressor Outlet Pressure Regulator

A number of simplifying assumptions were made at the outset of this model. They include:

1. The working fluid is an ideal gas.
2. The working fluid has constant specific heat.
3. The pressure drops across the valves and the regenerator/displacer are zero.
4. The valves have perfect operation.
5. The inlet and outlet gas temperatures are T_L.
6. The work required to drive the regenerator/displacer is zero.
7. The cylinder walls are perfectly insulated.
8. The hot and cold regions are both isothermal.
9. The fluid properties in the regenerator volume are evaluated at the average regenerator temperature.

One of the desired features of this model is the inclusion of regenerator volume. This is made difficult by the fact that there is a temperature gradient across the regenerator, and consequently fluid properties inside the regenerator must be approximated. It is first assumed that the temperature gradient across the regenerator is linear; therefore, the mean temperature of the regenerator will be used to evaluate the fluid properties of the gas inside the regenerator volume. Figure 5 illustrates this assumption. While the pressure inside the regenerator volume changes during operation, the temperature at which the fluid properties are evaluated is assumed to be constant at T_{REG}.

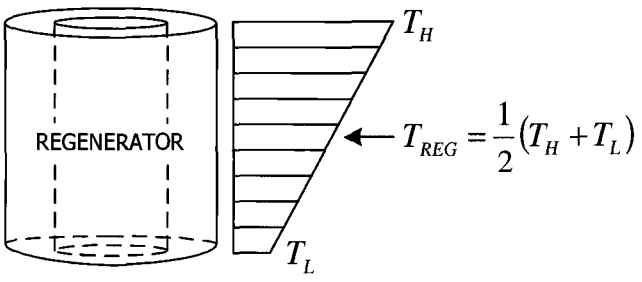

Figure 5 - Regenerator Temperature Profile

Perhaps the most significant assumption made in the model is that of isothermal hot and cold regions. This assumption is necessary to approximate fluid properties at both ends of the thermocompressor. However, it also carries more importance to the model because the thermal efficiency of the cycle is dependent upon it. In order for the cycle to reach Carnot efficiency, the hot and cold spaces must be isothermal. While this is the theoretical limit for thermal efficiency, it is not attainable practically. One of the primary reasons for this is imperfect regeneration. If the regenerator were perfect, the gas would leave the regenerator and enter the hot space at T_H and conversely enter the cold space at T_L. However, it has already been stated that the regenerator operates with some effectiveness less than unity. As a result, the gas enters the hot space at some temperature T_{HX} which is lower than T_H and enters the cold space at some temperature T_{LX} which is higher than T_L. Therefore, the regenerator effectiveness is given by

$$\varepsilon = \frac{T_{HX} - T_L}{T_H - T_L} \tag{1}$$

or, conversely, by

$$\varepsilon = \frac{T_H - T_{LX}}{T_H - T_L} \tag{2}$$

This discrepancy between regenerator exit temperature and cylinder temperature must be resolved by additional heat transfer to the gas in the hot space and away from the gas in the cold space. This additional heat transfer introduces irreversibilities into the cycle, which lowers its thermal efficiency. Some feature must be included in this model to account for that additional heat transfer, but still allow for the approximation of fluid properties by the isothermal assumption. This is accomplished by assuming that a fictitious zero volume heat exchanger exists on either end of the regenerator. This heat exchanger models the supplemental heat transfer, while the cylinder is assumed to be isothermal. The gas enters the respective heat exchanger at either T_{HX} or T_{LX} and leaves at T_H or T_L. This heat exchanger model is illustrated in Fig. 6.

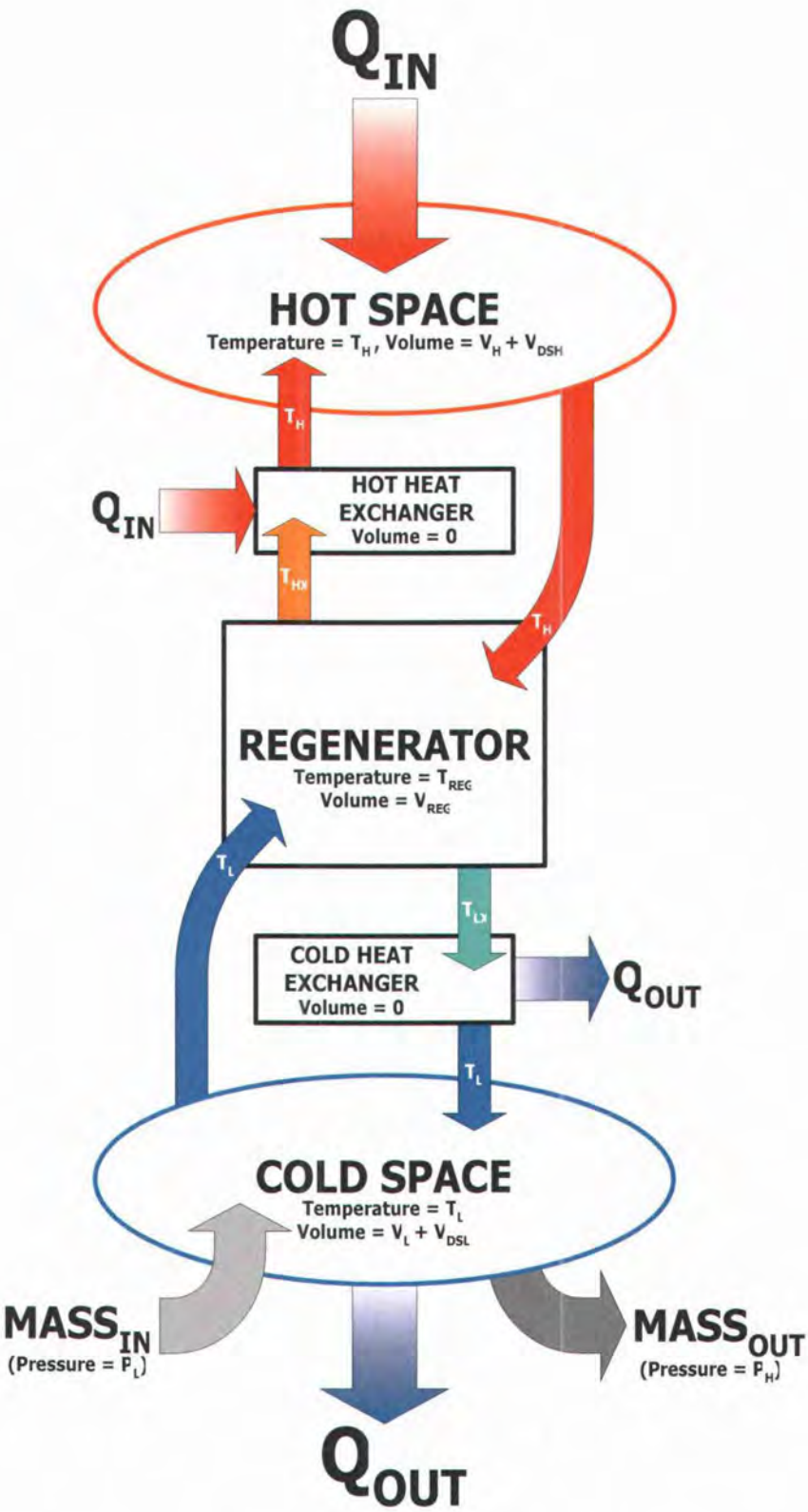

Figure 6 - Thermocompressor Model

Before examining the details of this model, a series of non-dimensional parameters must be defined. They are as follows:

$$P^* = \frac{P_L}{P_H}, \quad T^* = \frac{T_L}{T_H}, \quad T^*_{REG} = \frac{T_{REG}}{T_H} \tag{3}$$

$$V^* = \frac{V}{V_T}, \quad V^*_{REG} = \frac{V_{REG}}{V_T} \tag{4}$$

$$m^* = m\left(\frac{RT_H}{P_H V_T}\right), \quad Q^* = \frac{Q}{P_H V_T}, \quad W^* = \frac{W}{P_H V_T} \tag{5}$$

Where the total volume is given by

$$V_T = V_H + V_{DS,H} + V_{REG} + V_{DS,L} + V_L \tag{6}$$

This analytical model of the thermocompressor cycle is divided into seven sections. The first four sections (4.2-4.5) correspond to the four processes of the cycle. Each of the first four sections is divided into the five components of the system as shown in Fig. 6. The governing equations are presented for each component of the system during each process of the cycle. The fifth section (4.6) of the analysis gives an overview of the entire cycle. The sixth section (4.7) gives expressions for the cycle efficiency. Finally, the seventh section (4.8) presents an optimization study of the regenerator design.

4.2 PROCESS 1-2

Both a mass and an energy balance will be formulated for each component of the thermocompressor as illustrated in Fig. 6 for the first process of the cycle.

4.2.1 HOT SPACE 1-2

A mass balance on the hot space from State 1 to State 2 is given by

$$\Delta m_{H12} = (m_{in})_{H12} \tag{7}$$

$$\Delta m_{H12} = \frac{P_H V_{H2}}{RT_H} + \frac{(P_H - P_L)V_{DS,H}}{RT_H} \tag{8}$$

Non-dimensionalizing Eq. (8) gives

$$\boxed{\Delta m^*_{H12} = V^*_{H2} + (1 - P^*)V^*_{DS,H}} \tag{9}$$

An energy balance on the hot space from State 1 to State 2 can be written as

$$\Delta U_{H12} = Q_{H12} - W_{H12} + \left(m_{in}h_{in} - m_{out}h_{out}\right)_{H12} \tag{10}$$

Substituting constant specific heats, then simplifying yields

$$\Delta m_{H12}u_H = Q_{H12} - W_{H12} + \Delta m_{H12}h_H \tag{11}$$

$$Q_{H12} = W_{H12} + \Delta m_{H12}\left(c_v - c_p\right)T_H \tag{12}$$

Non-dimensionalizing Eq. (12) gives

$$\boxed{Q^*_{H12} = W^*_{H12} - \Delta m^*_{H12}} \tag{13}$$

Where W^*_{H12} is given by

$$W^*_{H12} = \int_0^{V^*_{H2}} P^* dV^*_H \tag{14}$$

The work term in Eq. (14) will be evaluated after V^*_{H2} has been determined.

4.2.2 HOT HEAT EXCHANGER 1-2

Because the hot heat exchanger has zero volume, it must have zero change in mass. Therefore, a mass balance on the hot heat exchanger from State 1 to State 2 is simply given by

$$\boxed{\Delta m^*_{HHX12} = 0} \tag{15}$$

Similarly, because it has zero volume, the hot heat exchanger must also have zero internal energy change and no work can be done in that space. Therefore, an energy balance on the hot heat exchanger can be written as

$$0 = Q_{HHX12} + \left(m_{in}h_{in} - m_{out}h_{out}\right)_{HHX12} \tag{16}$$

$$Q_{HHX12} = \Delta m_{H12}c_p\left(T_H - T_{HX}\right) \tag{17}$$

Non-dimensionalizing Eq. (17) gives

$$\boxed{Q^*_{HHX12} = \Delta m^*_{H12}\frac{\gamma}{\gamma - 1}\left(1 - T^*\right)\left(1 - \varepsilon\right)} \tag{18}$$

4.2.3 REGENERATOR 1-2

A mass balance on the regenerator from State 1 to State 2 is given by

$$\Delta m_{REG12} = (m_{in} - m_{out})_{REG12} \tag{19}$$

$$\Delta m_{REG12} = \frac{(P_H - P_L)V_{REG}}{RT_{REG}} \tag{20}$$

Non-dimensionalizing Eq. (20) gives

$$\boxed{\Delta m^*_{REG12} = \frac{(1-P^*)}{T^*_{REG}} V^*_{REG}} \tag{21}$$

Because the regenerator has no volume change, no work can be done in that space. Therefore, an energy balance on the regenerator can be written as

$$\Delta U_{REG12} = Q_{REG12} + (m_{in}h_{in} - m_{out}h_{out})_{REG12} \tag{22}$$

$$Q_{REG12} = \Delta m_{REG12} c_v T_{REG} - \Delta m_{REG12} c_p T_L + \Delta m_{H12} c_p (T_{HX} - T_L) \tag{23}$$

Substituting Eq. (1) into (23) gives

$$Q_{REG12} = \Delta m_{REG12} c_v T_{REG} - \Delta m_{REG12} c_p T_L + \Delta m_{H12} c_p (T_H - T_L)\varepsilon \tag{24}$$

Non-dimensionalizing Eq. (24) yields

$$\boxed{Q^*_{REG12} = \Delta m^*_{REG12} \frac{1}{\gamma - 1} T^*_{REG} - \Delta m^*_{REG12} \frac{\gamma}{\gamma - 1} T^* + \Delta m^*_{H12} \frac{\gamma}{\gamma - 1} (1 - T^*)\varepsilon} \tag{25}$$

4.2.4 COLD HEAT EXCHANGER 1-2

Gas leaves the cold space and enters the regenerator at T_L as shown in Fig. 6. Consequently, the cold heat exchanger has no impact on the gas during this part of the cycle. Therefore, the respective mass and energy balances on the cold heat exchanger are given by

$$\boxed{\Delta m^*_{LHX12} = 0} \tag{26}$$

and

$$\boxed{Q^*_{LHX12} = 0} \tag{27}$$

4.2.5 COLD SPACE 1-2

A mass balance on the cold space from State 1 to State 2 gives

$$\Delta m_{L12} = (m_{in} - m_{out})_{L12} \tag{28}$$

$$\Delta m_{L12} = \frac{(P_H - P_L)V_{DS,L}}{RT_L} - \frac{P_L V_{L1} - P_H V_{L2}}{RT_L} \tag{29}$$

Where V_{L1} and V_{L2} are given by

$$V_{L1} = V_T - (V_{DS,H} + V_{REG} + V_{DS,L}) \tag{30}$$

and

$$V_{L2} = V_T - (V_{H2} + V_{DS,H} + V_{REG} + V_{DS,L}) \tag{31}$$

Substituting Eq. (30) and (31) into Eq. (29), simplifying, and non-dimensionalizing yields

$$\boxed{\Delta m^*_{L12} = -\frac{1}{T^*}\left[V^*_{H2} - (1 - P^*)(1 - V^*_{DS,H} - V^*_{REG})\right]} \tag{32}$$

An energy balance on the regenerator from State 1 to State 2 can by written as

$$\Delta m_{L12} u_L = Q_{L12} - W_{L12} + \Delta m_{L12} h_L \tag{33}$$

$$Q_{L12} = W_{L12} + \Delta m_{L12}(c_v - c_p)T_L \tag{34}$$

Non-dimensionalizing Eq. (34) gives

$$\boxed{Q^*_{L12} = W^*_{L12} - \Delta m^*_{L12} T^*} \tag{35}$$

Because it is assumed that there is no pressure difference across the displacer as it moves down the piston, the work done in the cold space must be equal and opposite of the work done in the hot space. Therefore, W^*_{L12} is given by

$$\boxed{W^*_{L12} = -W^*_{H12}} \tag{36}$$

4.2.6 CYLINDER 1-2

Since both valves are closed during this part of the cycle, no mass enters or leaves the cylinder. Therefore, the mass balance for the entire cylinder can be written as

$$\Delta m^*_{H12} + \Delta m^*_{HHX12} + \Delta m^*_{REG12} + \Delta m^*_{LHX12} + \Delta m^*_{L12} = 0 \tag{37}$$

Substituting Eq. (9), (15), (21), (26), and (32) into Eq. (37) and simplifying yields

$$V_{H2}^* + (1-P^*)V_{DS,H}^* + \frac{(1-P^*)}{T_{REG}^*}V_{REG}^* \cdots$$
$$-\frac{1}{T^*}\left[V_{H2}^* - (1-P^*)(1-V_{DS,H}^* - V_{REG}^*)\right] = 0 \tag{38}$$

Solving Eq. (38) for V_{H2}^* gives

$$\boxed{V_{H2}^* = \left[\frac{1-P^*}{1-T^*}\right] - \left[\frac{1-P^*}{1-T^*}\right]\left[1-\frac{T^*}{T_{REG}^*}\right]V_{REG}^* - (1-P^*)V_{DS,H}^*} \tag{39}$$

Equation (38) can be rewritten as a mass balance for the entire cylinder from State 1 to some arbitrary point, X, between State 1 and State 2. That mass balance can be written as

$$P_X^* V_{HX}^* + (P_X^* - P^*)V_{DS,H}^* + \frac{(P_X^* - P^*)}{T_{REG}^*}V_{REG}^* \cdots$$
$$-\frac{1}{T^*}\left[P_X^* V_{HX}^* - (P_X^* - P^*)(1-V_{DS,H}^* - V_{REG}^*)\right] = 0 \tag{40}$$

Solving Eq. (40) for P_X gives

$$P_X^* = \frac{P^*\left(\left[\frac{1}{1-T^*}\right] - \left[\frac{1}{1-T^*}\right]\left[1-\frac{T^*}{T_{REG}^*}\right]V_{REG}^* - V_{DS,H}^*\right)}{\left(\left[\frac{1}{1-T^*}\right] - \left[\frac{1}{1-T^*}\right]\left[1-\frac{T^*}{T_{REG}^*}\right]V_{REG}^* - V_{DS,H}^* - V_{HX}^*\right)} \tag{41}$$

Substituting Eq. (41) into Eq. (14) yields

$$W_{H12}^* = \int_0^{V_{H2}^*} P_X^* dV_H^* \tag{42}$$

Integrating Eq. (42) and simplifying gives

$$\boxed{W_{H12}^* = -\left(\left[\frac{1}{1-T^*}\right] - \left[\frac{1}{1-T^*}\right]\left[1-\frac{T^*}{T_R^*}\right]V_R^* - V_{DS,H}^*\right)P^* \ln(P^*)} \tag{43}$$

4.3 PROCESS 2-3

Both a mass and an energy balance will be formulated for each component of the thermocompressor as illustrated in Fig. 6 for the second process of the cycle.

4.3.1 HOT SPACE 2-3

A mass balance on the hot space from State 2 to State 3 can be written as

$$\Delta m_{H23} = \frac{P_H (V_{H3} - V_{H2})}{RT_H} \tag{44}$$

Where V_{H3} is given by

$$V_{H3} = V_T - (V_{DS,H} + V_{REG} + V_{DS,L}) \tag{45}$$

Substituting Eq. (45) into Eq. (44) and non-dimensionalizing yields

$$\boxed{\Delta m^*_{H23} = 1 - (V^*_{H2} + V^*_{DS,H} + V^*_{REG} + V^*_{DS,L})} \tag{46}$$

An energy balance on the hot space from State 2 to State 3 gives

$$Q_{H23} = W_{H23} + \Delta m_{H23}(c_v - c_p)T_H \tag{47}$$

Where W_{H12} can be written as

$$W_{H23} = P_H (V_{H3} - V_{H2}) \tag{48}$$

Substituting Eq. (45) into Eq. (48) and non-dimensionalizing gives

$$\boxed{W^*_{H23} = 1 - (V^*_{H2} + V^*_{DS,H} + V^*_{REG} + V^*_{DS,L})} \tag{49}$$

Substituting Eq. (46) and (49) into Eq. (47) and non-dimensionalizing yields

$$\boxed{Q^*_{H12} = 0} \tag{50}$$

4.3.2 HOT HEAT EXCHANGER 2-3

Just as in the first part of the cycle, the respective mass and energy balances for the hot heat exchanger in the second part of the cycle are given by

$$\boxed{\Delta m^*_{HHX23} = 0} \tag{51}$$

and

$$Q_{HHX23} = \Delta m_{H23} c_p (T_H - T_{HX}) \tag{52}$$

Non-dimensionalizing Eq. (52) gives

$$\boxed{Q^*_{HHX23} = \Delta m^*_{H23} \frac{\gamma}{\gamma - 1}(1 - T^*)(1 - \varepsilon)} \tag{53}$$

4.3.3 REGENERATOR 2-3

Because there is no pressure or volume change in the regenerator from State 2 to State 3, its mass balance is given by

$$\boxed{\Delta m^*_{REG\,23} = 0} \tag{54}$$

An energy balance on the regenerator from State 2 to State 3 can be written as

$$0 = Q_{REG\,23} + \left(m_{in}h_{in} - m_{out}h_{out}\right)_{REG\,23} \tag{55}$$

$$Q_{REG\,23} = \Delta m_{H\,23} c_p \left(T_{HX} - T_L\right) \tag{56}$$

Substituting Eq. (1) into (56) gives

$$Q_{REG\,23} = \Delta m_{H\,23} c_p \left(T_H - T_L\right)\varepsilon \tag{57}$$

Non-dimensionalizing Eq. (57) yields

$$\boxed{Q^*_{REG\,23} = \Delta m^*_{H\,23} \frac{\gamma}{\gamma - 1}\left(1 - T^*\right)\varepsilon} \tag{58}$$

4.3.4 COLD HEAT EXCHANGER 2-3

Just as in the first process in the cycle, no mass passes through the cold heat exchanger during the second part of the cycle, therefore, the respective mass and energy balances are given by

$$\boxed{\Delta m^*_{LHX\,23} = 0} \tag{59}$$

and

$$\boxed{Q^*_{LHX\,23} = 0} \tag{60}$$

4.3.5 COLD SPACE 2-3

A mass balance on the cold space from State 2 to State 3 gives

$$\Delta m_{L23} = -\frac{P_H V_{L2}}{RT_L} \tag{61}$$

Substituting Eq. (31) into Eq. (61) and non-dimensionalizing yields

$$\boxed{\Delta m^*_{L23} = -\frac{1}{T^*}\left[1 - \left(V^*_{H2} + V^*_{DS,H} + V^*_{REG} + V^*_{DS,L}\right)\right]} \tag{62}$$

An energy balance on the cold space from State 2 to State 3 can by written as

$$Q_{L23} = W_{L23} + \Delta m_{L23}(c_v - c_p)T_L \tag{63}$$

Where W^*_{L23} is given by

$$\boxed{W^*_{L23} = -W^*_{H23}} \tag{64}$$

Substituting Eq. (49), (64), and (62) into Eq. (63) and non-dimensionalizing gives

$$\boxed{Q^*_{L23} = 0} \tag{65}$$

4.3.6 CYLINDER 2-3

A mass balance on the entire cylinder for the second part of the cycle can be solved for the mass flow out of the cylinder per cycle. The mass balance is given by

$$\Delta m^*_{23} = \Delta m^*_{H23} + \Delta m^*_{HHX23} + \Delta m^*_{REG23} + \Delta m^*_{LHX23} + \Delta m^*_{L23} \tag{66}$$

Substituting Eq. (46), (51), (54), (59), and (62) into Eq. (66) and simplifying gives

$$\boxed{\Delta m^*_{23} = -\left[\frac{1}{T^*} - 1\right]\left[1 - \left(V^*_{H2} + V^*_{DS,H} + V^*_{REG} + V^*_{DS,L}\right)\right]} \tag{67}$$

4.4 PROCESS 3-4

Both a mass and an energy balance will be formulated for each component of the thermocompressor as illustrated in Fig. 6 for the third process of the cycle.

4.4.1 HOT SPACE 3-4

A mass balance on the hot space from State 3 to State 4 can be written as

$$\Delta m_{H34} = -\left(\frac{P_H V_{H3} - P_L V_{H4}}{RT_H} + \frac{(P_H - P_L)V_{DS,H}}{RT_H}\right) \tag{68}$$

Non-dimensionalizing Eq. (68) gives

$$\boxed{\Delta m^*_{H34} = -\left(1 - P^* V^*_{H4} - P^* V^*_{DS,H} - V^*_{REG} - V^*_{DS,L}\right)} \tag{69}$$

An energy balance on the hot space from State 3 to State 4 can be written as

$$Q_{H34} = W_{H34} + \Delta m_{H34}(c_v - c_p)T_H \tag{70}$$

Non-dimensionalizing Eq. (70) gives

$$\boxed{Q^*_{H34} = W^*_{H34} - \Delta m^*_{H34}} \tag{71}$$

Where W^*_{H34} is given by

$$\boxed{W^*_{H34} = \int_{V^*_{H3}}^{V^*_{H4}} P^* dV^*_H} \tag{72}$$

The work term in Eq. (72) will be evaluated after V^*_{H4} has been determined.

4.4.2 HOT HEAT EXCHANGER 3-4

Gas leaves the hot space and enters the regenerator at T_H as shown in Fig. 6. Consequently, the hot heat exchanger has no impact on the gas during this part of the cycle. Therefore, the respective mass and energy balances are given by

$$\boxed{\Delta m^*_{HHX34} = 0} \tag{73}$$

and

$$\boxed{Q^*_{HHX34} = 0} \tag{74}$$

4.4.3 REGENERATOR 3-4

A mass balance on the regenerator from State 3 to State 4 is given by

$$\Delta m_{REG34} = -\frac{(P_H - P_L)V_{REG}}{RT_{REG}} \tag{75}$$

Non-dimensionalizing Eq. (75) gives

$$\boxed{\Delta m^*_{REG34} = -\frac{(1-P^*)}{T^*_{REG}} V^*_{REG}} \tag{76}$$

An energy balance on the regenerator from State 3 to State 4 can be written as

$$\Delta U_{REG34} = Q_{REG34} + (m_{in}h_{in} - m_{out}h_{out})_{REG34} \tag{77}$$

$$Q_{REG34} = \Delta m_{REG34} c_v T_{REG} + \Delta m_{REG34} c_p T_{LX} - \Delta m_{H34} c_p (T_H - T_{LX}) \tag{78}$$

Substituting Eq. (2) into (78) gives

$$Q_{REG34} = \Delta m_{REG34} c_v T_{REG} + \Delta m_{REG34} c_p T_{LX} - \Delta m_{H34} c_p (T_H - T_L)\varepsilon \tag{79}$$

Non-dimensionalizing Eq. (79) yields

$$\boxed{\begin{aligned} Q^*_{REG34} &= \Delta m^*_{REG34}\frac{1}{\gamma-1}T^*_{REG}\cdots \\ &+\Delta m^*_{REG34}\frac{\gamma}{\gamma-1}\left(1-\left(1-T^*\right)\varepsilon\right)-\Delta m^*_{H34}\frac{\gamma}{\gamma-1}\left(1-T^*\right)\varepsilon \end{aligned}} \tag{80}$$

4.4.4 COLD HEAT EXCHANGER 3-4

A mass balance on the cold heat exchanger from State 3 to State 4 is given by

$$\boxed{\Delta m^*_{LHX34}=0} \tag{81}$$

An energy balance on the cold heat exchanger can be written as

$$0=Q_{LHX34}+\left(m_{in}h_{in}-m_{out}h_{out}\right)_{LHX34} \tag{82}$$

$$Q_{LHX34}=\Delta m_{H34}c_p\left(T_{LX}-T_L\right) \tag{83}$$

Non-dimensionalizing Eq. (83) gives

$$\boxed{Q^*_{LHX34}=\Delta m^*_{H34}\frac{\gamma}{\gamma-1}\left(1-T^*\right)\left(1-\varepsilon\right)} \tag{84}$$

4.4.5 COLD SPACE 3-4

A mass balance on the cold space from State 3 to State 4 gives

$$\Delta m_{L34}=\frac{P_L V_{L4}}{RT_L}-\frac{\left(P_H-P_L\right)V_{DS,L}}{RT_L} \tag{85}$$

Where V_{L4} is given by

$$V_{L4}=V_T-\left(V_{H4}+V_{DS,H}+V_{REG}+V_{DS,L}\right) \tag{86}$$

Substituting Eq. (86) into Eq. (85), simplifying, and non-dimensionalizing yields

$$\boxed{\Delta m^*_{L34}=\frac{1}{T^*}\left[P^*\left(1-V^*_{H4}\right)-P^*V^*_{DS,H}-P^*V^*_{REG}-V^*_{DS,L}\right]} \tag{87}$$

An energy balance on the regenerator from State 3 to State 4 can by written as

$$Q_{L34}=W_{L34}+\Delta m_{L34}\left(c_v-c_p\right)T_L \tag{88}$$

Non-dimensionalizing Eq. (88) gives

$$\boxed{Q^*_{L34}=W^*_{L34}-\Delta m^*_{L34}T^*} \tag{89}$$

Where W^*_{L34} is given by

$$\boxed{W^*_{L34} = -W^*_{H34}} \tag{90}$$

4.4.6 CYLINDER 3-4

Both valves are closed during this part of the cycle; therefore, no mass enters or leaves the cylinder. The mass balance for the entire cylinder can be written as

$$\Delta m^*_{H34} + \Delta m^*_{HHX34} + \Delta m^*_{REG34} + \Delta m^*_{LHX34} + \Delta m^*_{L34} = 0 \tag{91}$$

Substituting Eq. (69), (73), (76), (81), and (87) into Eq. (91) and simplifying yields

$$\begin{aligned} &-\left(1 - P^* V^*_{H4} - P^* V^*_{DS,H} - V^*_{REG} - V^*_{DS,L}\right) - \frac{\left(1-P^*\right)}{T^*_{REG}} V^*_{REG} \cdots \\ &+\frac{1}{T^*}\left[P^*\left(1 - V^*_{H4}\right) - P^* V^*_{DS,H} - P^* V^*_{REG} - V^*_{DS,L}\right] = 0 \end{aligned} \tag{92}$$

Solving Eq. (92) for V^*_{H4} gives

$$\boxed{\begin{aligned} V^*_{H4} = &\left[\frac{P^* - T^*}{P^*\left(1-T^*\right)}\right] - V^*_{DS,H} - \left[\frac{1-P^*}{P^*\left(1-T^*\right)}\right]\frac{T^*}{T^*_{REG}} V^*_{REG} \cdots \\ &-\left[\frac{P^* - T^*}{P^*\left(1-T^*\right)}\right] V^*_{REG} - \frac{1}{P^*} V^*_{DS,L} \end{aligned}} \tag{93}$$

Equation (93) can be rewritten as a mass balance for the entire cylinder from State 3 to some arbitrary point, Y, between State 3 and State 4. That mass balance can be written as

$$\begin{aligned} &-\left(1 - P^*_Y V^*_{HY} - P^*_Y V^*_{DS,H} - V^*_{REG} - V^*_{DS,L}\right) - \frac{\left(1-P^*_Y\right)}{T^*_{REG}} V^*_{REG} \cdots \\ &+\frac{1}{T^*}\left[P^*_Y\left(1 - V^*_{HY}\right) - P^*_Y V^*_{DS,H} - P^*_Y V^*_{REG} - V^*_{DS,L}\right] = 0 \end{aligned} \tag{94}$$

Solving Eq. (94) for P_Y gives

$$P^*_Y = \frac{\left(1 + \left[\frac{1}{T^*_{REG}} - 1\right] V^*_{REG} + \left[\frac{1}{T^*} - 1\right] V^*_{DS,L}\right)}{\left(\frac{1}{T^*} - \left[\frac{1}{T^*} - 1\right] V^*_{HB} - \left[\frac{1}{T^*} - 1\right] V^*_{DS,H} + \left[\frac{1}{T^*_{REG}} - \frac{1}{T^*}\right] V^*_{REG}\right)} \tag{95}$$

Substituting Eq. (95) into Eq. (72) yields

$$W_{H34}^{*} = \int_{V_{H3}^{*}}^{V_{H4}^{*}} P_{Y}^{*} dV_{H}^{*} \tag{96}$$

Integrating Eq. (96) and simplifying gives

$$\boxed{W_{H34}^{*} = \left(\left[\frac{T^{*}}{T^{*}-1} \right] - \left[\frac{1-T_{REG}^{*}}{1-T^{*}} \right] \left[\frac{T^{*}}{T_{REG}^{*}} \right] V_{REG}^{*} - V_{DS,L}^{*} \right) \ln\left(\frac{1}{P^{*}} \right)} \tag{97}$$

4.5 PROCESS 4-1

Both a mass and an energy balance will be formulated for each component of the thermocompressor as illustrated in Fig. 6 for the fourth process of the cycle.

4.5.1 HOT SPACE 4-1

A mass balance on the hot space from State 4 to State 1 can be written as

$$\Delta m_{H41} = -\frac{P_{L} V_{H4}}{R T_{H}} \tag{98}$$

Non-dimensionalizing Eq. (98) yields

$$\boxed{\Delta m_{H41}^{*} = -P^{*} V_{H4}^{*}} \tag{99}$$

An energy balance on the hot space from State 4 to State 1 gives

$$Q_{H41} = W_{H41} + \Delta m_{H41} \left(c_{v} - c_{p} \right) T_{H} \tag{100}$$

Where W_{H41} can be written as

$$W_{H41} = P_{L} \left(0 - V_{H4} \right) \tag{101}$$

Non-dimensionalizing Eq. (101) yields

$$\boxed{W_{H41}^{*} = -P^{*} V_{H4}^{*}} \tag{102}$$

Substituting Eq. (99) and (102) into Eq. (100) and non-dimensionalizing gives

$$\boxed{Q_{H41}^{*} = 0} \tag{103}$$

4.5.2 HOT HEAT EXCHANGER 4-1

Just as in the third process of the cycle, no mass passes through the hot heat exchanger during the fourth part of the cycle, therefore, the respective mass and energy balances are given by

$$\boxed{\Delta m^*_{HHX\,41} = 0} \tag{104}$$

and

$$\boxed{Q^*_{HHX\,41} = 0} \tag{105}$$

4.5.3 REGENERATOR 4-1

A mass balance on the regenerator from State 4 to State 1 gives

$$\boxed{\Delta m^*_{REG\,41} = 0} \tag{106}$$

An energy balance on the regenerator from State 4 to State 1 can be written as

$$Q_{REG\,41} = \Delta m_{H\,41} c_p (T_{LX} - T_H) \tag{107}$$

Substituting Eq. (2) into (107) gives

$$Q_{REG\,41} = \Delta m_{H\,41} c_p (T_H - T_L)\varepsilon \tag{108}$$

Non-dimensionalizing Eq. (108) yields

$$\boxed{Q^*_{REG\,41} = -\Delta m^*_{H\,41} \frac{\gamma}{\gamma - 1}(1 - T^*)\varepsilon} \tag{109}$$

4.5.4 COLD HEAT EXCHANGER 4-1

A mass balance on the cold heat exchanger from State 4 to State 1 is given by

$$\boxed{\Delta m^*_{LHX\,41} = 0} \tag{110}$$

An energy balance on the cold heat exchanger can be written as

$$0 = Q_{LHX\,41} + (m_{in} h_{in} - m_{out} h_{out})_{LHX\,41} \tag{111}$$

$$Q_{LHX\,41} = \Delta m_{H\,41} c_p (T_L - T_{LX}) \tag{112}$$

Non-dimensionalizing Eq. (112) gives

$$\boxed{Q^*_{LHX\,41} = -\Delta m^*_{H\,41} \frac{\gamma}{\gamma - 1}(1 - T^*)(1 - \varepsilon)} \tag{113}$$

4.5.5 COLD SPACE 4-1

A mass balance on the cold space from State 4 to State 1 gives

$$\Delta m_{L41} = \frac{P_L(V_{L1} - V_{L4})}{RT_L} \tag{114}$$

Substituting Eq. (86) into Eq. (114), simplifying, and non-dimensionalizing yields

$$\boxed{\Delta m^*_{L41} = \frac{P^* V^*_{H4}}{T^*}} \tag{115}$$

An energy balance on the regenerator from State 4 to State 1 can by written as

$$Q_{L41} = W_{L41} + \Delta m_{L41}(c_v - c_p)T_L \tag{116}$$

Where W^*_{L41} is given by

$$\boxed{W^*_{L41} = -W^*_{H41}} \tag{117}$$

Substituting Eq. (115) and (117) into Eq. (116) and non-dimensionalizing gives

$$\boxed{Q^*_{L41} = 0} \tag{118}$$

4.5.6 CYLINDER 4-1

A mass balance on the entire cylinder for the fourth part of the cycle can be solved for the mass flow into the cylinder per cycle. The mass balance is given by

$$\Delta m^*_{41} = \Delta m^*_{H41} + \Delta m^*_{HHX41} + \Delta m^*_{REG41} + \Delta m^*_{LHX41} + \Delta m^*_{L41} \tag{119}$$

Substituting Eq. (99), (104), (106), (110), and (115) into Eq. (119) and simplifying gives

$$\boxed{\Delta m^*_{41} = P^*\left(\frac{1}{T^*} - 1\right)V^*_{H4}} \tag{120}$$

4.6 CYCLE OVERVIEW

Examining the cycle from a global perspective will be beneficial to show the inputs and outputs to the system. The total heat input to the thermocompressor can be written as

$$\boxed{Q^*_{in} = Q^*_{H12} + Q^*_{HHX12} + Q^*_{HHX23} + Q^*_{H34}} \tag{121}$$

Next, the work output of the thermocompressor must be defined. It is assumed that the gas enters and leaves the thermocompressor at T_L. Therefore, the output gas is at P_H and T_L and has some energy availability relative to the input gas, which is at P_L and T_L. It is further assumed that a hypothetical isothermal expansion process from P_H to P_L operating outside of the thermocompressor could be used to convert that availability into mechanical work. For an ideal gas, that isothermal expansion is given by the integral of pressure with respect to volume, which is given by

$$W_{out} = \int \frac{\Delta m R T_L}{V} dV \tag{122}$$

Integrating Eq. (122) gives

$$W_{out} = \Delta m_{41} R T_L \ln\left(\frac{P_H}{P_L}\right) \tag{123}$$

Non-dimensionalizing Eq. (123) gives

$$\boxed{W^*_{out} = \Delta m^*_{41} T^* \ln\left(\frac{1}{P^*}\right)} \tag{124}$$

The mass flow through the regenerator can be written as

$$\Delta m_{REG} = \Delta m_{REG12} + \Delta m_{REG22} + \Delta m_{REG34} + \Delta m_{REG41} \tag{125}$$

Substituting Eq. (21), (54),(76), and (106) into (125) gives

$$\boxed{\Delta m_{REG} = 0} \tag{126}$$

Equation (126) verifies that there is no net mass accumulation or loss in the regenerator during a cycle. It is assumed that the temperature profile of the regenerator does not change during a cycle; therefore Eq. (126) is consistent with conservation of mass for a fixed volume.

The heat flow through the regenerator can be given by

$$Q_{REG} = -Q_{REG12} - Q_{REG22} + Q_{REG34} + Q_{REG41} \tag{127}$$

Substituting Eq. (25), (58), (80), and (109) into (127) gives

$$\boxed{Q_{REG} = 0} \tag{128}$$

Equation (128) verifies that there is no net energy increase or decrease in the regenerator during a cycle. Again, it is assumed that the temperature profile of the regenerator does not change during a cycle; therefore Eq. (128) is consistent with conservation of energy for a fixed mass.

Figure 7 shows the non-dimensionalized mass flow rate through the thermocompressor as a function of pressure ratio for a range of temperature ratios. The maximum mass flow rate occurs with the pressure ratio is one, which corresponds to zero pressure increase. In this case the thermocompressor would not actually be producing any work. The minimum mass flow rate is zero, which corresponds to the maximum pressure increase. For an ideal gas the theoretical maximum pressure increase would produce a pressure ratio equal to the temperature ratio as indicated in the figure.

Figure 8 shows the non-dimensionalized work output of the thermocompressor as a function of pressure ratio for a range of temperature ratios. The curve indicates that the maximum work output of the device does not occur at its maximum pressure ratio, but at some intermediate pressure ratio. This is due to the fact that work output is a function of both pressure ratio, and mass flow rate. As shown in Eq. (124), work output increases exponentially with increased pressure ratio, and it increases linearly with increased mass flow rate. However, as shown in Fig. 7, the mass flow rate decreases exponentially with increased pressure ratio. Therefore, at low pressure ratios, the mass flow rate is high, but the work output is still very low. Similarly, at high pressure ratios, the mass flow rate is very low, and consequently the work output is low. Therefore, there is an intermediate pressure ratio, which produces the maximum work output for the device.

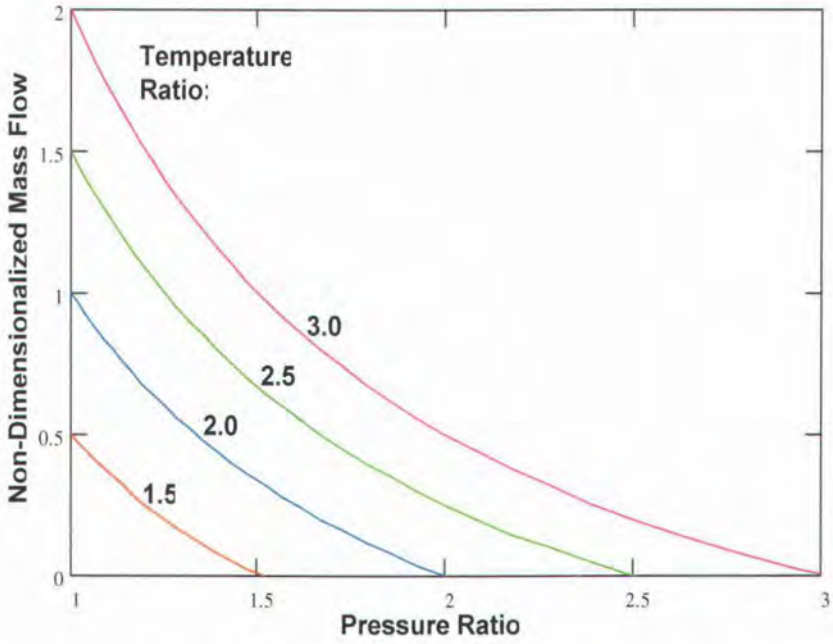

Figure 7 - Non-Dimensionalized Mass Flow Rate

$V_{REG} = 0$, $V_{DSL} = 0$, $V_{DSH} = 0$, $\varepsilon = 1$, $\gamma = 1.4$

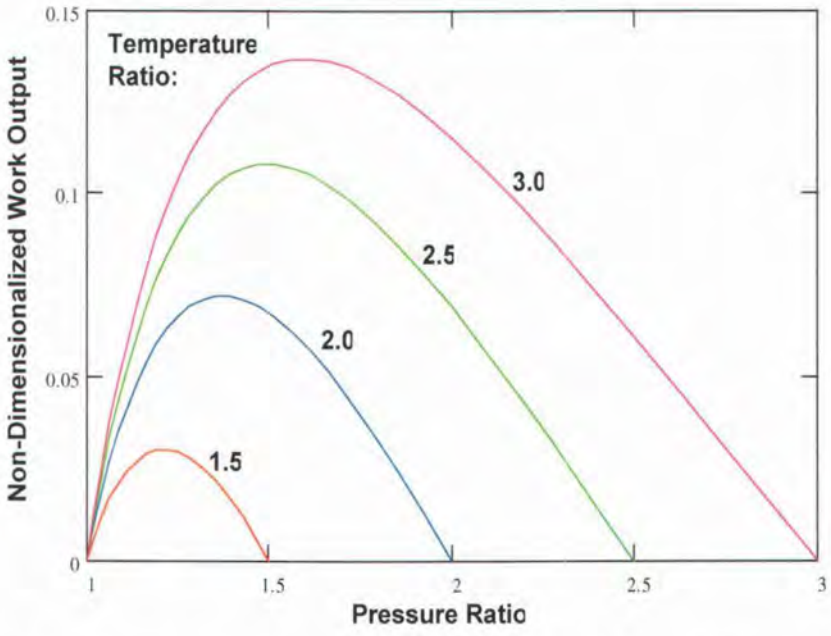

Figure 8 - Non-Dimensionalized Work Output vs. Pressure Ratio and Temperature Ratio

$V_{REG} = 0$, $V_{DSL} = 0$, $V_{DSH} = 0$, $\varepsilon = 1$, $\gamma = 1.4$

Figure 9 shows the non-dimensionalized heat input of the thermocompressor as a function of pressure ratio for a range of temperature ratios. As expected, the heat input follows a similar trend as the work output, and therefore has a maximum at the same intermediate pressure ratio.

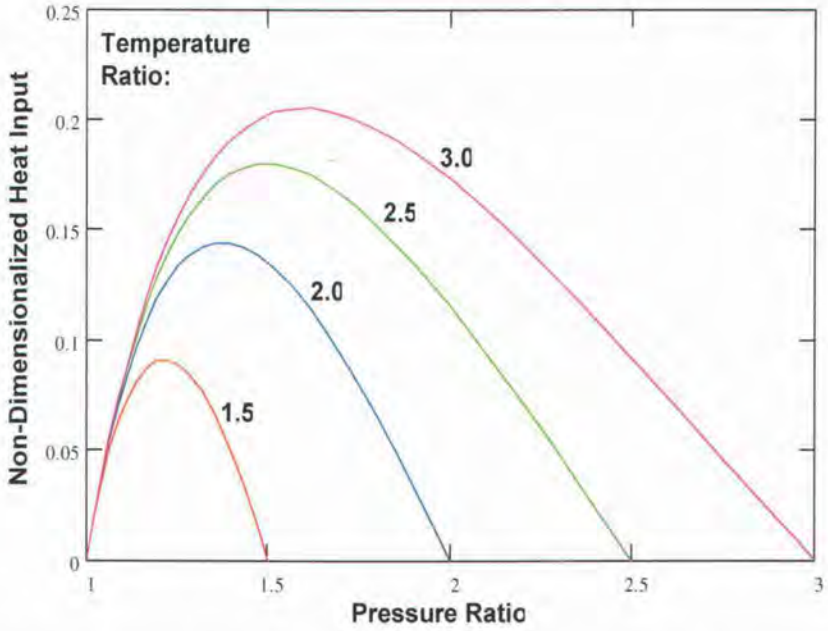

Figure 9 - Non-Dimensionalized Heat Input vs. Pressure Ratio and Temperature Ratio

$V_{REG} = 0$, $V_{DSL} = 0$, $V_{DSH} = 0$, $\varepsilon = 1$, $\gamma = 1.4$

4.7 CYCLE EFFICIENCY

Now that each component of the thermocompressor has been characterized for the entire cycle, it is possible to derive expressions for the efficiency of the device. The thermal efficiency is defined as

$$\eta_{TH} = \frac{W^*_{out}}{Q^*_{in}} \tag{129}$$

Substituting Eq. (121) and (124) into Eq. (129) gives

$$\boxed{\eta_{TH} = \frac{\Delta m^*_{41} T^* \ln\left(\frac{1}{P^*}\right)}{Q^*_{H12} + Q^*_{HHX12} + Q^*_{HHX23} + Q^*_{H34}}} \tag{130}$$

Substituting $\varepsilon=1$, $V_{DS,H}=0$, $V_{REG}=0$, and $V_{DS,L}=0$ into Eq. (130) and simplifying gives

$$\eta_{TH} = 1 - T^* \tag{131}$$

Equation (131) is equal to Carnot efficiency. This demonstrates that a thermocompressor operating under ideal, perfect conditions operates with the same efficiency as a fully reversible heat engine with no entropy generation. This requires a perfectly insulated cylinder, no dead volume in the system, and perfect regeneration. This result is consistent with a traditional ideal Stirling cycle, which also operates at Carnot efficiency.

Another measure of merit for the performance of the cycle is volumetric efficiency. It is defined as follows:

$$\eta_{VOL} = \frac{\text{(Mass Flow Per Cycle)}}{\text{(Inlet Density)(Volume Displacement)}}$$

Therefore, volumetric efficiency can be written as

$$\eta_{VOL} = \frac{\Delta m_{41}}{\left[\frac{P_L}{RT_L}\right]\left[V_T - \left(V_{DS,H} + V_{REG} + V_{DS,L}\right)\right]} \tag{132}$$

Non-dimensionalizing Eq. (132) gives

$$\boxed{\eta_{VOL} = \frac{\Delta m_{41}^* T^*}{P^*\left[1 - \left(V_{DS,H}^* + V_{REG}^* + V_{DS,L}^*\right)\right]}} \tag{133}$$

Volumetric efficiency is plotted in Fig. 10 as a function of pressure ratio. As expected, it follows a similar trend to the mass flow rate.

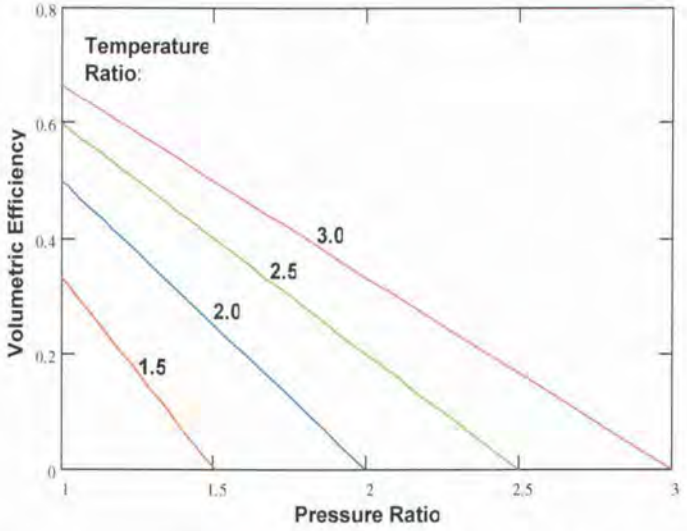

Figure 10 - Volumetric Efficiency vs. Pressure Ratio and Temperature Ratio

$V_{REG} = 0$, $V_{DSL} = 0$, $V_{DSH} = 0$, $\varepsilon = 1$, $\gamma = 1.4$

The thermal efficiency of the thermocompressor is given in Fig. 11 as a function of pressure ratio and regenerator effectiveness. Figure 11 illustrates that the maximum thermal efficiency of the thermocompressor occurs at an intermediate pressure ratio. Comparing Fig. 11 to Fig. 8, demonstrates that the maximum thermal efficiency corresponds to the maximum work output.

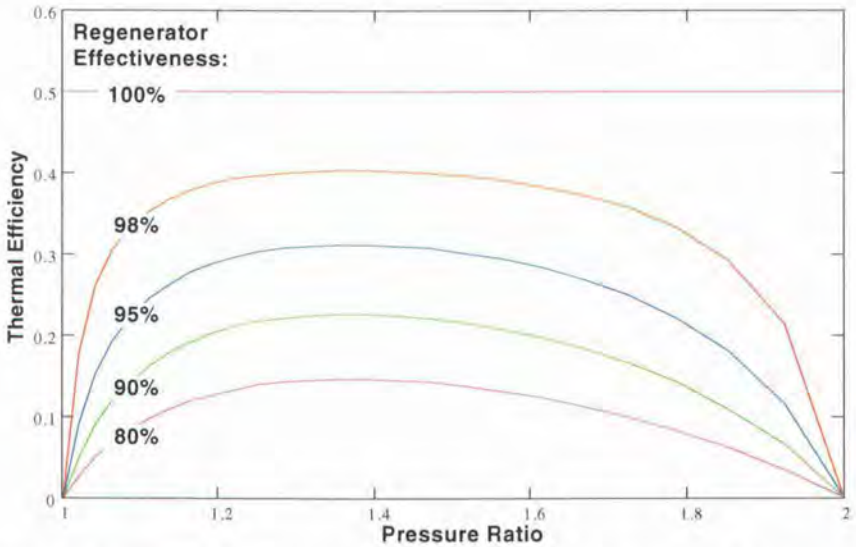

Figure 11 - Thermal Efficiency vs. Pressure Ratio and Regenerator Effectiveness

$T_{RATIO} = 2$, $V_{REG} = 0$, $V_{DSL} = 0$, $V_{DSH} = 0$, $\gamma = 1.4$

Thermal efficiency is plotted as a function of regenerator effectiveness in Figs. 12, 13, and 14. Figure 12 for a range of regenerator dead volumes, Fig. 13 for a range of cold side dead volumes, and Fig. 14 for a range of hot side dead volumes.

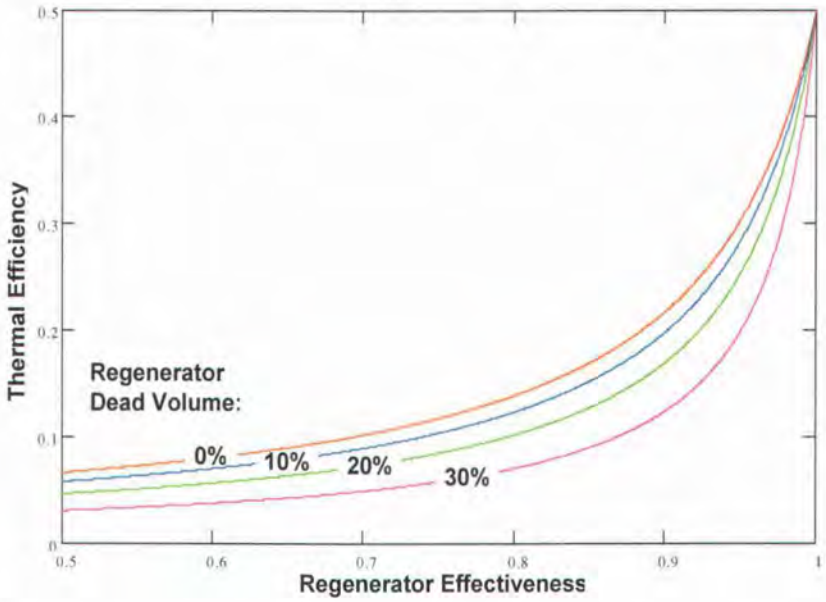

Figure 12 - Thermal Efficiency vs. Regenerator Effectiveness and Regenerator Dead Volume

$T_{RATIO} = 2$, $P_{RATIO} = 1.5$, $V_{DSL} = 0$, $V_{DSH} = 0$, $\gamma = 1.4$

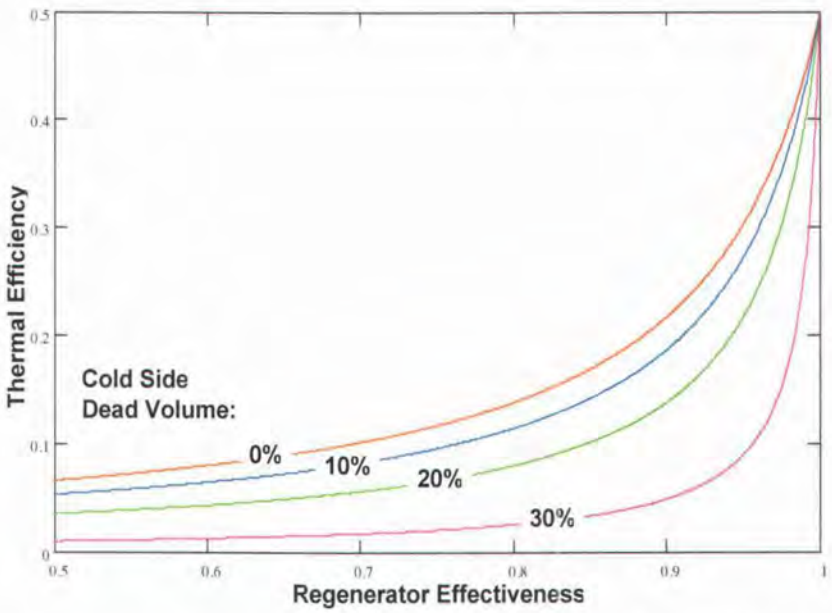

Figure 13 - Thermal Efficiency vs. Regenerator Effectiveness and Cold Side Dead Volume

$T_{RATIO} = 2$, $P_{RATIO} = 1.5$, $V_{REG} = 0$, $V_{DSH} = 0$, $\gamma = 1.4$

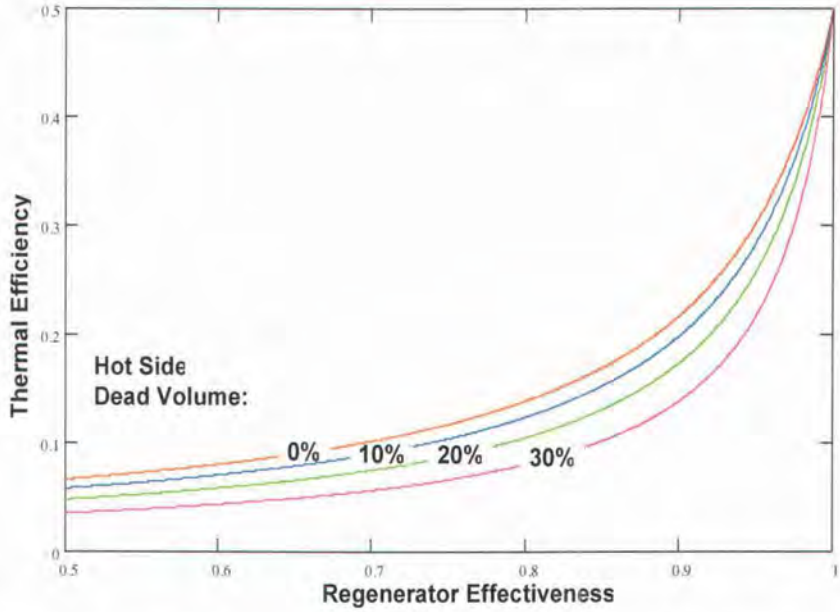

Figure 14 - Thermal Efficiency vs. Regenerator Effectiveness and Hot Side Dead Volume

$T_{RATIO} = 2$, $P_{RATIO} = 1.5$, $V_{DSL} = 0$, $V_{REG} = 0$, $\gamma = 1.4$

As indicated in Figs. 12, 13, and 14, thermal efficiency is highly sensitive to regenerator effectiveness. This is due to the additional heat transfer to the hot side that is required when the gas leaves the regenerator at some temperature less than T_H, as illustrated in Fig. 6. Figure 15 shows that the supplemental heat transfer is large compared to the rest of the heat input to the hot side and increases rapidly as regenerator effectiveness is reduced. This increase in heat input without an increase in work output, accounts for the decrease in thermal efficiency.

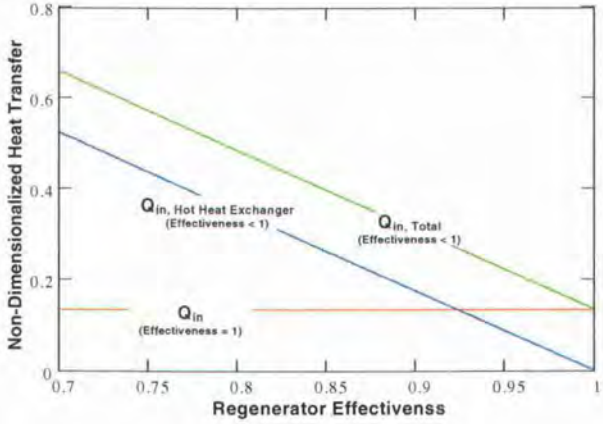

Figure 15 - Non-Dimensionalized Heat Transfer vs. Regenerator Effectiveness

4.8 REGENERATOR OPTIMIZATION

Because the thermal efficiency of the thermocompressor has a high sensitivity to the regenerator effectiveness, it is necessary to investigate the regenerator design parameters to see if there is an optimum configuration. As the regenerator surface area increases, its effectiveness increases, which improves thermal efficiency. However, the increased surface area also corresponds to an increase in regenerator volume, which has an adverse affect on thermal efficiency. It is the purpose of this section to explore those variables to find an optimum balance between regenerator effectiveness and regenerator volume.

First, the design parameters of the regenerator must be defined. For the purpose of this study, the regenerator design will be as shown in Fig. 16. A series of holes running through the length of the regenerator/displacer will serve as the surface area of the regenerator.

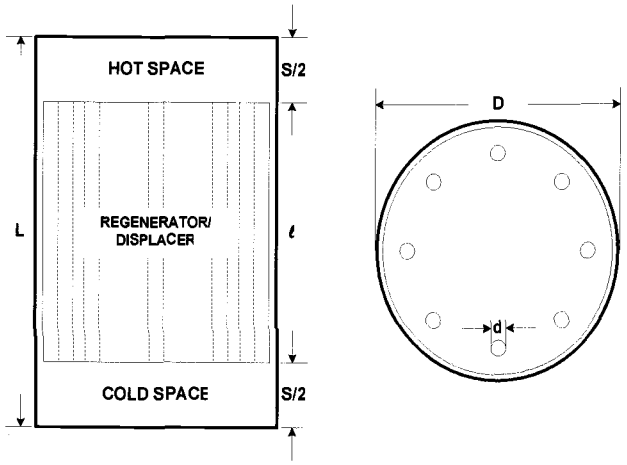

Figure 16 - Regenerator Design

The system parameters include: the length of the cylinder L, the diameter of the cylinder, D, the number of holes, n, the diameter of the holes, d, and the length of the regenerator, ℓ. Two parameters will be defined as follows: the aspect ratio of the cylinder, AR = L/D, and the aspect ratio of the regenerator, $\lambda = \ell/L$. These system parameters will serve as the independent variables in this study, and the dependent

variables will include: pressure drop across the regenerator, regenerator effectiveness, regenerator volume, and the thermal efficiency of the device.

It is preferable to maximize surface area and minimize volume in the regenerator. Therefore, a large number of small diameter holes are preferable. However, as the hole diameter gets smaller the pressure drop across the regenerator/displacer increases, which negatively affects the performance of the device. The pressure drop, therefore, will limit the diameter of the holes. As a baseline, it will be assumed that an acceptable pressure drop is 1% of the low pressure of the device, which will be assumed to be atmospheric pressure.

The cross-sectional area, the perimeter, and the length of all the individual holes are given as

$$a = n\frac{\pi}{4}d^2, \quad p = n \cdot \pi \cdot d, \quad \ell = \lambda \cdot L \tag{134}$$

The mass flow rate through the regenerator is a function of the pressure ratio, however, if the low pressure and temperature are assumed to both be at atmospheric conditions, the maximum flow rate through the regenerator would be given as

$$\dot{m} = \frac{1}{2f} \cdot \frac{P_{atm} V_T}{R T_{atm}} \tag{135}$$

where f is the frequency of oscillation of the regenerator/displacer. This mass flow rate will be used for simplicity as it represents a theoretical characteristic flow rate. The fluid velocity through the regenerator is given by

$$v = \frac{\dot{m}}{\rho \cdot a} \tag{136}$$

The Reynolds number characterizing the flow through the regenerator is given by

$$\mathrm{Re} = \frac{\rho \cdot v \cdot d}{\mu} \tag{137}$$

where μ is the viscosity of the working fluid. The pressure drop across the regenerator/displacer can now be written as

$$\Delta P = F \cdot \frac{\rho \cdot v^2}{2} \cdot \frac{(\lambda \cdot L)}{d} \tag{138}$$

where F is the friction factor assumed to be 64/Re, which is valid for laminar, fully-developed pipe flow.

Figure 17 shows a plot of the pressure drop across the regenerator/displacer for a series of regenerator hole diameters. The case presented in Fig. 17 is considered to be an extreme case for a small-scale device.

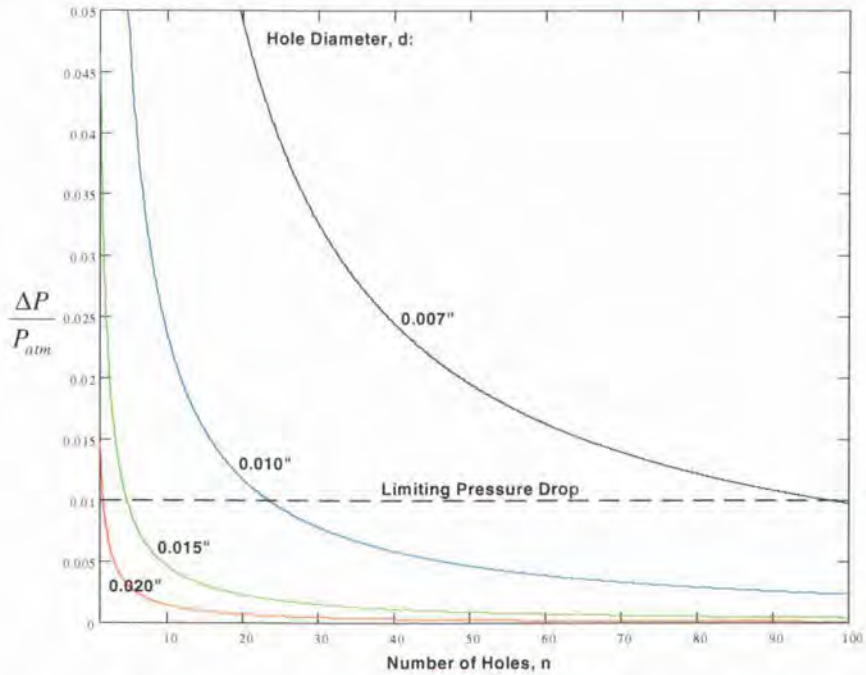

Figure 17 – Pressure Drop vs. Number of Holes, n; Working Fluid = N_2, $\rho = 0.75$ [kg/m^3], $\mu = 2.4e\text{-}5$ [N-s/m^2], f = 10 [Hz], $\lambda = 0.9$, Cylinder Length = 2 in, $P_{atm} = 101.325$ [kPa], $T_{atm} = 300$ [K]

The plot indicates that hole diameters ranging from 0.010-0.020 inches would have acceptable pressure drops. However, it can be argued that machining holes smaller than 0.020 inches in diameter through material two inches thick is not practical without considerable expense. Therefore, for the purpose of this study, the hole diameter will be set at 0.020 inches, which is practical and will not incur a large pressure drop.

Next, an expression must be developed for the regenerator effectiveness in terms of the number of the regenerator holes and the regenerator hole diameter.

Incropera and DeWitt [17] give the Nusselt number of internal, fully developed, laminar flow as

$$Nu = 3.66 \tag{139}$$

The film coefficient can be written as

$$h = \frac{Nu \cdot k}{d} \tag{140}$$

The number of transfer units for the regenerator is given by

$$NTU = \frac{h \cdot p \cdot (\lambda \cdot L)}{c_p \cdot \dot{m}} \tag{141}$$

Finally, the regenerator effectiveness can be approximated by

$$\varepsilon = \frac{NTU}{1 - NTU} \tag{142}$$

In addition, the regenerator volume can be written as

$$V_{REG} = \frac{a \cdot (\lambda \cdot L)}{V_T} \tag{143}$$

Therefore, substituting Eq. (142) and (143) into (130) gives the thermal efficiency of the device in terms of n and λ. The next step is to plot a contour of Eq. (130) for a range of n and λ, which is shown in Fig. 18.

In Fig. 18, as λ and n increase, the length of the regenerator and the number of holes in the regenerator increase. Consequently, the regenerator surface area increases with lambda and n along with the regenerator effectiveness and regenerator dead volume. Therefore, as you move up the graph, the increasing regenerator effectiveness drives up the thermal efficiency, but at the same time the regenerator dead volume is also increasing. At some point, the increase of regenerator effectiveness at the cost of increased regenerator dead volume is no longer advantageous. At that point as you continue to move up the graph, the thermal efficiency starts to decrease. Therefore, there is a maximum thermal efficiency which corresponds to optimal values of n and λ. The maximum thermal efficiency for the given temperature ratio of two is indicated as 0.28 in Fig. 18.

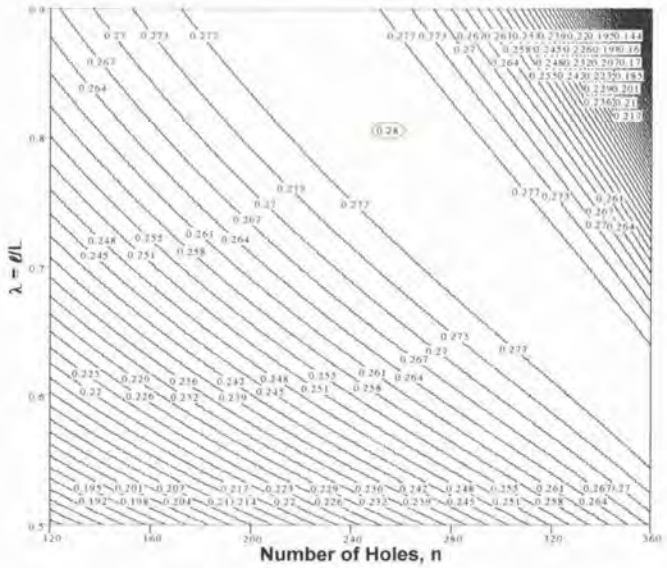

Figure 18 - Thermal Efficiency vs. n and λ, T_{RATIO} = 2, P_{RATIO} = 1.5, V_{DSL} = 0, V_{DSH} = 0, γ = 1.4, V_T = 0.175 [in^3], AR = 1, d = 0.020 [in]

Next a contour of regenerator effectiveness is plotted for the same ranges of n and λ, as shown in Fig. 19.

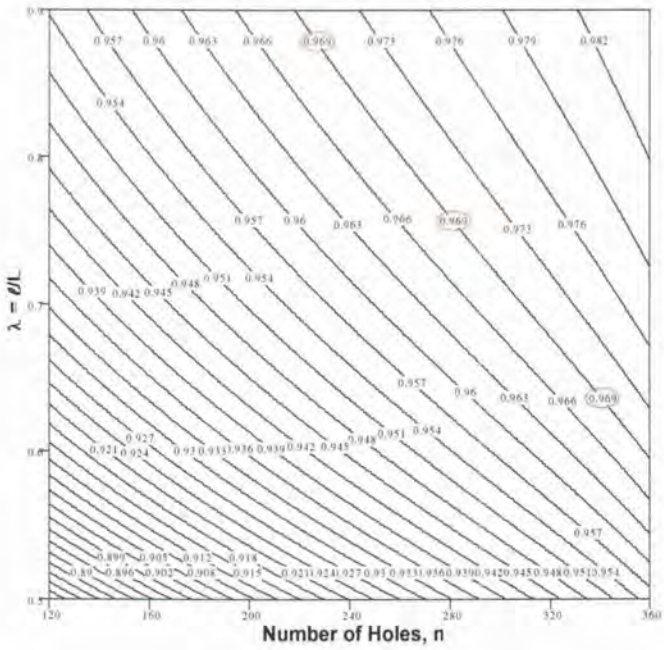

Figure 19 – Regenerator Effectiveness vs. n and λ, T_{RATIO} = 2, P_{RATIO} = 1.5, V_{DSL} = 0, V_{DSH} = 0, γ = 1.4, V_T = 0.175 [in^3], AR = 1, d = 0.020 [in]

Figure 20 shows a contour of regenerator volume for the same ranges of n and λ.

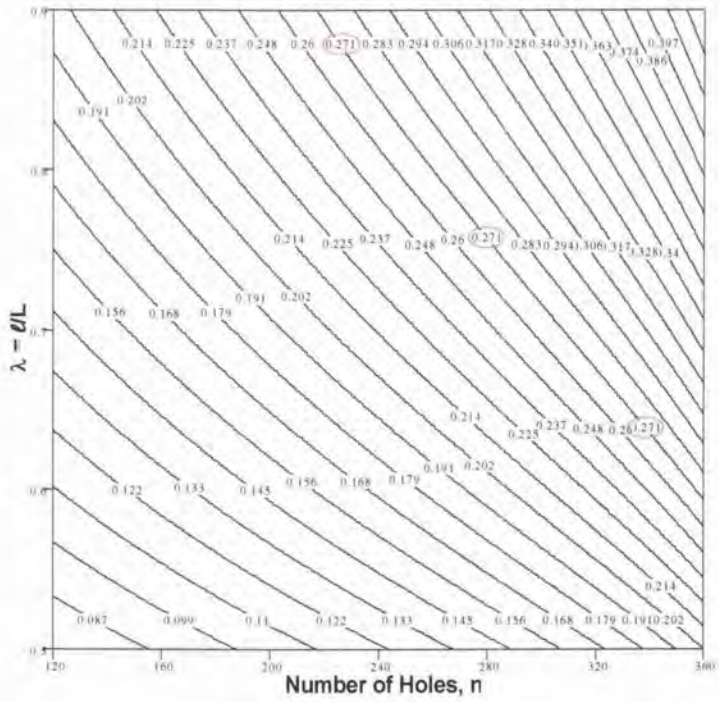

Figure 20 - Regenerator Effectiveness vs. n and λ, T_{RATIO} = 2, P_{RATIO} = 1.5, V_{DSL} = 0, V_{DSH} = 0, γ = 1.4, V_T = 0.175 [in^3], AR = 1, d = 0.020 [in]

As indicated in Figs. 19 and 20, there are contours of regenerator effectiveness and regenerator volume which correspond to the same contour in Fig. 18 which gives the maximum thermal efficiency. Therefore, these are the optimal values of regenerator effectiveness and regenerator volume, which give the maximum thermal efficiency for the device. A program was written in MathCAD, which produces these plots for any given configuration of inputs. That program is given in Appendix B. These optimization plots were produced for a range of temperature ratios. However, for the sake of brevity, a summary of those results is given in Figs. 21 and 22. Figure 21 compares the predicted maximum thermal efficiency of the device to the ideal maximum efficiency, namely Carnot efficiency. Figure 22 gives the ideal regenerator effectiveness and regenerator volume which correspond to the predicted maximum thermal efficiency.

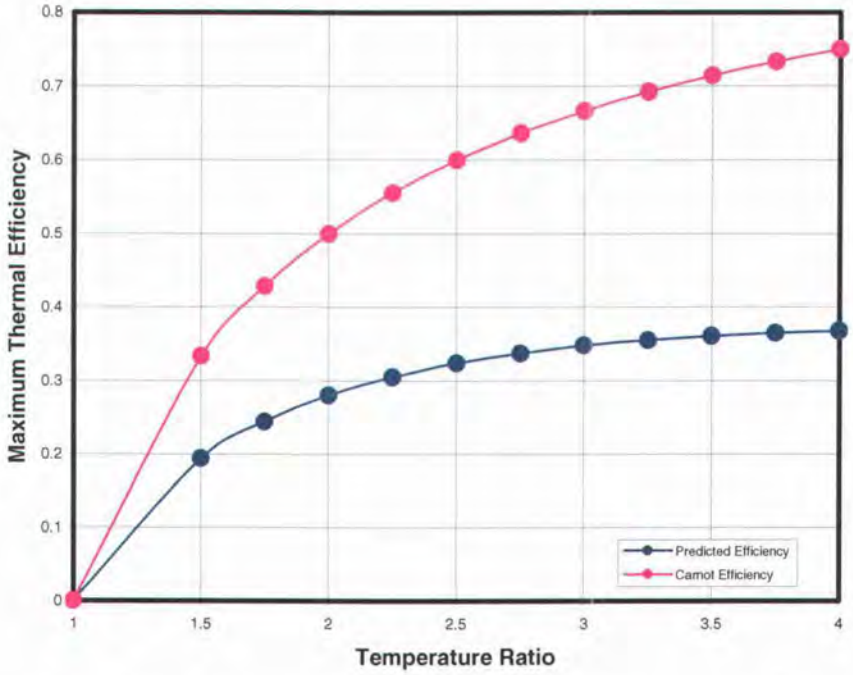

Figure 21 - Maximum Predicted Thermal Efficiency vs. T_{RATIO},

$P_{RATIO} = 1+0.5(T_{RATIO}-1)$, $V_{DSL} = 0$, $V_{DSH} = 0$, $\gamma = 1.4$, d = 0.020 [in]

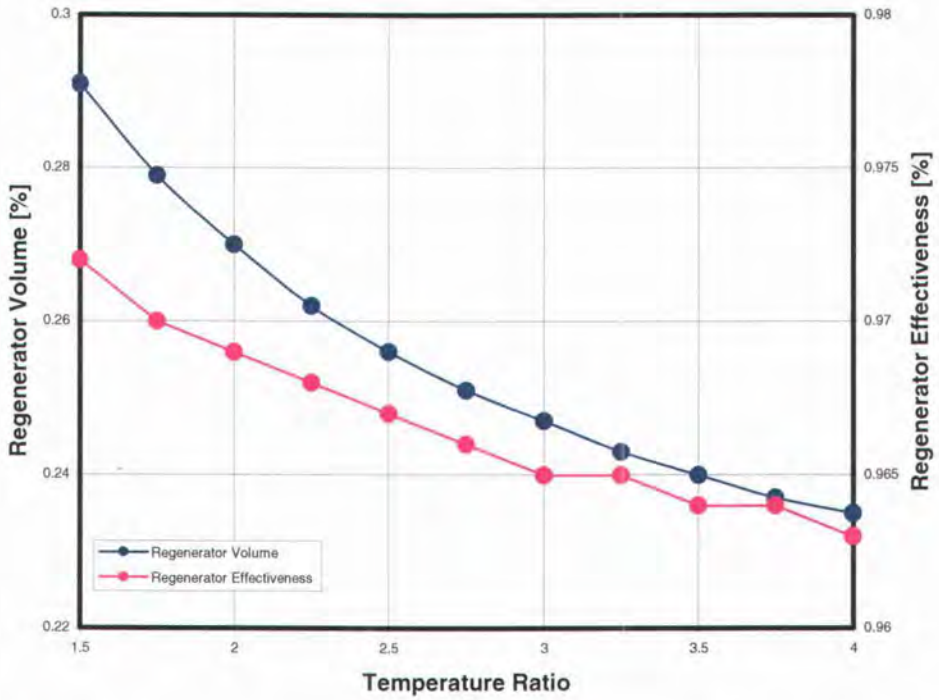

Figure 22 - Optimum Regenerator Effectiveness and Regenerator Volume vs. T_{RATIO},

$P_{RATIO} = 1+0.5(T_{RATIO}-1)$, $V_{DSL} = 0$, $V_{DSH} = 0$, $\gamma = 1.4$, d = 0.020 [in]

5 EXPERIMENTAL METHODS

5.1 THERMOCOMPRESSOR DESIGN

A first order experimental device was developed which was intended to serve as a platform to explore some of the key design considerations of a thermocompressor. The design can be broken into three sub-systems. First, the cylinder, which includes a heater on the hot side and a cooling loop on the cold side, second the regenerator/displacer, and finally the regenerator/displacer drive system. The thermocompressor is shown in Fig. 23 and 24.

Because this was a first-order device, it was not intended to necessarily represent all of the complexities of the system. Therefore, for the sake of simplicity, no valves were included in the design. Consequently, the mass inside the device was fixed, and no mass crossed the system boundary. With no mass flowing through the thermocompressor there was no meaningful way to define its thermal efficiency. However, dynamic pressure and temperature measurements were made inside the cylinder to characterize the performance of the device.

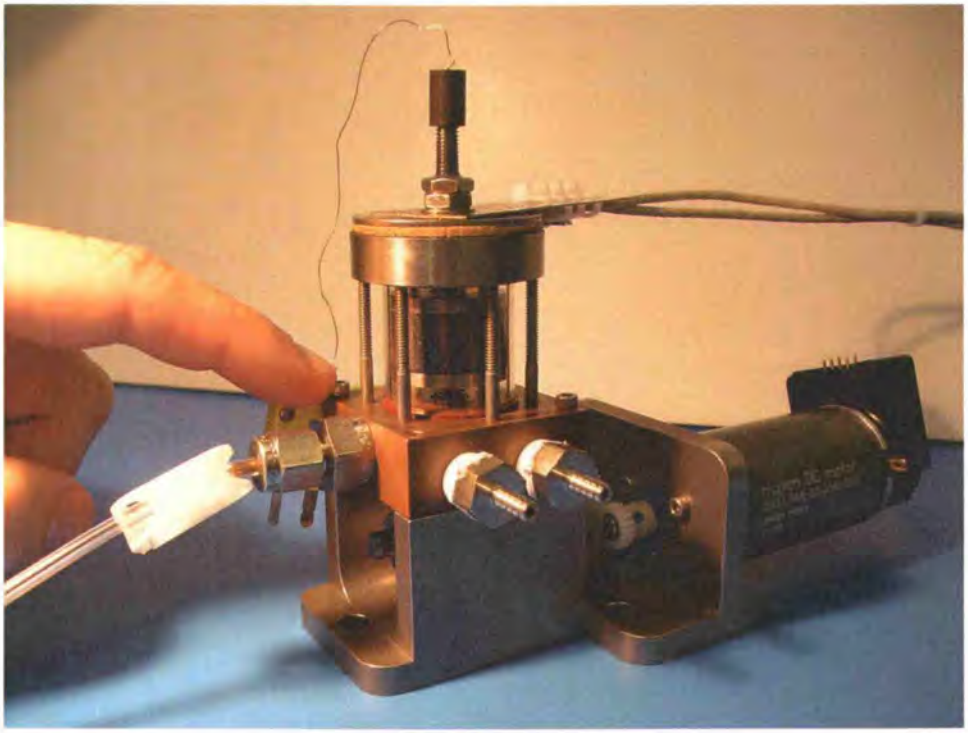

Figure 23 - Thermocompressor - Front/Side

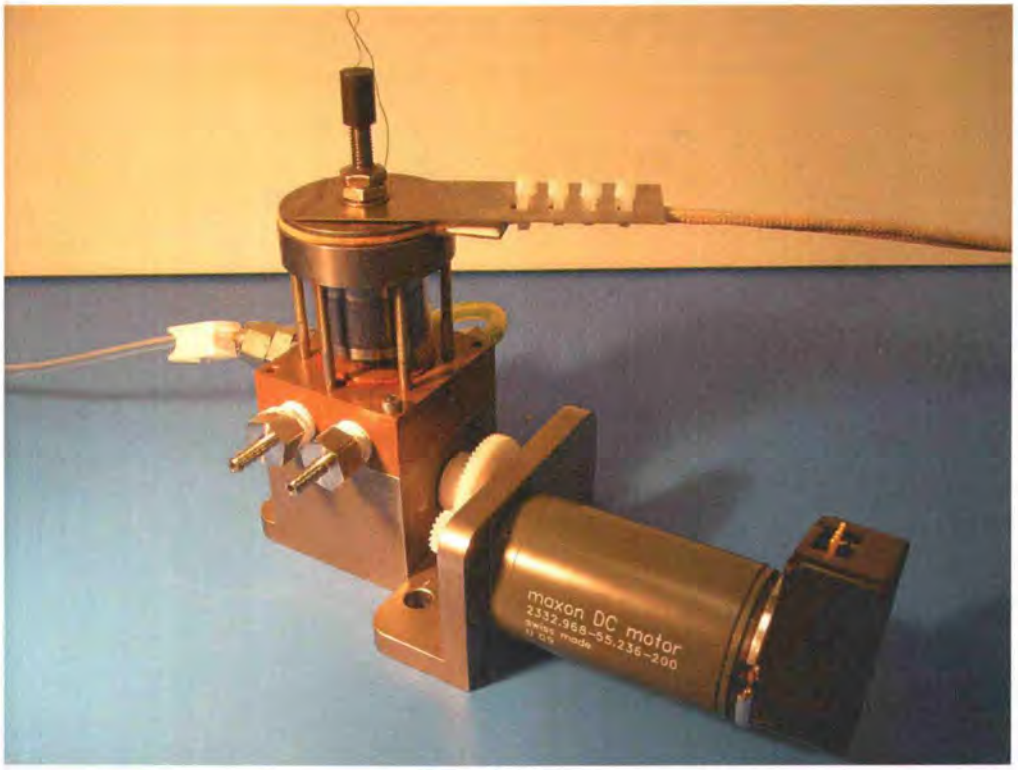

Figure 24 - Thermocompressor - Back/Side

5.1.1 CYLINDER DESIGN

There are a number of concerns associated with the cylinder design. Two primary concerns are axial conduction along the cylinder, and friction on the regenerator/displacer. Either of these two factors have the potential to severely impair the performance of the device.

Axial conduction is detrimental to the device in that it represents potentially useful energy that is lost from the system. Therefore, it is imperative that the hot side be isolated from the cold side. Axial conduction is directly proportional to the thermal conductivity of the cylinder material, the cross-sectional area of the cylinder, and the temperature gradient along the cylinder. With any thermomechanical device, in general, the larger the temperature difference across the device, the higher its thermal efficiency. Therefore, small-scale devices in particular tend to have large temperature gradients. Consequently, it is critical to choose cylinder materials with low thermal conductivity and design the cylinder with minimal cross-sectional area.

Friction also represents energy that is lost from the system. Friction is influenced by several factors: the orientation of the device, side loads on the regenerator/displacer due to its drive system, and the coefficient of friction between the regenerator/displacer and the cylinder. It is, therefore, imperative to design a cylinder, which minimizes each of these factors.

The Thermocompressor presented in this thesis addresses these issues by incorporating a modified dashpot (Airpot 2K240) to serve as the cylinder. This approach was chosen for its low coefficient of friction, tight tolerance between the piston and cylinder, and low thermal conductivity. The coefficient of friction between the piston and cylinder was 0.2, and the piston was fit to the cylinder within a few microns. The piston material was graphite and the cylinder material was Pyrex with respective thermal conductivities of approximately 5.7 and 1.4 W/m-K at 300 K. The cylinder top was made of 303 stainless steel, and the base was made of copper. The Pyrex cylinder was sealed to both the top and base with high-temperature silicone gaskets. An electric mica-insulated heater (Minco HM6807R3.9L12T1) was mounted to the top of the cylinder. Water was pumped through a cooling loop in the base of the cylinder. The base also included a single port with a shut-off clamp used to evacuate and fill the cylinder. All ports in the base were designed to minimize dead space in the system. The cylinder assembly was held together by a bolt pattern of six screws around the cylinder. Because the screws also provided a path for axial conduction, stainless steel screws with a thermal conductivity of approximately 12-14 W/m-K were used. Figure 25 illustrates the cylinder design and gives its dimensions.

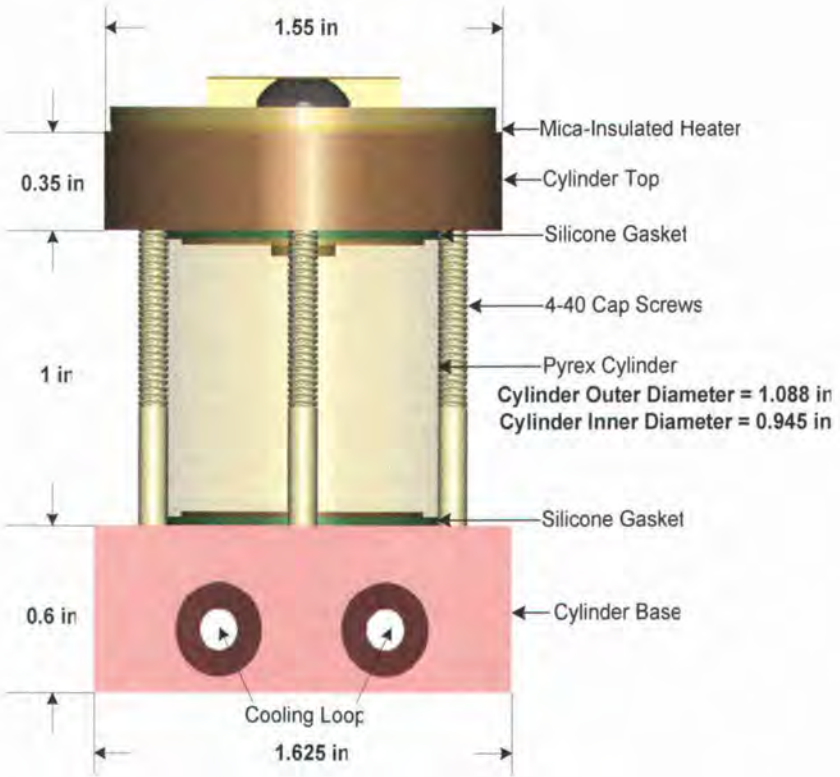

Figure 25 - Cylinder Design and Dimensions

5.1.2 REGENERATOR/DISPLACER DESIGN

There are several important issues associated with the regenerator/displacer design. Three of which are axial conduction along the regenerator/displacer, regenerator dead volume, and regenerator effectiveness. All concerns connected with axial conduction in the cylinder are present with the regenerator/displacer; therefore, the same design considerations apply. The regenerator dead volume and regenerator effectiveness also significantly influence the thermal efficiency of the device as has been shown in Section 4.8.

The regenerator/displacer presented in this thesis incorporates several design features which address the key considerations listed above. The regenerator/displacer is made of a hollow stainless steel core with a graphite sleeve acting as the sliding surface. The graphite sleeve was a modified dashpot piston. Thirty six holes around the perimeter of the core serve as the flow path for the working fluid. The hole diameter was 0.022 ±0.002 inches. This diameter was chosen to minimize

regenerator dead space without creating a large pressure drop across the regenerator/displacer. The regenerator dead space of this design was estimated to be 5.5% of the total volume of the thermocompressor, and the regenerator effectiveness was estimated to be 79%. The calculations to estimate regenerator effectiveness are shown in Appendix C. The regenerator/displacer design is shown in Fig. 26 with its respective dimensions.

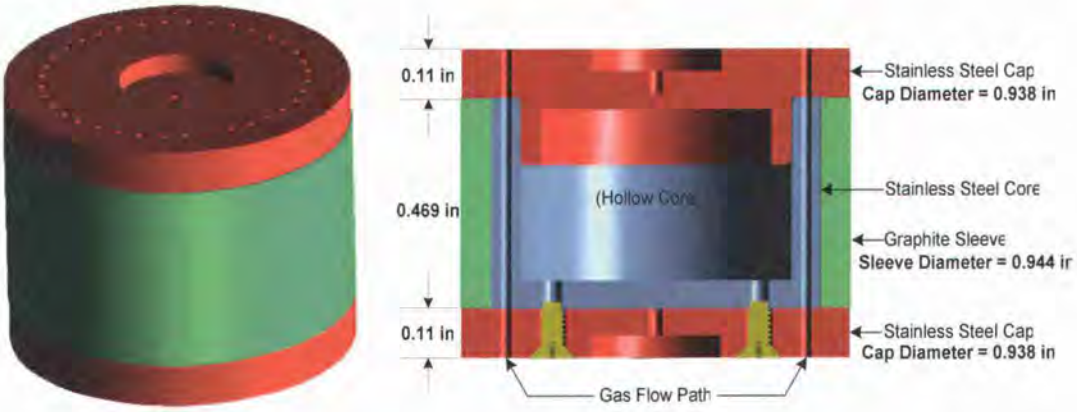

Figure 26 - Regenerator/Displacer Design and Dimensions

5.1.3 REGENERATOR/DISPLACER DRIVE SYSTEM DESIGN

The regenerator/displacer drive system is an equally challenging design problem to the previous two sub-systems discussed. The system must incorporate some type of sliding seal without incurring significant frictional losses. Also, the system must minimize the side loads applied to the regenerator/displacer as they are directly proportional to its friction. Finally, the drive system can be a significant source of dead space in the cylinder, which adversely affects the performance of the device.

The thermocompressor presented here utilizes a magnetic rotor to drive the reciprocating motion of the regenerator/displacer. This system is illustrated in Fig. 27 and Fig. 28 with its respective dimensions. As the rotor spins it alternately attracts or repels an auxiliary magnet, which is coupled to the regenerator displacer. In this way, it completely bypasses the problem of a sliding seal. The regenerator/displacer was seated between two coil springs above and below, which facilitate its oscillation. The

bottom spring (Century Spring, NN-62) has a constant of 0.46 lb/in, while the top spring (Century Spring, II-84) has a lower constant of 0.13 lb/in. This system applies a minimal side load on the regenerator/displacer, which occurs when the polarity of the magnets changes as the rotor spins. The magnet rotor was driven by a DC motor (Maxon, S2332), which was controlled by a motor controller (Maxon, 4-Q-DC LSC 30/2). Because the motor was difficult to control at low speeds a 3:1 gear reduction between the motor and the magnet rotor accommodated the speed range of the drive system. The regenerator/displacer was driven at 10-13 Hz. The biggest disadvantage of this design in its current form is its dead space. The dead space of this design was estimated to be 12% of the total volume of the thermocompressor.

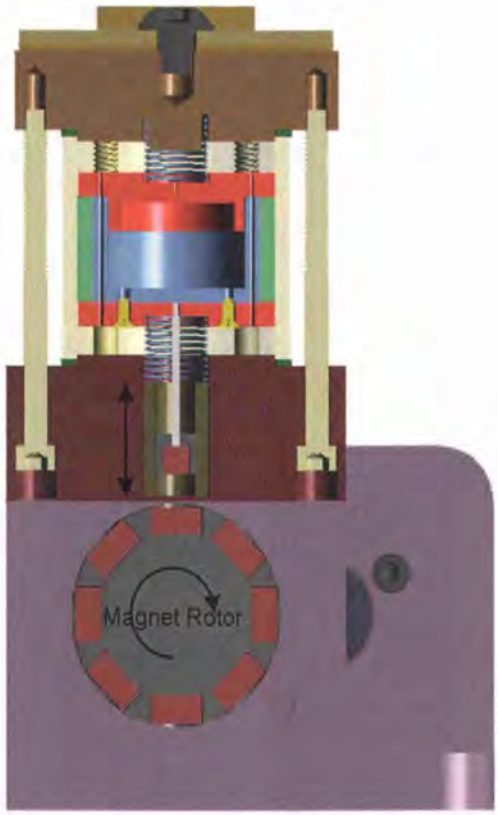

Figure 27 - Regenerator/Displacer Drive System

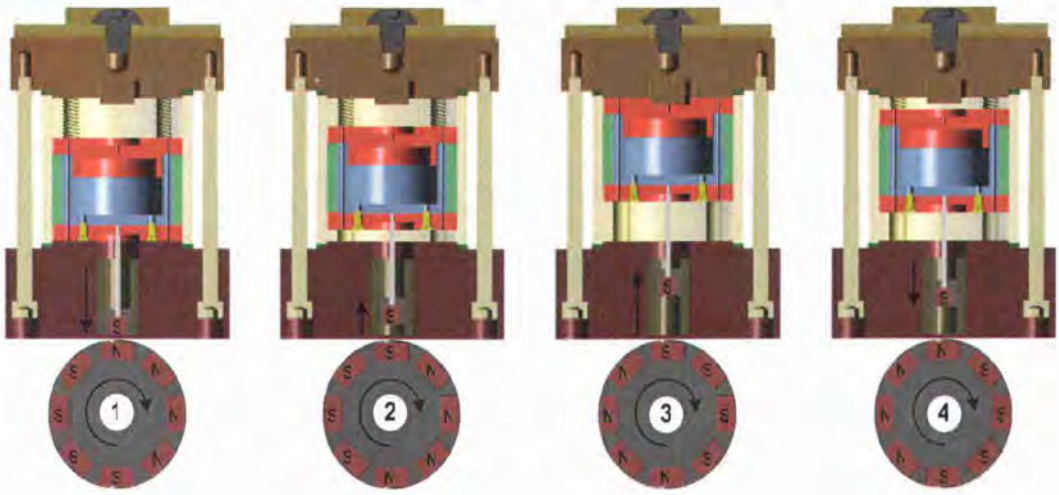

Figure 28 - Regenerator/Displacer Drive System Motion

5.2 EXPERIMENTAL SETUPS AND PROCEDURES

Several tests were performed with the experimental apparatus. The primary interest of which was to measure pressure verses time during its operation at various speeds and temperature ratios with different working fluids. In addition, the regenerator/displacer position verses time was also measured and plotted against the pressure measurements. Also of interest was some dynamic measurement of temperature inside the cylinder during operation to indicate how much temperature variation exists in the hot and cold spaces.

5.2.1 POSITION MEASUREMENT SETUP

Accurately measuring the position of the regenerator/displacer requires a means of instrumentation which does not itself interfere with the motion of the regenerator/displacer. Therefore, a system was developed which incorporates the use of a strobe light (Omega, HHT41), which is triggered by the digital signal from an encoder mounted on the drive motor (Maxon, S2332). The encoder signal is sent to a signal conditioner and next to a digital delay generator (California Avionics Laboratories, Model 101BR). The digital delay generator can be manually set to

delay the digital pulse from 0.1 μs to 9.9999999 seconds in 0.1 μs increments. Finally, the digital pulse signal is sent to the strobe light, which fires once per pulse. This setup allowed the position of the regenerator/displacer to be observed at various time intervals relative to the encoder pulse. A ruler with 1/64 inch increments was mounted next to the cylinder from which the position of the regenerator/displacer was measured. Two additional components of the setup include a feedback motor controller (Maxon, 4-Q-DC LSC 30/2), which receives a signal from the encoder, and a digital oscilloscope (Tektronix, TDS 220), which receives a signal from the signal conditioner. The motor controller was used to set the speed of the motor, and the oscilloscope was used to display the frequency of the regenerator/displacer's oscillation. This setup is shown in Fig. 29.

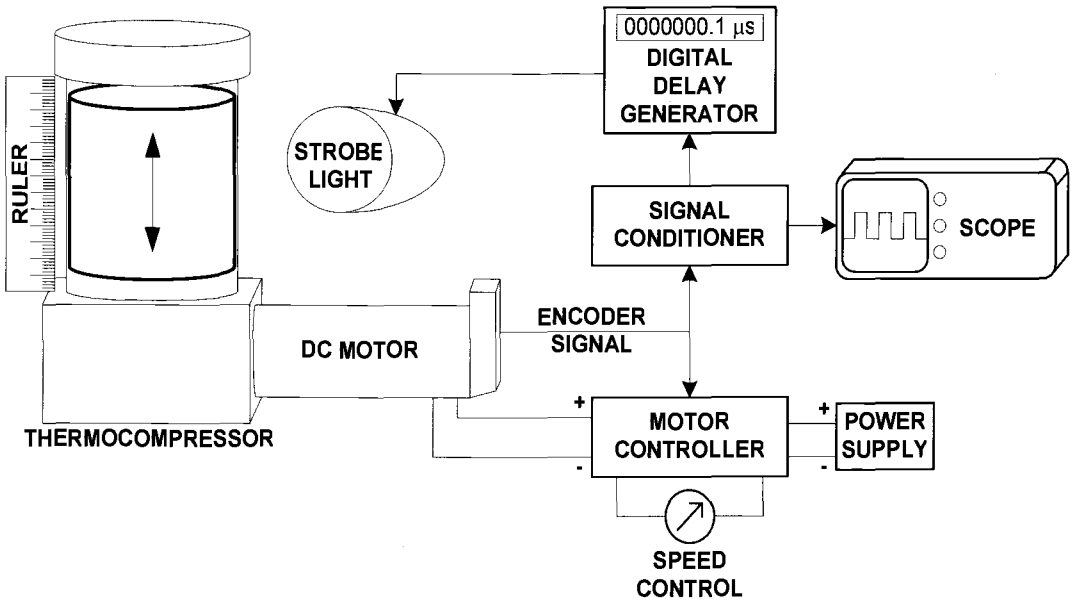

Figure 29 - Regenerator/Displacer Position Measurement Setup

5.2.2 POSITION MEASUREMENT PROCEDURE

The position of the regenerator/displacer during operation was measured and plotted verses time at two speeds, 10 Hz and 13 Hz. First, the motor speed was adjusted manually on the motor controller until the oscilloscope indicated the targeted frequency. The encoder pulse was displayed on the oscilloscope for reference. The frequency of the regenerator/displacer could be consistently controlled within ±0.1

Hz. The digital delay generator would first be set to 0.1 μs, which corresponds to a strobe flash firing 0.1 μs after the encoder pulse. The position of the regenerator displacer was then measured visually on the ruler and recorded. The regenerator/displacer position was recorded as the distance between the base of the cylinder and the bottom edge of the regenerator/displacer. Next, the digital delay was set to 0.0025 seconds, and the regenerator/displacer position was then measured and recorded. Subsequent to this, the digital delay was sequentially incremented by 0.0025 seconds until an entire period of oscillation was reached. At each increment the regenerator/displacer position was measured and recorded.

5.2.3 PRESSURE MEASUREMENT SETUP

The pressure measurements were made with a 50-psia piezoresistive pressure transducer (Endevco, 8530C-50) through a pressure tap in the cold side of the cylinder. The signal from the pressure transducer was read by a digital oscilloscope, which transferred the data to a PC. In addition, the oscilloscope received a signal from the encoder mounted to the drive motor, which was also transferred to the PC. A Labview program facilitated the interface between the PC and the oscilloscope. Just as in the position measurement setup, the drive motor speed was controlled by the motor controller. The cold side temperature of the cylinder was maintained by water flowing through a cooling loop, and the hot side temperature was maintained by a mica insulated electric heater (Minco, HM6807R3.9L12T1), which was controlled manually with a variable transducer (Variac, TDGC-0.5KM). The hot and cold side temperatures were measured with thermocouples (Omega, KMQSS-062U-6) mounted in the cylinder top block and base respectively. Those thermocouples were read manually with handheld readouts. The pressure measurement setup is illustrated in Fig. 30.

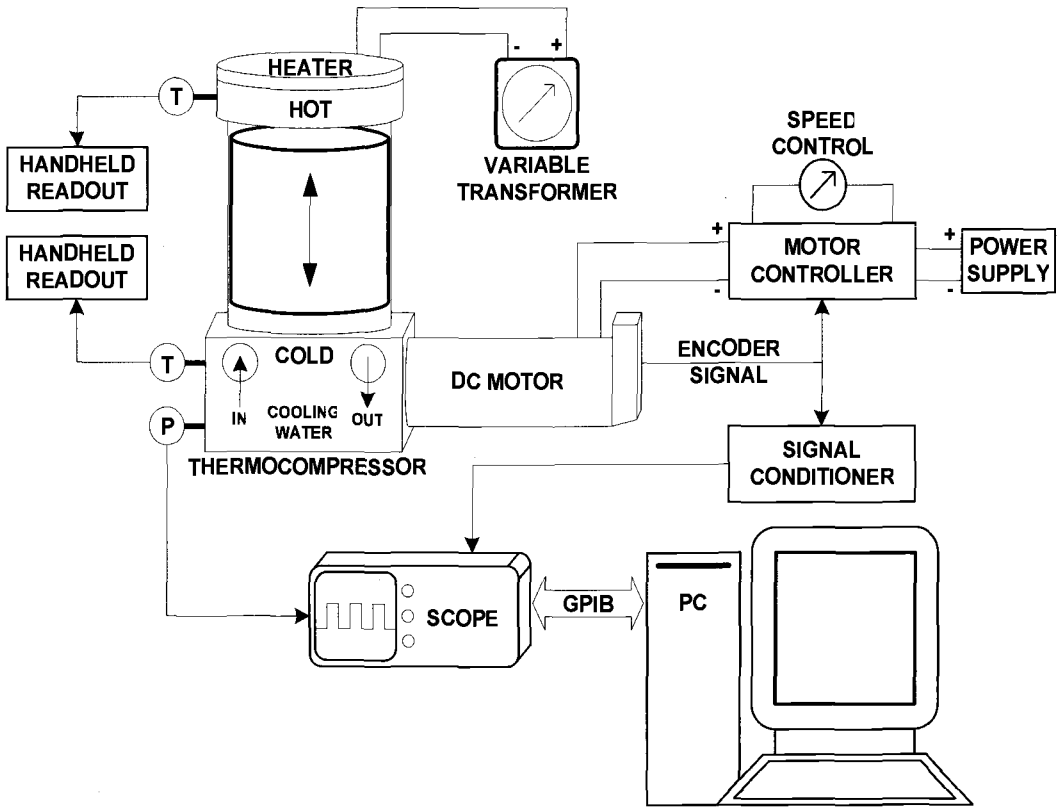

Figure 30 - Pressure Measurement Setup

5.2.4 PRESSURE MEASUREMENT PROCEDURE

The pressure in the cylinder was measured verses time through a range of temperature ratios from 1.2 to 2. Tests were done on two different working fluids, nitrogen and helium. Both working fluids were tested at two operating speeds, 10 Hz and 13 Hz. This test produced four data sets corresponding to two working fluids at two operating speeds.

Before running any tests, the pressure transducer was calibrated. The pressure transducer was installed in a calibration station where it measured pressure concurrently with a high accuracy test gauge (Dwyer, 7314D). The mV output of the pressure transducer was displayed on the oscilloscope while the test gauge was read manually. Atmospheric pressure was read on a barometer (Oakton, WD-03316-80). The pressure applied to the calibration station was controlled either by a vacuum pump or a high pressure nitrogen tank. The mV output of the pressure transducer was

recorded at five pressure points including a vacuum, atmospheric pressure, and three points up to approximately 30 psia. The transducer readings were calibrated to the test gauge readings, and a linear calibration curve was established for the pressure measurements.

Next, the thermocompressor was assembled with the pressure transducer installed and checked for leaks. The cylinder was pressurized with Nitrogen to approximately 22.8 psia and left static for ten minutes. After ten minutes the pressure reading dropped approximately 0.02 psia. With the cylinder still pressurized, the regenerator/displacer was then run at 10 Hz for ten minutes. After driving the regenerator/displacer for ten minutes, the pressure reading dropped approximately 0.01 psia. This test confirmed that the cylinder leak rate was minimal.

The same procedure was followed for all the pressure measurement tests. First, the cooling water was supplied to the looping loop from a laboratory sink faucet. After exiting the base, the water was discharged to the drain. The cooling water ran continuously during all tests. Next, a vacuum was pulled on the cylinder. Then, the heater was powered by the variable transducer, and the hot and cold temperatures were monitored. Insulation was placed over the hot side of the cylinder to reduce heat loss into the room. Once the temperature ratio between the hot and cold sides had nearly approached 1.2, the cylinder was filled with the working fluid.

The fill process included clamping off the cylinder inlet, disconnecting the vacuum pump, connecting a gas tank to the cylinder inlet, unclamping the cylinder inlet, and slowly allowing the working fluid to enter the cylinder. The pressure increase in the cylinder was closely monitored as the working fluid was let into the cylinder. Once the cylinder pressure reached approximately atmospheric pressure, the cylinder inlet was clamped off.

Once the fill process was complete, the motor was turned on, and its speed was adjusted until the appropriate operating speed was reached. As in the position measurement test, the frequency of the regenerator/displacer could be consistently controlled to within ±0.1 Hz. At this point, the pressure oscillation inside the cylinder was displayed on the oscilloscope along with the drive motor encoder signal. Once

the temperature ratio across the thermocompressor reached 1.2, the oscilloscope data would be downloaded and stored in the PC. All of the other necessary information, such as the heater voltage and the high and low temperatures, was recorded manually.

Once the pressure curve was downloaded at a specific temperature ratio the heater voltage was increased, and the temperatures were monitored until the temperature ratio reached the next point at which the pressure curve was recorded again. The temperature ratio was incrementally increased from 1.2 to 2.0 in increments of 0.1. During any given test run, the speed of the thermocompressor was maintained constant at either 10 or 13 Hz.

5.2.5 TEMPERATURE MEASUREMENT SETUP

Dynamic temperature measurements were made inside the cylinder by feeding a thermocouple (Omega, SCASS-010E-6) through a small hole in the top of the cylinder and sealing it with high temperature epoxy (Duralco, 4525). The thermocouple had a 0.010 inch diameter stainless steel sheath with a 0.0015 inch diameter exposed tip. This thermocouple was chosen for its low time constant. According to the manufacturer's specification, this thermocouple has a time constant of approximately 0.005 seconds. The temperature variation in the hot side of the cylinder occurs in half of one period of oscillation, which when operating at 10 Hz is 0.05 seconds. Therefore, the temperature variation occurs in 10 thermocouple time constants, which indicates that the thermocouple should be able to accurately measure the temperature variation.

It should be noted that dynamic temperature measurements were not practical on the cold side of the cylinder due to the fact that the regenerator/displacer drive system included a magnet rotor, which was spinning immediately below the base of the cylinder. The motion of the magnets moving close to the thermocouple on the cold side caused erroneous measurements.

The signal from the thermocouple was sent to a signal conditioner and subsequently to the oscilloscope. Just as in the pressure measurement test, the drive

motor encoder signal was also sent to the oscilloscope, and both signals were downloaded to the PC. The rest of this experimental setup was, in fact, identical to that described in the previous test with the exception of the pressure transducer, which was not used for the majority of this test. The pressure transducer was only used during the thermocompressor fill procedure. The temperature measurement setup is shown in Fig. 31.

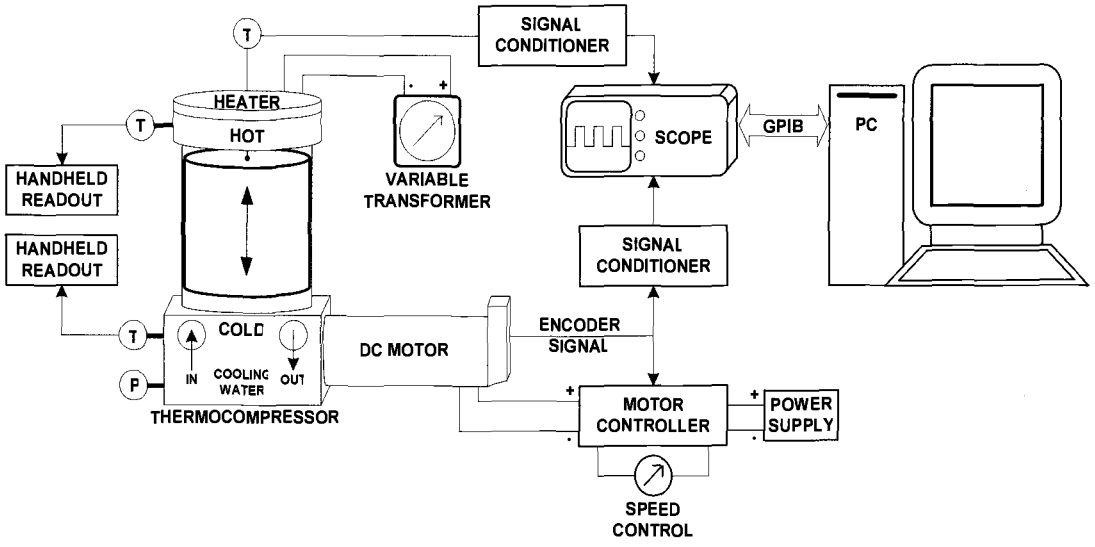

Figure 31 - Dynamic Hot Side Temperature Measurement Setup

5.2.6 TEMPERATURE MEASUREMENT PROCEDURE

The temperature in the hot side of the cylinder was measured verses time through a range of temperature ratios from 1.2 to 2. Tests were done on two different working fluids, nitrogen and helium. This test was only done at a single operating speed of 10 Hz because the thermocouple's time response was not fast enough to accurately measure the temperature variation at 13 Hz. This test produced two sets of data corresponding to the two working fluids.

The procedure for the temperature measurements is nearly identical to that for the pressure measurements. Once the thermocompressor was brought up to temperature, and the cylinder was filled with the working fluid, the pressure transducer was disconnected from the oscilloscope, and the thermocouple was connected. The reason why both instruments were not measured simultaneously is

that the oscilloscope was limited to two channels, and the second channel was occupied by the drive motor encoder signal.

Once the thermocouple was connected to the oscilloscope and the temperature ratio across the thermocompressor reached 1.2, the oscilloscope data would be downloaded and stored in the PC. All of the other necessary information, such as the heater voltage and the high and low temperatures, was recorded manually.

Once the temperature curve was downloaded at a specific temperature ratio the heater voltage was increased, and the temperatures were monitored until the temperature ratio reached the next point at which the temperature curve was recorded again. The temperature ratio was incrementally increased from 1.2 to 2.0 in increments of 0.1. During both test runs, the speed of the thermocompressor was maintained constant at 10 Hz.

6 RESULTS AND DISCUSSION

The results of the experimental work will provide insight into the performance of the themocompressor. First, the position measurements of the regenerator/displacer are given. Next, the cylinder pressure measurements are presented and compared to the regenerator/displacer position. Finally, the hot side temperature measurements are plotted. In is the intention of this work to evaluate some of the design features of the device.

6.1 REGENERATOR/DISPLACER POSITION VS. TIME

Ideally, the regenerator/displacer would exhibit perfect sinusoidal motion. However, this is very difficult to achieve given a drive system, which incorporates a magnetic coupler and uses permanent magnets. The motion of the system is determined by many variables including the choice of magnets, the configuration of the magnets, the springs, and the mass of the regenerator/displacer; just to name a few. When all of these variables are fixed in the design, there is a range of speeds at which the device will operate and, even then, its motion will vary depending upon its speed. For the system presented here, the motion is plotted at two different speeds.

The position of the regenerator/displacer was measured from its bottom edge to the bottom of the cylinder as shown in Fig. 32. Accordingly, a position of zero inches corresponds to bottom dead center, and a position of 0.250 inches corresponds to top dead center.

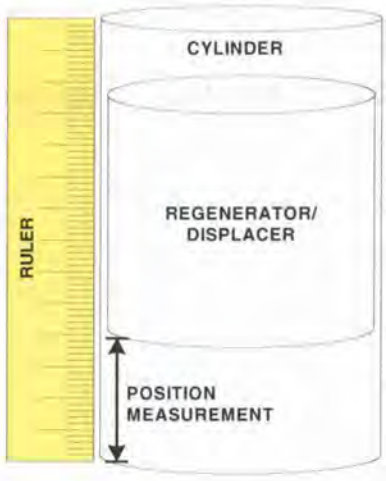

Figure 32 - Regenerator/Displacer Position Measurement

Figure 33 shows the position of the regenerator/displacer verses time when it is oscillating at 10 Hz. In some ways, the curve resembles a triangle wave, however, it has some distinct features, which are very different from a triangle wave. When the regenerator/displacer reaches bottom dead center, it stays there for approximately 0.02 seconds before moving back up. This flat section is a result of the magnetic coupling in the drive system. The magnet rotor spins one revolution per oscillation of the regenerator/displacer. For half of a rotation the magnetic coupler pulls the regenerator/displacer down and for the other half, it pushes the regenerator/displacer up. At this speed the regenerator/displacer moves down the cylinder to bottom dead center faster than the magnet rotor rotates to the opposite poles, which push the regenerator/displacer back up the cylinder. There is a period of time during which the magnet rotor simply holds the regenerator/displacer at bottom dead center. Also, the curve indicates that as the regenerator/displacer moves down the cylinder its linear speed is increasing. This is evidenced by the fact that the slope of its position verses time curve appears to get steeper as it gets closer to bottom dead center. This is also a result of the magnetic coupler. As the coupling magnets get closer together the attractive force between them increases, which increases the speed of the regenerator/displacer.

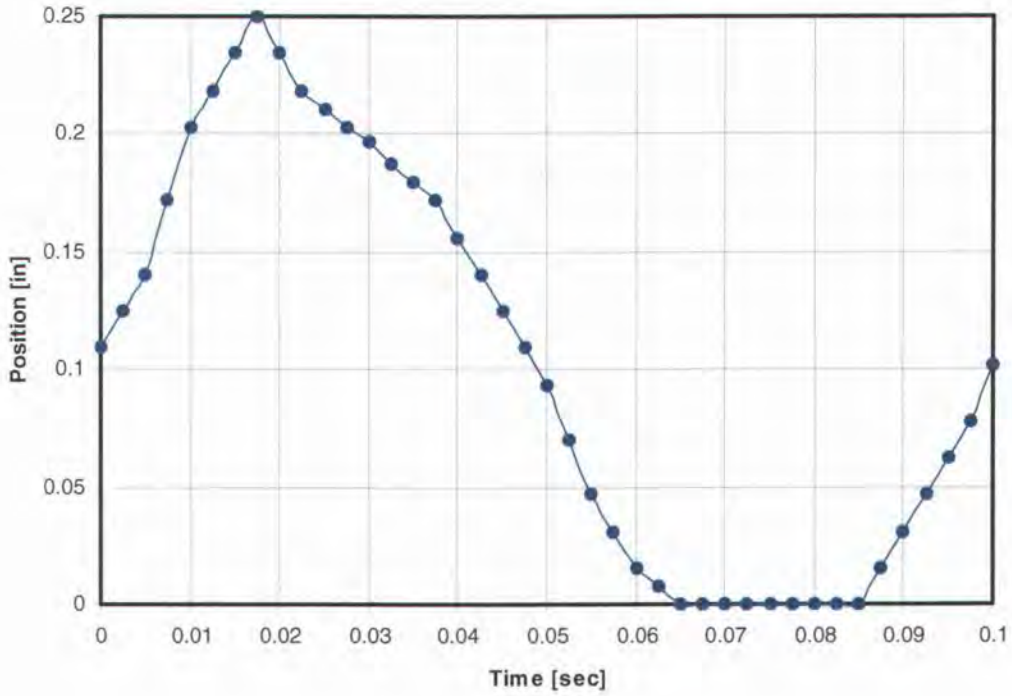

Figure 33 - Position vs. Time, Speed = 10 [Hz] - 10/18/04

Figure 34 shows the position of the regenerator/displacer verses time when it is oscillating at 13 Hz. Again, the curve resembles a triangle wave in some ways; however, it also has some distinct features, which are very different from a triangle wave. At this speed, the magnet rotor is spinning fast enough that it does not hold the regenerator/displacer down at bottom dead center. However, the curve again indicates that the speed the regenerator/displacer increases as it moves down the cylinder. This is the same characteristic that was observed in Fig. 33

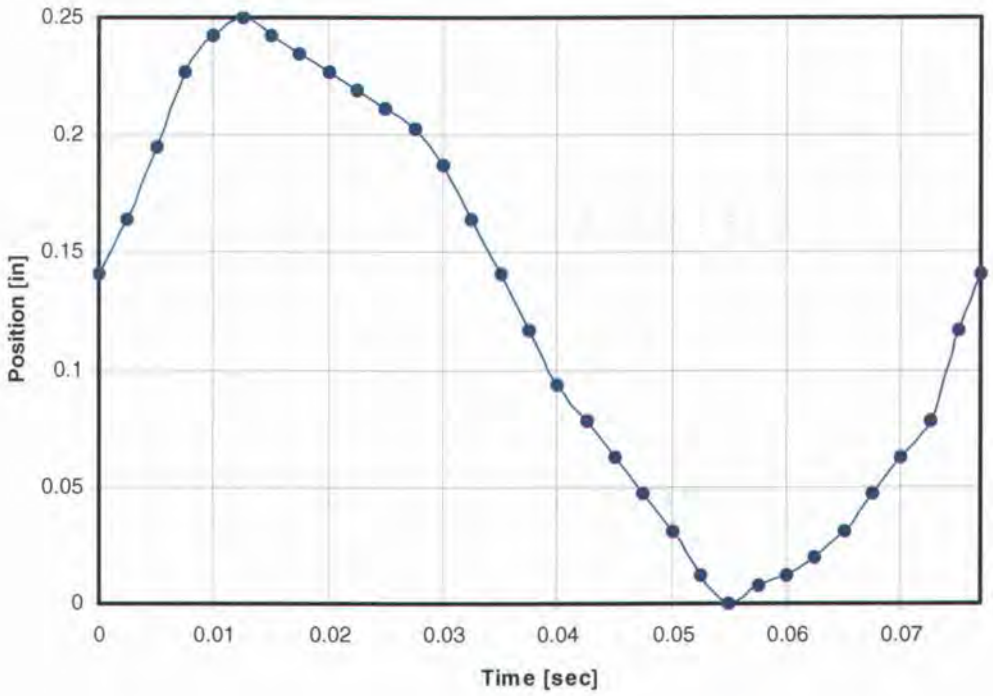

Figure 34 - Position vs. Time, Speed = 13 [Hz] - 10/18/04

6.2 CYLINDER PRESSURE VS. TIME

The cylinder pressure measurements comprise the bulk of the experiments. Because the thermal efficiency of the thermocompressor is not meaningful without mass flowing through the device, this data represents the best figure of merit for the thermocompressor.

6.2.1 PRESSURE RATIO VS. TEMPERATURE RATIO

Figure 35 shows the pressure ratio of the thermocompressor verses temperature ratio for each of the test runs. As expected, the curves show that there is a linear relationship between pressure ratio and temperature ratio. Overall, there appears to be very little difference between any of the runs. The pressure ratios for the runs with N_2 appear to be very similar to those with He. The pressure ratios appear to be slightly higher for the runs at 10 Hz compared to those at 13 Hz. This may be because there is more time for heat to transfer to the cylinder when the

regenerator/displacer is moving slower. Consequently, the pressure increase is greater. However, even this is a very slight difference between the curves.

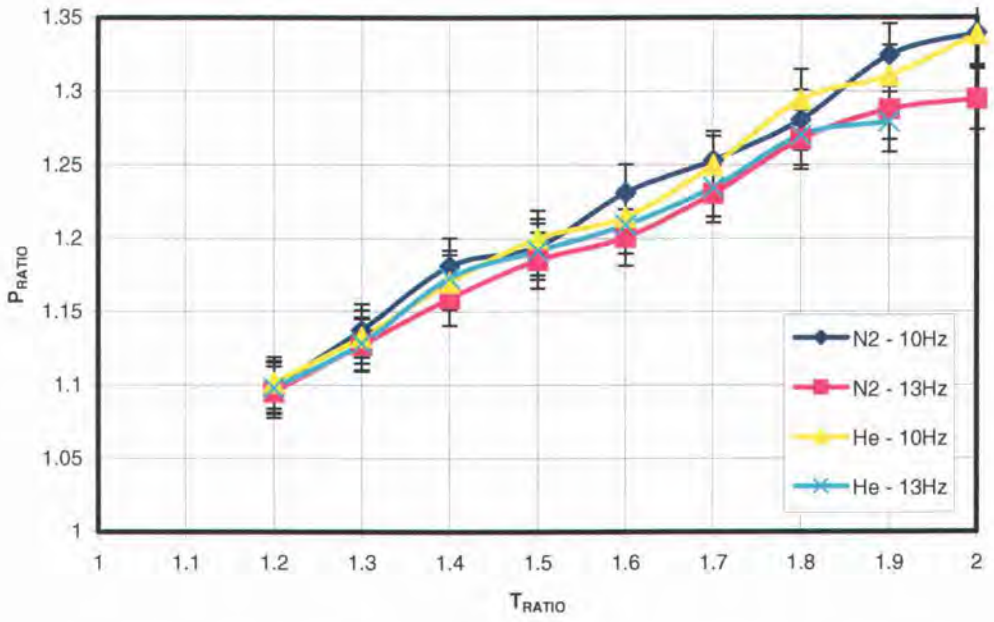

Figure 35 - Pressure Ratio vs. Temperature Ratio

6.2.2 PRESSURE VS. TIME – N_2, 10 Hz

Figures 36-44 show the pressure variation inside the cylinder along with the position of the regenerator/displacer. The working fluid for this run was N_2, and the operating speed was 10 Hz. As can be seen, the pressure curves closely follow the position curves. The cylinder pressure appears to be directly proportional to the regenerator/displacer position. The highest pressure ratio in this run is 1.32 for a temperature ratio of 2.0. The pressure transducer used (Endevco, 8530C-50) had a specified accuracy of ±0.11 psia and, as shown in Appendix D, the maximum uncertainty for these pressure measurements is ±0.274 psia.

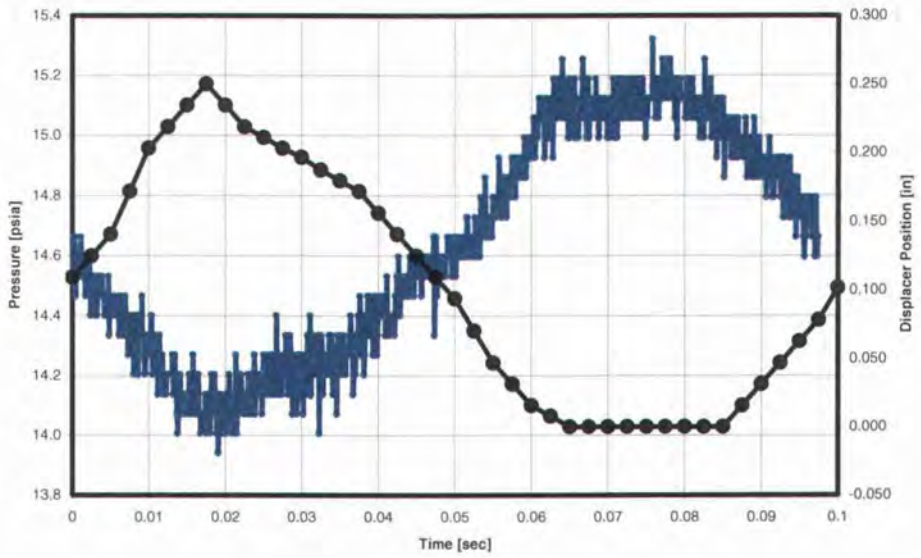

Figure 36 - Pressure vs. Time (Blue) & Position vs. Time (Black) – 10/06/04
Working Fluid = N_2, Speed = 10 [Hz], T_{RATIO} = 1.2, P_{RATIO} = 1.08

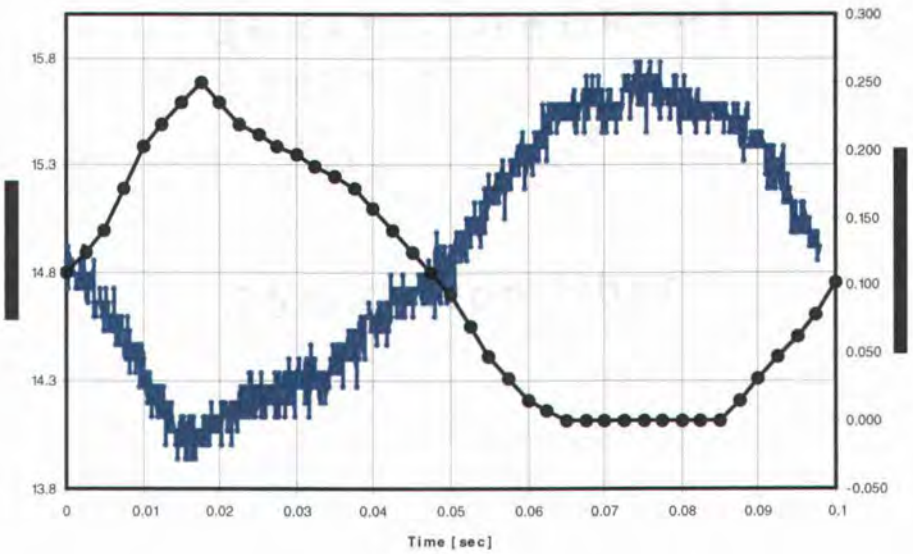

Figure 37 - Pressure vs. Time (Blue) & Position vs. Time (Black) – 10/06/04
Working Fluid = N_2, Speed = 10 [Hz], T_{RATIO} = 1.3, P_{RATIO} = 1.12

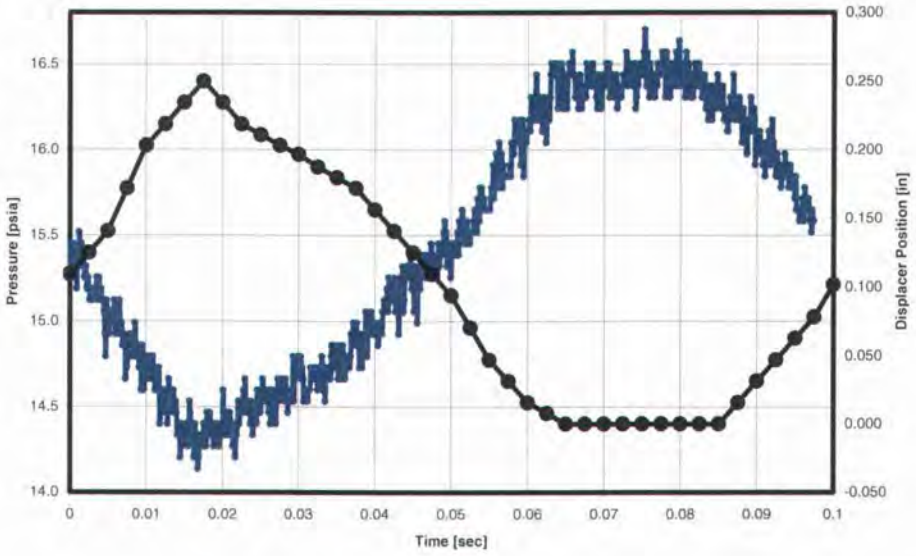

Figure 38 - Pressure vs. Time (Blue) & Position vs. Time (Black) – 10/06/04
Working Fluid = N_2, Speed = 10 [Hz], T_{RATIO} = 1.4, P_{RATIO} = 1.15

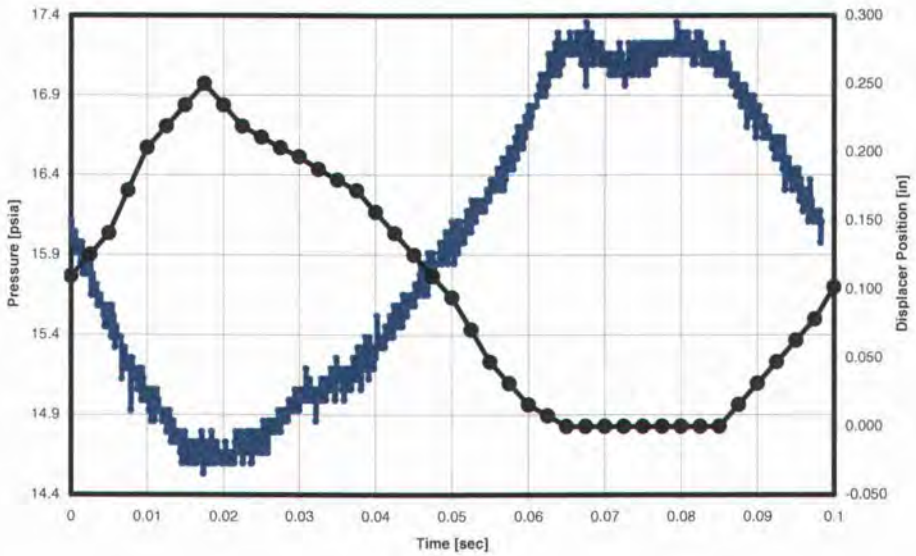

Figure 39 - Pressure vs. Time (Blue) & Position vs. Time (Black) – 10/06/04
Working Fluid = N_2, Speed = 10 [Hz], T_{RATIO} = 1.5, P_{RATIO} = 1.17

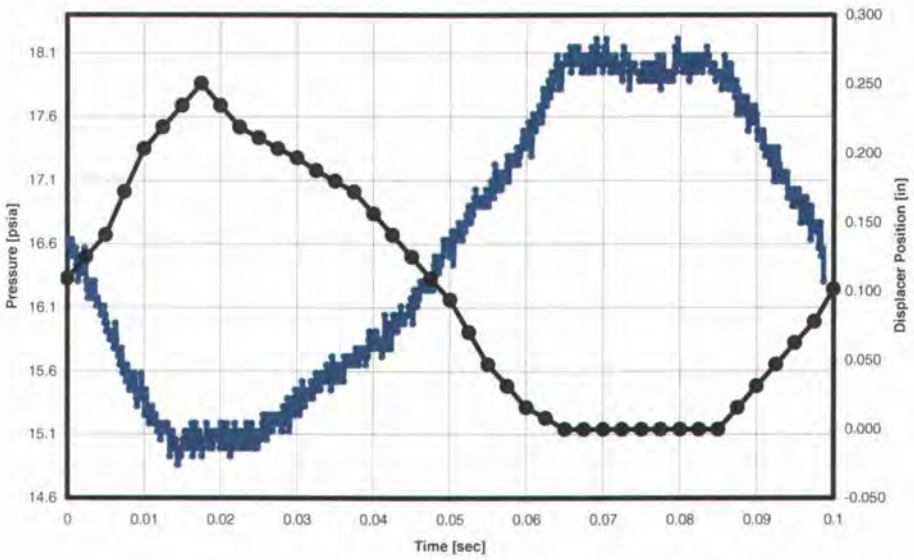

Figure 40 - Pressure vs. Time (Blue) & Position vs. Time (Black) – 10/06/04
Working Fluid = N_2, Speed = 10 [Hz], T_{RATIO} = 1.6, P_{RATIO} = 1.2

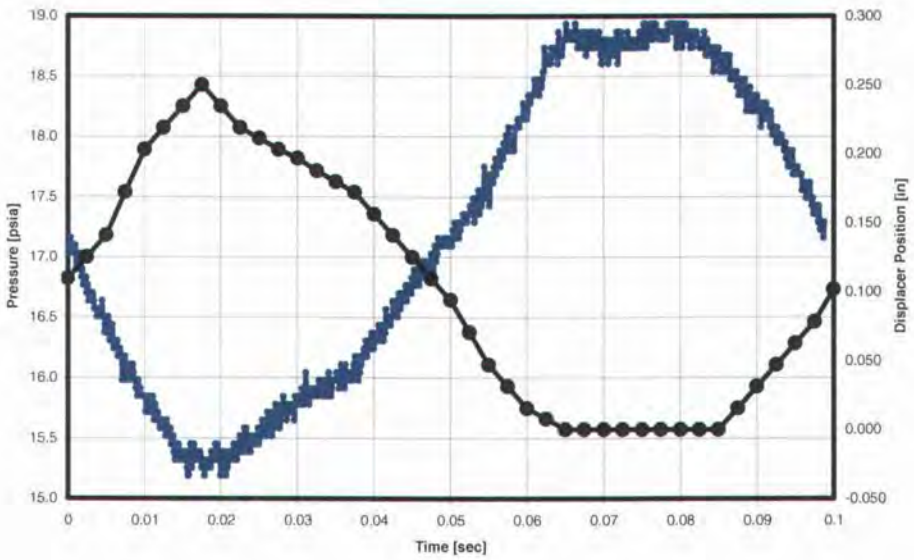

Figure 41 - Pressure vs. Time (Blue) & Position vs. Time (Black) – 10/06/04
Working Fluid = N_2, Speed = 10 [Hz], T_{RATIO} = 1.7, P_{RATIO} = 1.23

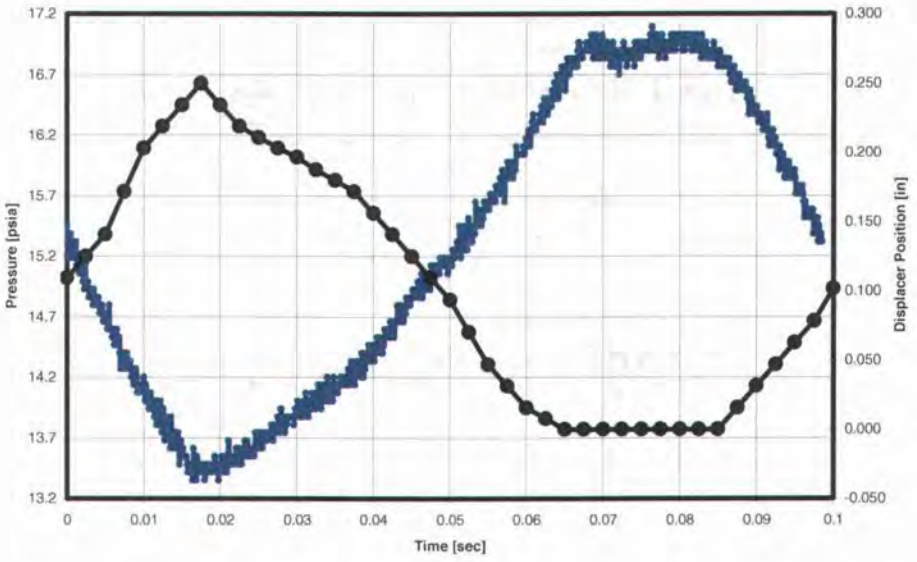

Figure 42 - Pressure vs. Time (Blue) & Position vs. Time (Black) – 10/12/04
Working Fluid = N_2, Speed = 10 [Hz], T_{RATIO} = 1.8, P_{RATIO} = 1.26

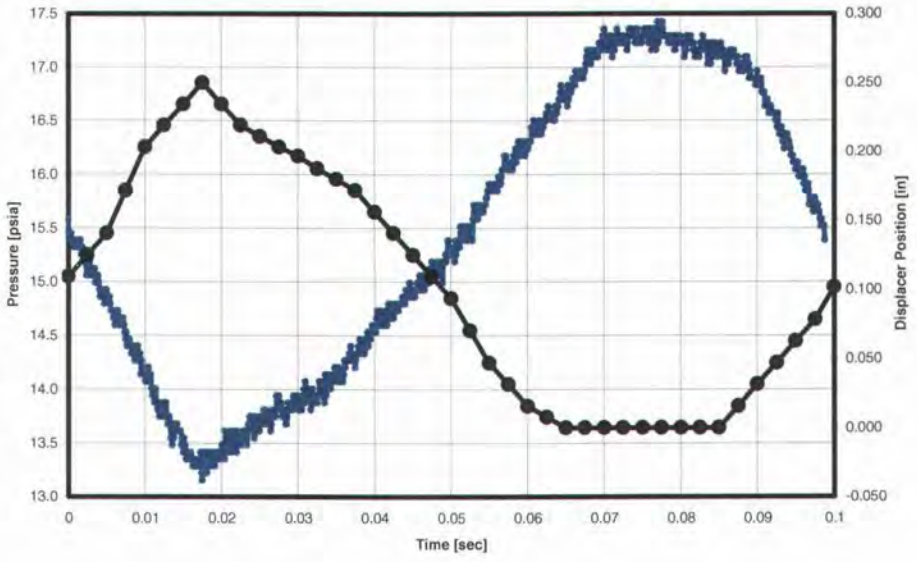

Figure 43 - Pressure vs. Time (Blue) & Position vs. Time (Black) – 10/12/04
Working Fluid = N_2, Speed = 10 [Hz], T_{RATIO} = 1.9, P_{RATIO} = 1.3

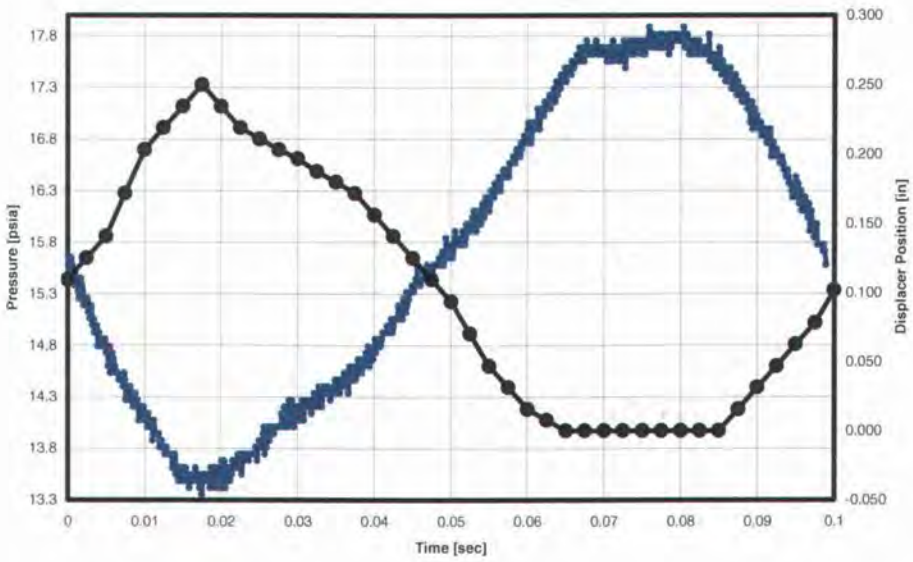

Figure 44 - Pressure vs. Time (Blue) & Position vs. Time (Black) – 10/12/04
Working Fluid = N_2, Speed = 10 [Hz], T_{RATIO} = 2.0, P_{RATIO} = 1.32

6.2.3 PRESSURE VS. TIME – N_2, 13 Hz

Figures 45-53 show the pressure variation inside the cylinder along with the position of the regenerator/displacer for an experimental run with N_2, operating at 13 Hz. Again, the pressure curves closely follow the position curves. The highest pressure ratio in this run is 1.29 for a temperature ratio of 2.0. Also, the maximum uncertainty for these pressure measurements is ±0.274 psia.

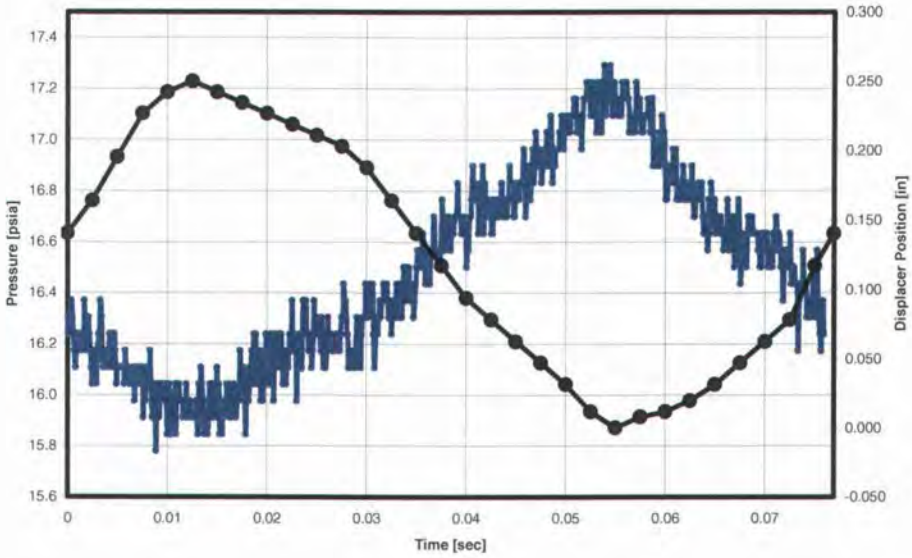

Figure 45 - Pressure vs. Time (Blue) & Position vs. Time (Black) – 10/05/04
Working Fluid = N_2, Speed = 13 [Hz], T_{RATIO} = 1.2, P_{RATIO} = 1.08

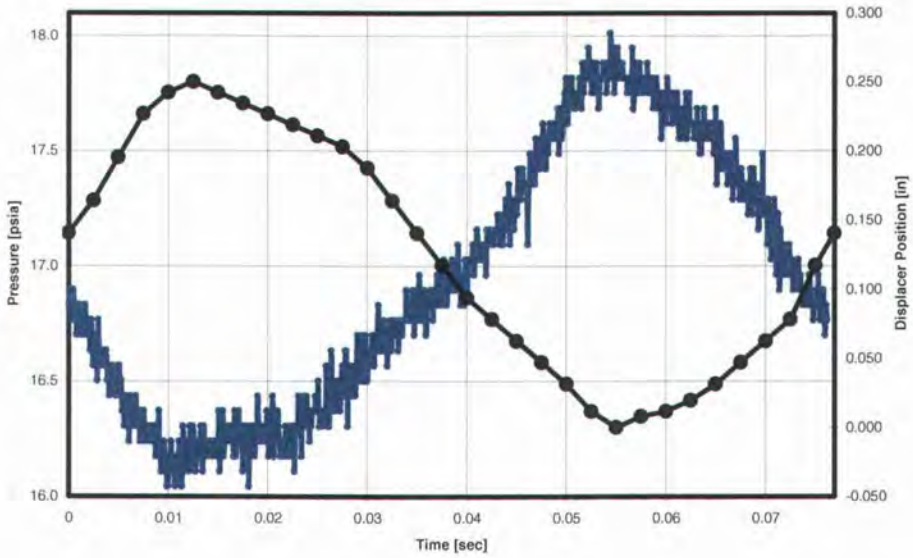

Figure 46 - Pressure vs. Time (Blue) & Position vs. Time (Black) – 10/05/04
Working Fluid = N_2, Speed = 13 [Hz], T_{RATIO} = 1.3, P_{RATIO} = 1.11

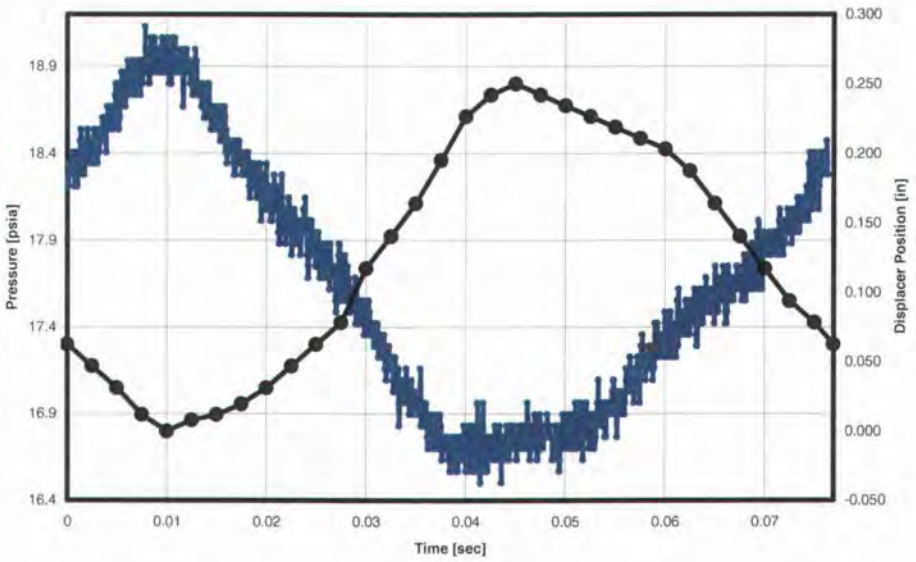

Figure 47 - Pressure vs. Time (Blue) & Position vs. Time (Black) – 10/05/04
Working Fluid = N_2, Speed = 13 [Hz], T_{RATIO} = 1.4, P_{RATIO} = 1.13

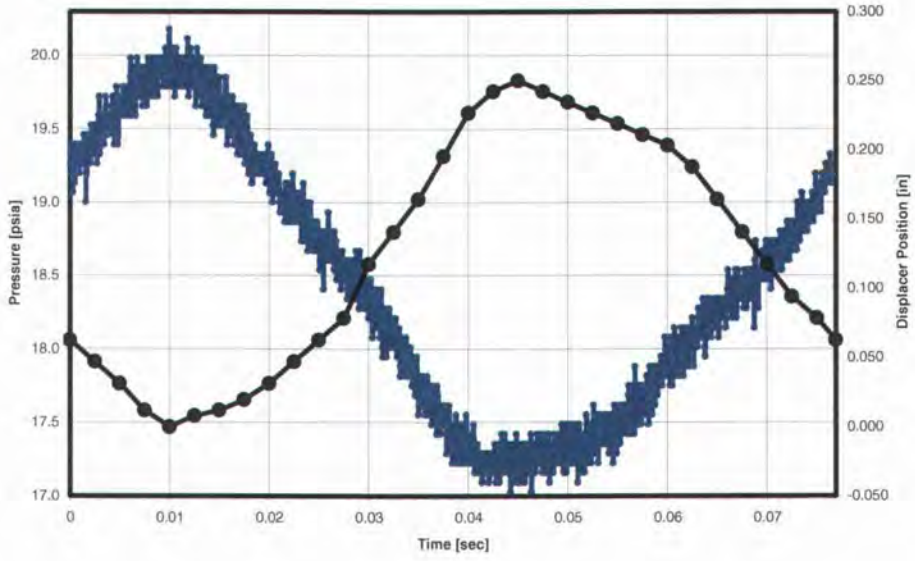

Figure 48 - Pressure vs. Time (Blue) & Position vs. Time (Black) – 10/05/04
Working Fluid = N_2, Speed = 13 [Hz], T_{RATIO} = 1.5, P_{RATIO} = 1.16

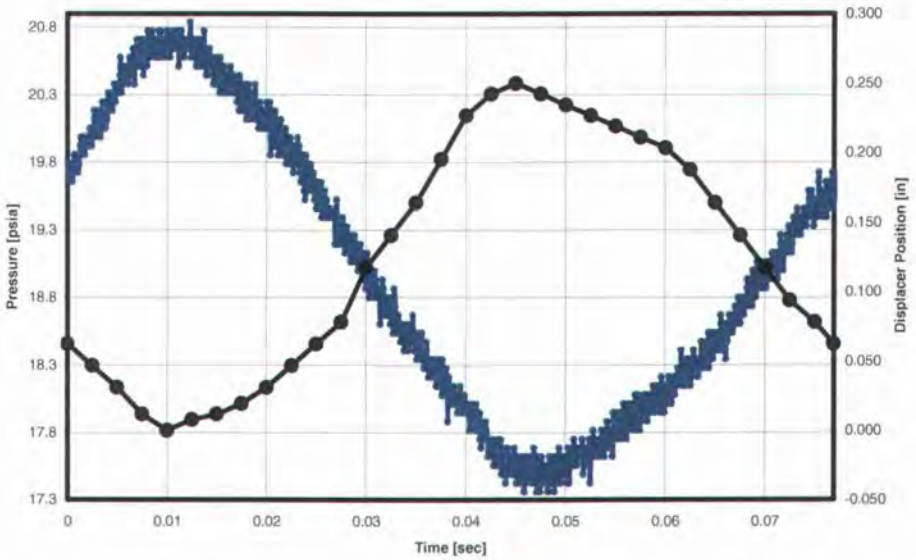

Figure 49 - Pressure vs. Time (Blue) & Position vs. Time (Black) – 10/05/04
Working Fluid = N_2, Speed = 13 [Hz], T_{RATIO} = 1.6, P_{RATIO} = 1.19

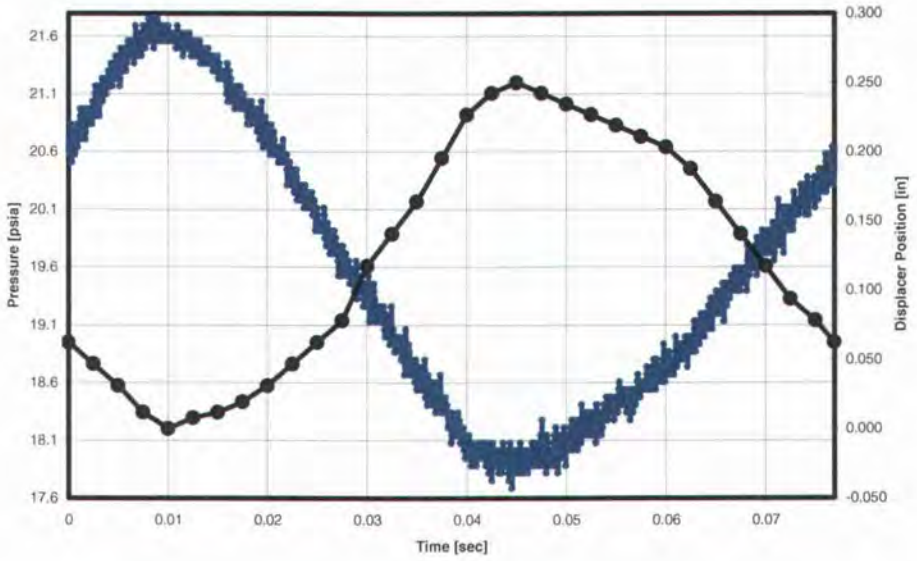

Figure 50 - Pressure vs. Time (Blue) & Position vs. Time (Black) – 10/05/04
Working Fluid = N_2, Speed = 13 [Hz], T_{RATIO} = 1.7, P_{RATIO} = 1.21

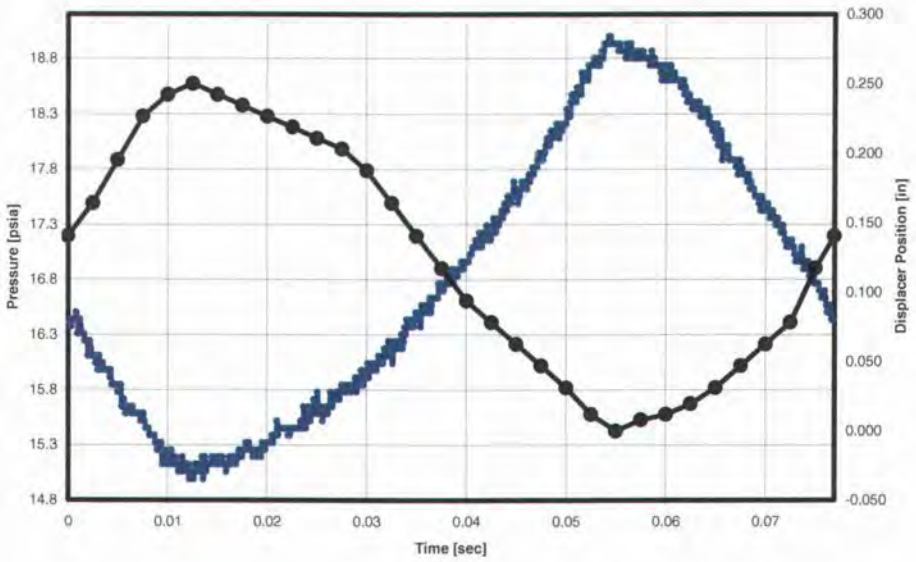

Figure 51 - Pressure vs. Time (Blue) & Position vs. Time (Black) – 10/13/04
Working Fluid = N_2, Speed = 13 [Hz], T_{RATIO} = 1.8, P_{RATIO} = 1.26

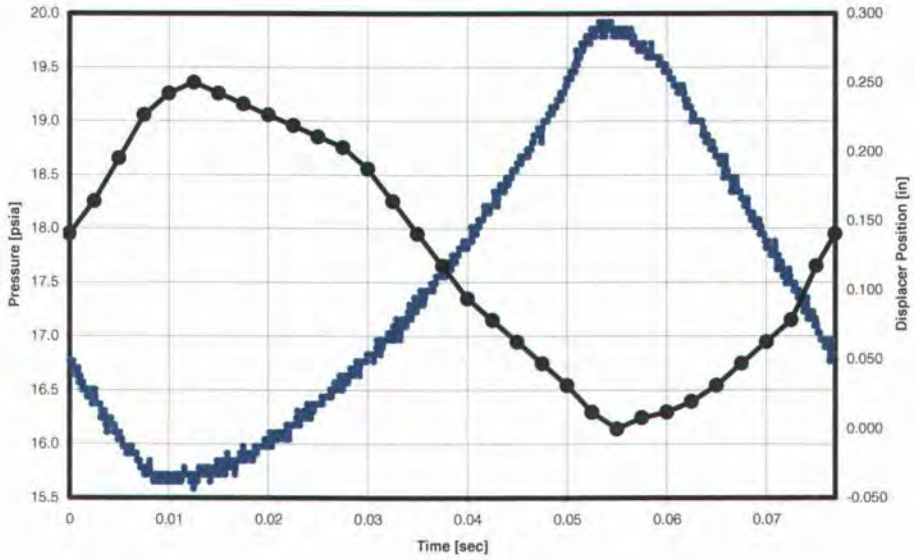

Figure 52 - Pressure vs. Time (Blue) & Position vs. Time (Black) – 10/13/04
Working Fluid = N_2, Speed = 13 [Hz], T_{RATIO} = 1.9, P_{RATIO} = 1.28

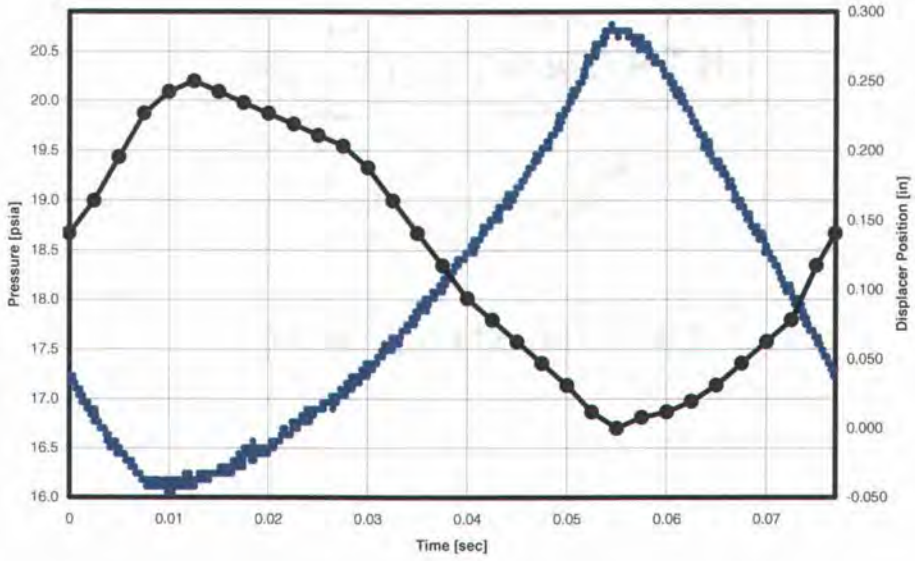

Figure 53 - Pressure vs. Time (Blue) & Position vs. Time (Black) – 10/13/04
Working Fluid = N_2, Speed = 13 [Hz], T_{RATIO} = 2.0, P_{RATIO} = 1.29

6.2.4 PRESSURE VS. TIME – He, 10 Hz

Figures 54-62 show the pressure variation inside the cylinder along with the position of the regenerator/displacer for an experimental run with He, operating at 10 Hz. Again, the pressure curves closely follow the position curves. The highest pressure ratio in this run is 1.32 for a temperature ratio of 2.0. The maximum uncertainty of the pressure measurements is ±0.274 psia.

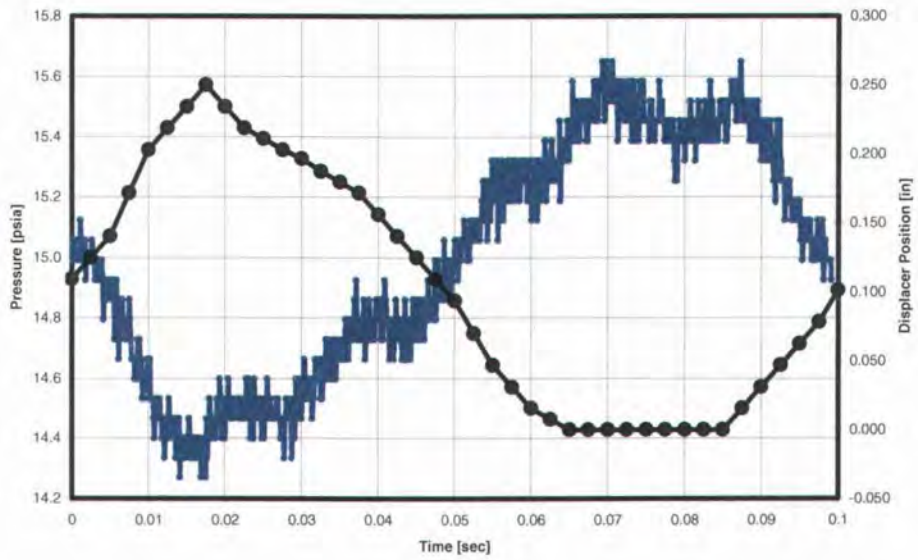

Figure 54 - Pressure vs. Time (Blue) & Position vs. Time (Black) – 10/09/04
Working Fluid = He, Speed = 10 [Hz], T_{RATIO} = 1.2, P_{RATIO} = 1.08

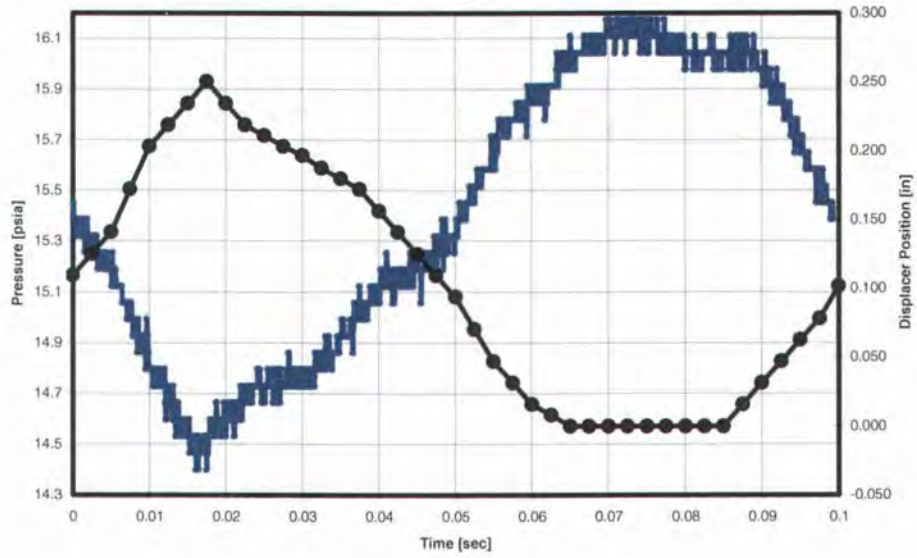

Figure 55 - Pressure vs. Time (Blue) & Position vs. Time (Black) – 10/09/04
Working Fluid = He, Speed = 10 [Hz], T_{RATIO} = 1.3, P_{RATIO} = 1.11

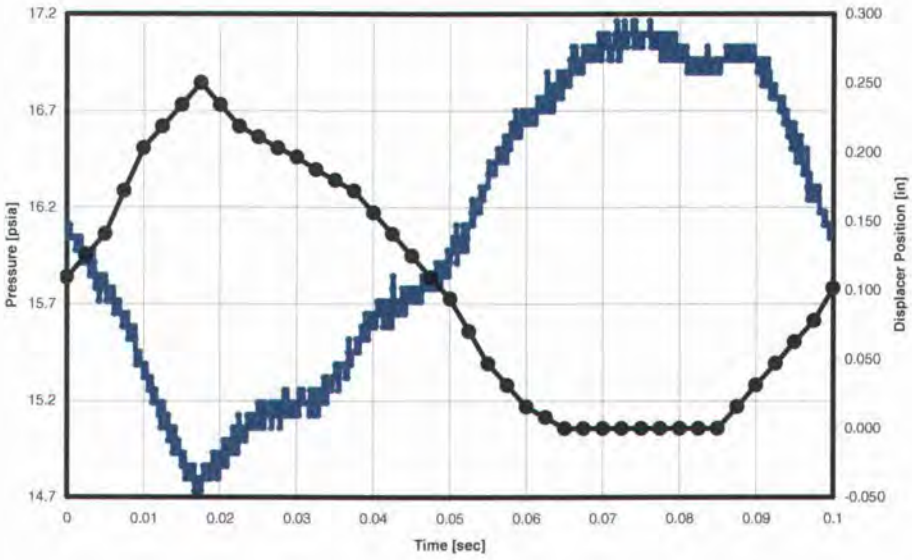

Figure 56 - Pressure vs. Time (Blue) & Position vs. Time (Black) – 10/09/04
Working Fluid = He, Speed = 10 [Hz], T_{RATIO} = 1.4, P_{RATIO} = 1.16

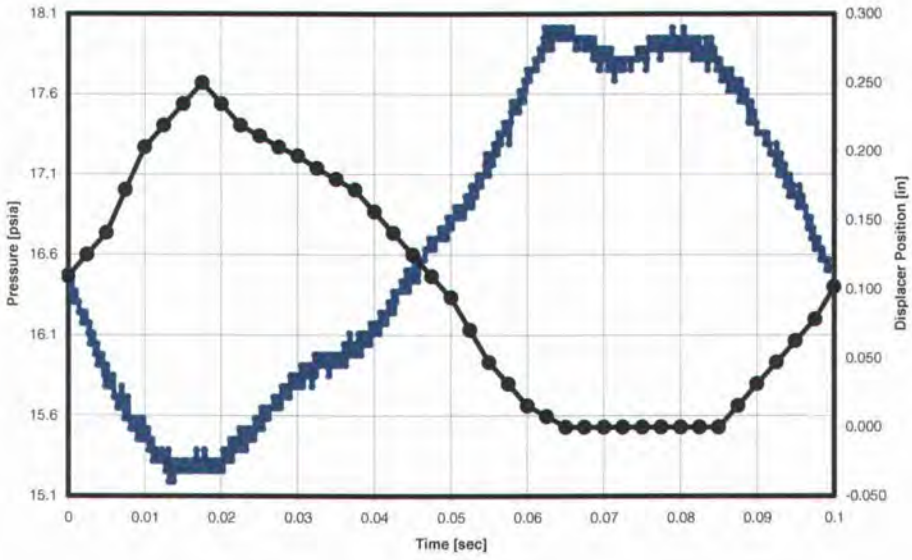

Figure 57 - Pressure vs. Time (Blue) & Position vs. Time (Black) – 10/09/04
Working Fluid = He, Speed = 10 [Hz], T_{RATIO} = 1.5, P_{RATIO} = 1.18

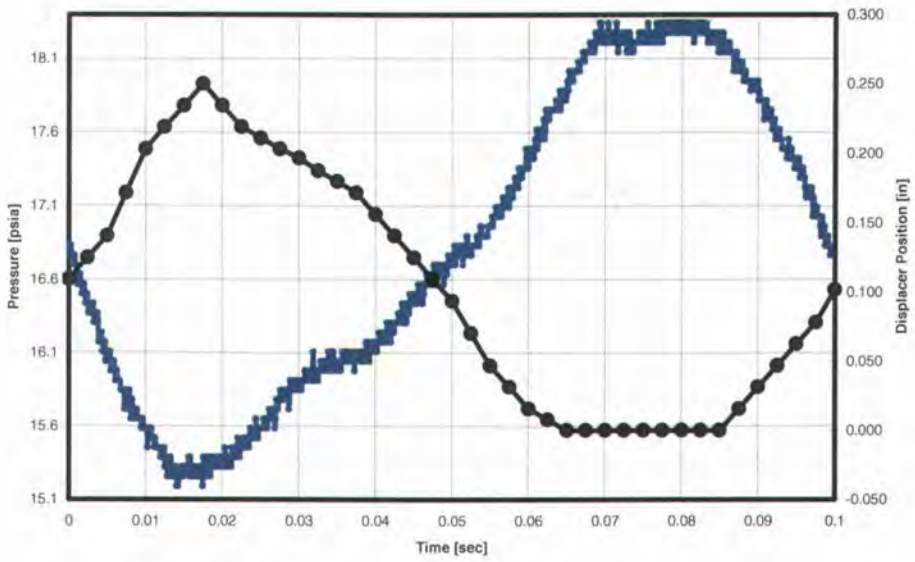

Figure 58 - Pressure vs. Time (Blue) & Position vs. Time (Black) – 10/09/04
Working Fluid = He, Speed = 10 [Hz], T_{RATIO} = 1.6, P_{RATIO} = 1.2

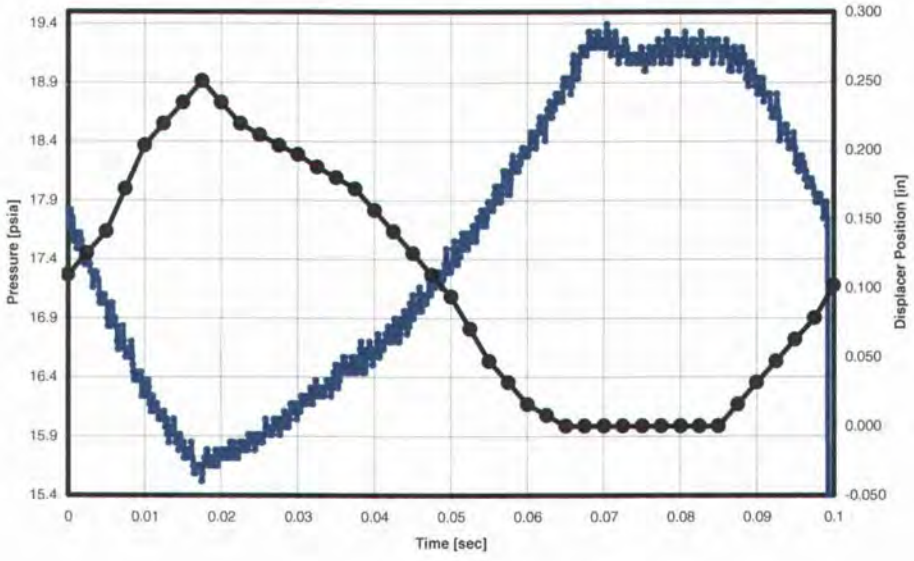

Figure 59 - Pressure vs. Time (Blue) & Position vs. Time (Black) – 10/09/04
Working Fluid = He, Speed = 10 [Hz], T_{RATIO} = 1.7, P_{RATIO} = 1.23

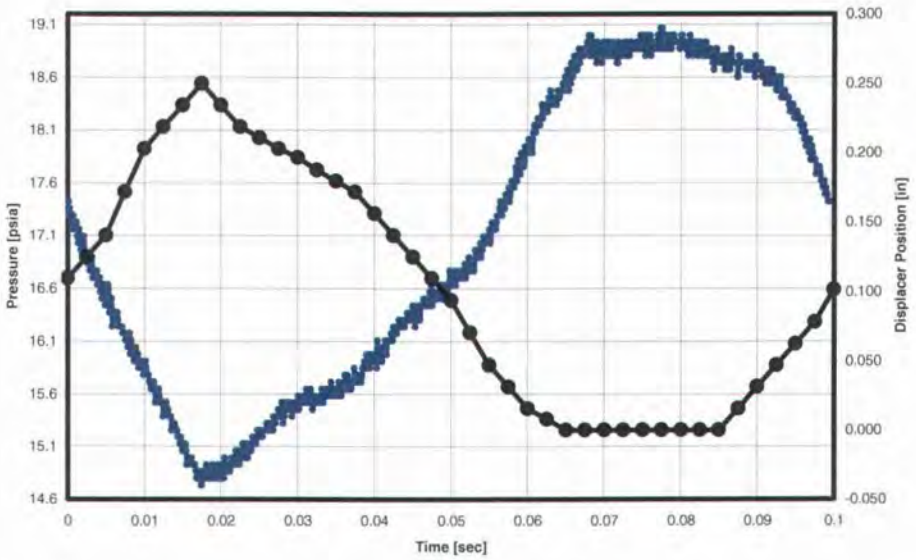

Figure 60 - Pressure vs. Time (Blue) & Position vs. Time (Black) – 10/12/04
Working Fluid = He, Speed = 10 [Hz], T_{RATIO} = 1.8, P_{RATIO} = 1.28

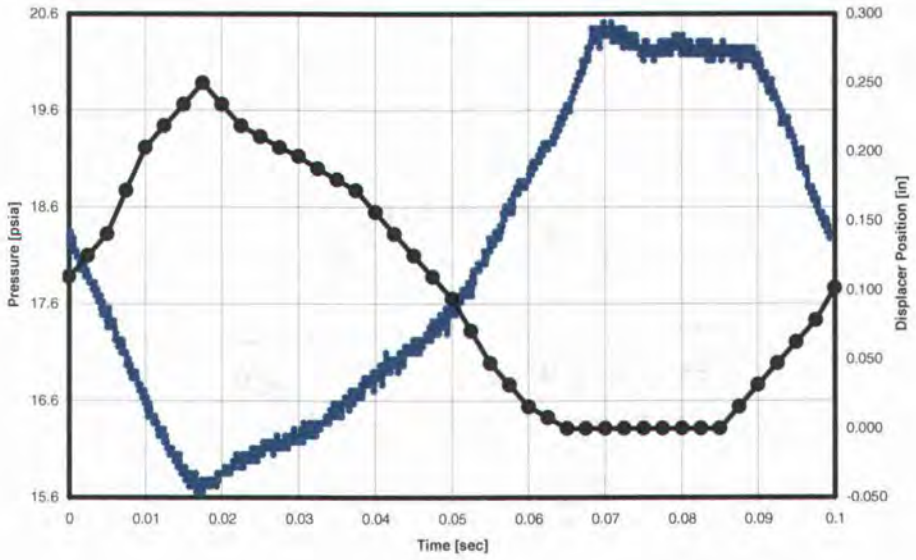

Figure 61 - Pressure vs. Time (Blue) & Position vs. Time (Black) – 10/12/04
Working Fluid = He, Speed = 10 [Hz], T_{RATIO} = 1.9, P_{RATIO} = 1.3

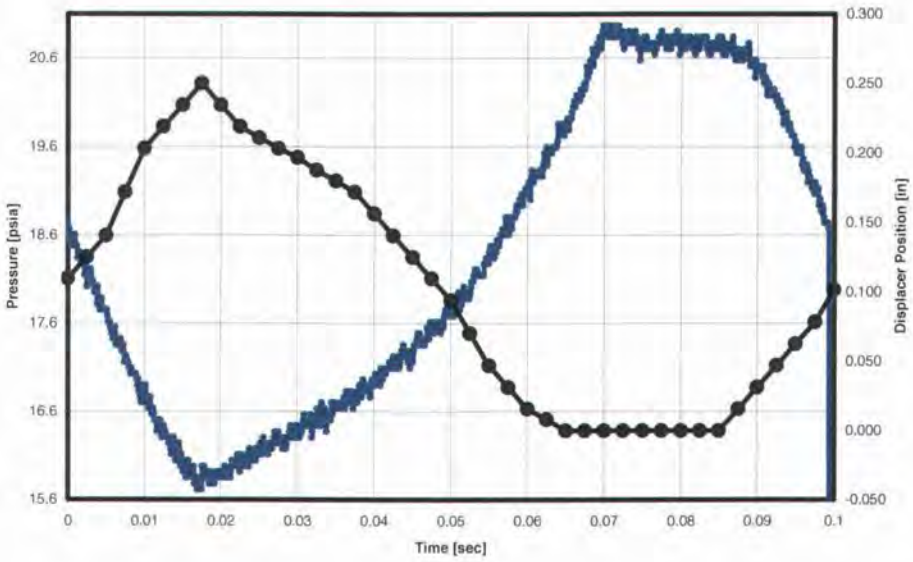

Figure 62 - Pressure vs. Time (Blue) & Position vs. Time (Black) – 10/12/04
Working Fluid = He, Speed = 10 [Hz], T_{RATIO} = 2.0, P_{RATIO} = 1.32

6.2.5 PRESSURE VS. TIME – He, 13 Hz

Figures 63-70 show the pressure variation inside the cylinder along with the position of the regenerator/displacer for an experimental run with He, operating at 13 Hz. Again, the pressure curves closely follow the position curves. The highest pressure ratio in this run is 1.27 for a temperature ratio of 1.9. Unfortunately, this run does not include a measurement at a temperature ratio of 2.0 because the thermocompressor was not operating correctly at that speed for this run. The maximum uncertainty for these pressure measurements is also ±0.274 psia.

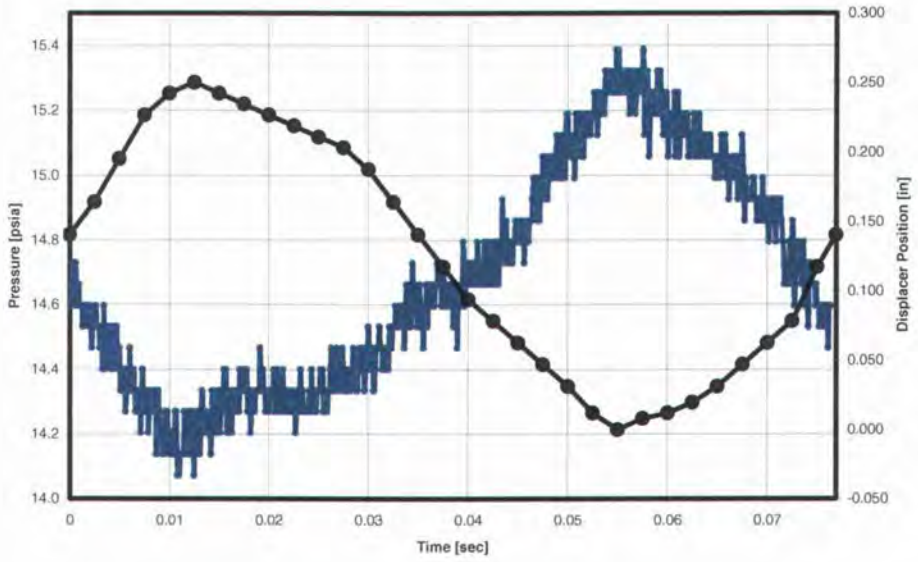

Figure 63 - Pressure vs. Time (Blue) & Position vs. Time (Black) – 10/07/04
Working Fluid = He, Speed = 13 [Hz], T_{RATIO} = 1.2, P_{RATIO} = 1.08

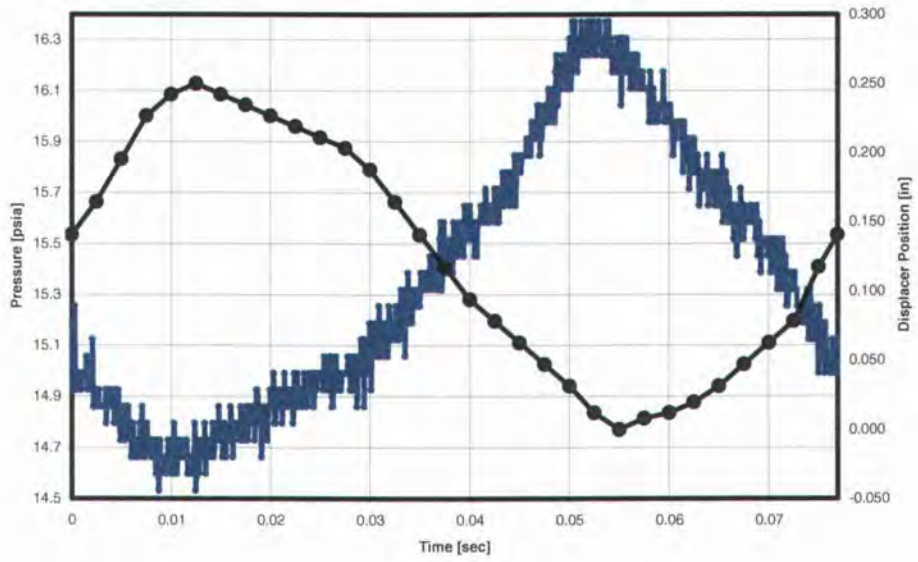

Figure 64 - Pressure vs. Time (Blue) & Position vs. Time (Black) – 10/07/04
Working Fluid = He, Speed = 13 [Hz], T_{RATIO} = 1.3, P_{RATIO} = 1.11

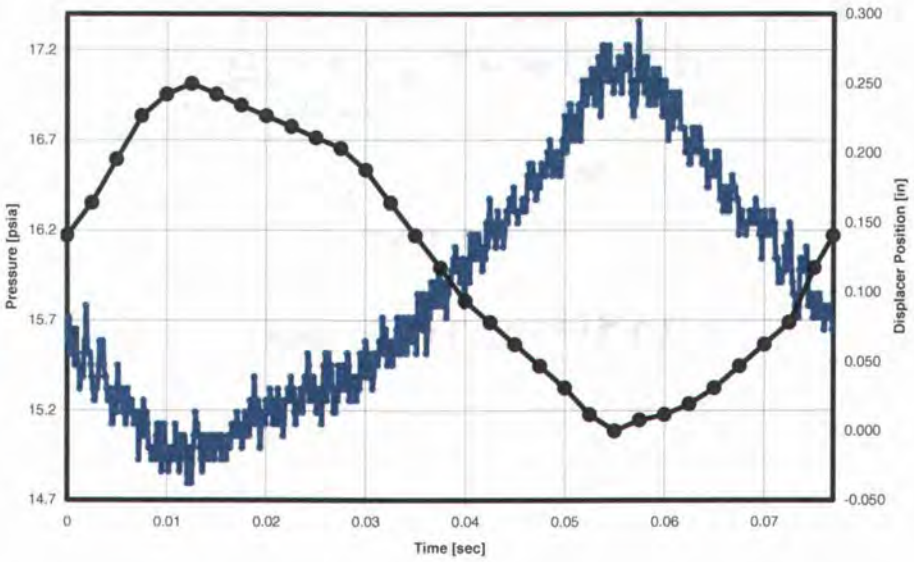

Figure 65 - Pressure vs. Time (Blue) & Position vs. Time (Black) – 10/07/04
Working Fluid = He, Speed = 13 [Hz], T_{RATIO} = 1.4, P_{RATIO} = 1.14

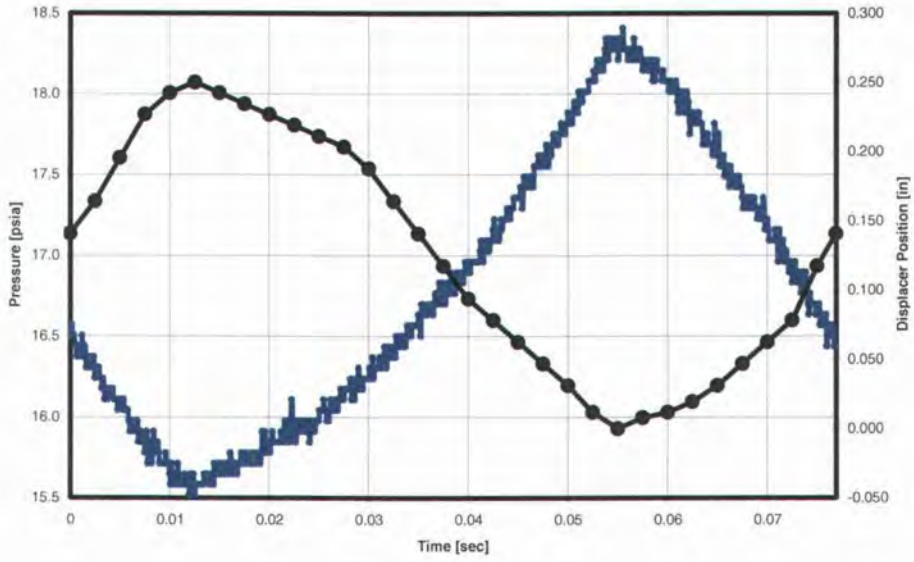

Figure 66 - Pressure vs. Time (Blue) & Position vs. Time (Black) – 10/09/04
Working Fluid = He, Speed = 13 [Hz], T_{RATIO} = 1.5, P_{RATIO} = 1.17

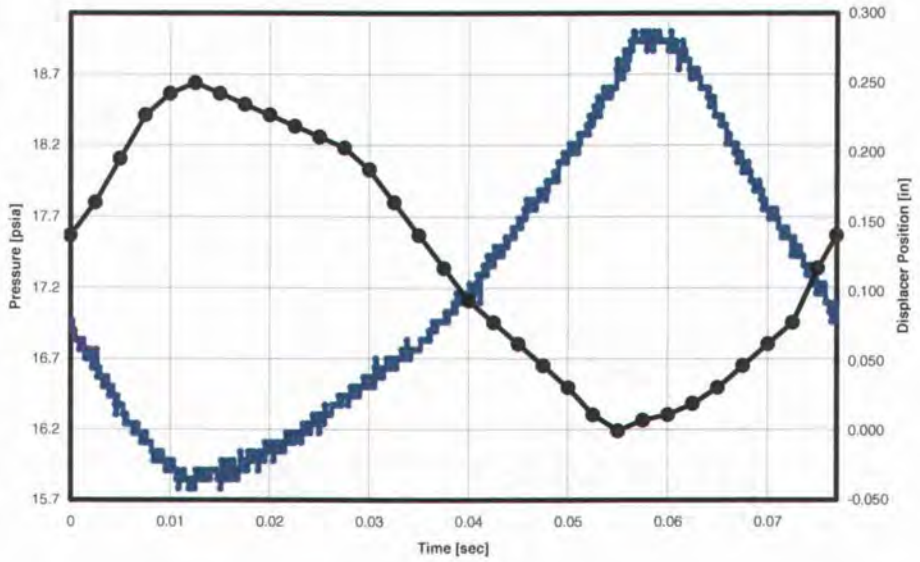

Figure 67 - Pressure vs. Time (Blue) & Position vs. Time (Black) – 10/09/04
Working Fluid = He, Speed = 13 [Hz], T_{RATIO} = 1.6, P_{RATIO} = 1.20

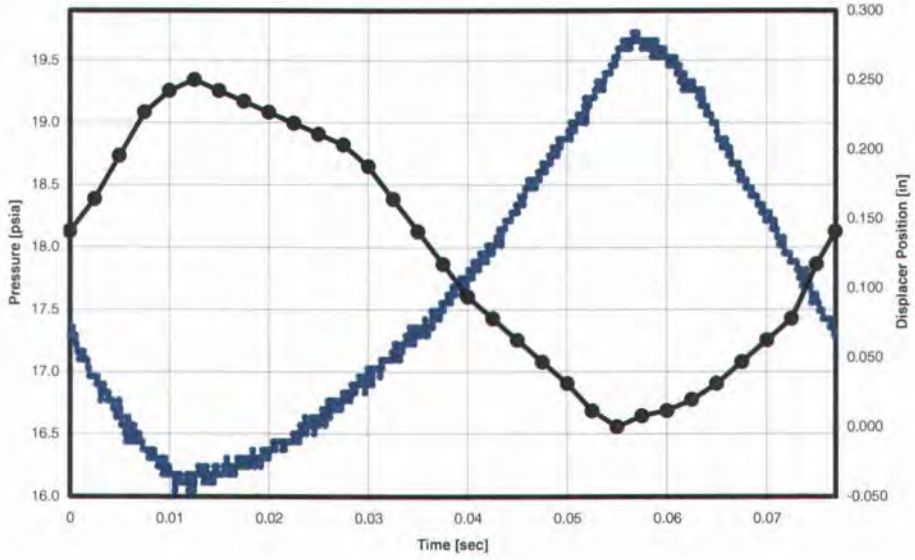

Figure 68 - Pressure vs. Time (Blue) & Position vs. Time (Black) – 10/09/04
Working Fluid = He, Speed = 13 [Hz], T_{RATIO} = 1.7, P_{RATIO} = 1.22

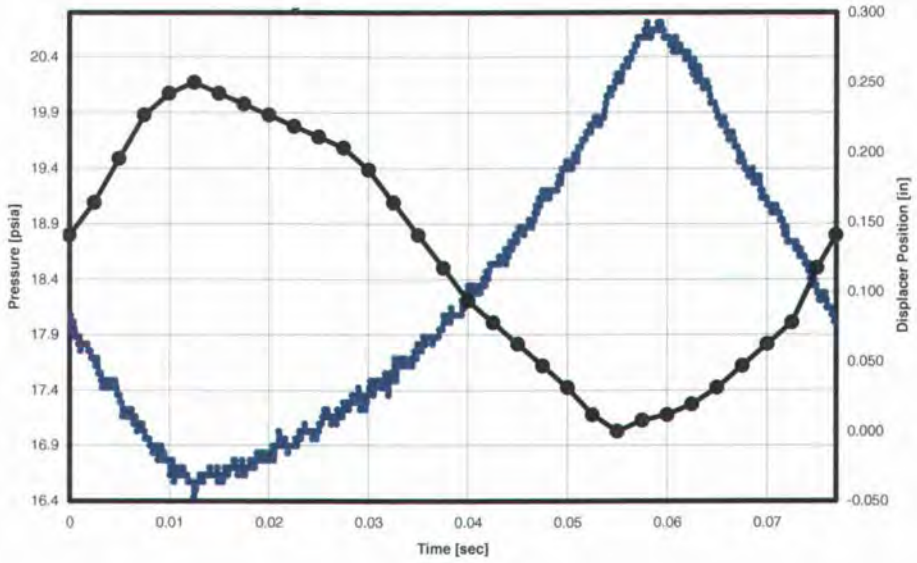

Figure 69 - Pressure vs. Time (Blue) & Position vs. Time (Black) – 10/09/04
Working Fluid = He, Speed = 13 [Hz], T_{RATIO} = 1.8, P_{RATIO} = 1.24

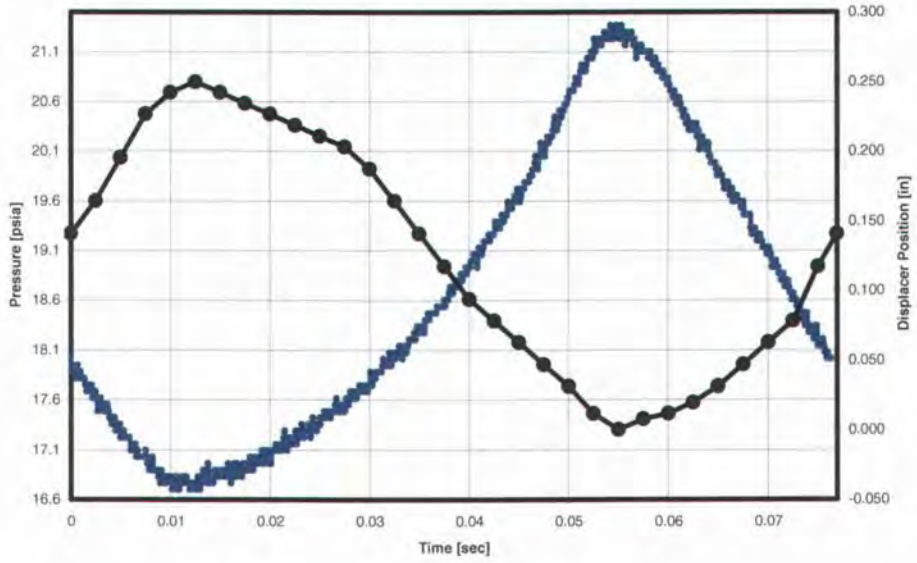

Figure 70 - Pressure vs. Time (Blue) & Position vs. Time (Black) – 10/12/04
Working Fluid = He, Speed = 13 [Hz], T_{RATIO} = 1.9, P_{RATIO} = 1.27

6.3 HOT SIDE TEMPERATURE VS. TIME

When examining the temperature measurements made inside the cylinder, it is necessary to consider the location of the thermocouple. As shown in Fig. 71, the thermocouple was inserted into the center of the hot space a distance of 0.030 inches below the top of the cylinder. The thermocouple mated with a hole in the top center of the regenerator/displacer, which had a depth of 0.050 inches. The temperature measurements, therefore, indicate the change in temperature of the thermocouple, which is near the top surface of the cylinder. The measurements do not, however, accurately reflect the full temperature variation inside the cylinder.

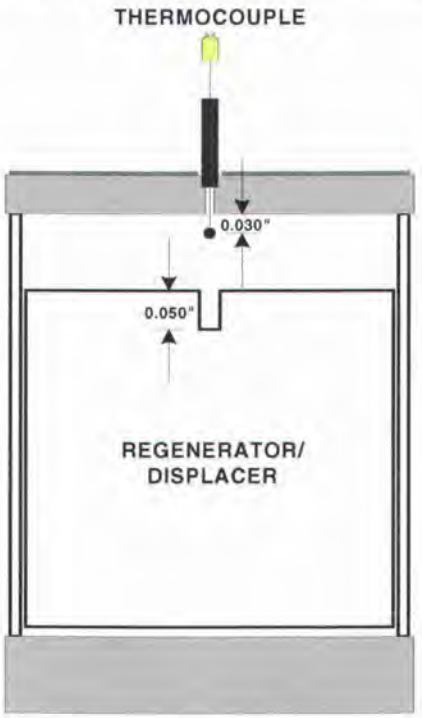

Figure 71 - Hot Side Thermocouple Placement

Because the thermocouple is placed near the top of the cylinder in the center, its measurements may be influenced by several factors. First, as the regenerator/displacer starts to move down from top dead center, the gas rushes into the hot space from the sides of the cylinder. Therefore, there is a slight delay before the incoming gas reaches the thermocouple. When it does reach the thermocouple, it may be experiencing turbulent mixing, which would help facilitate heat transfer. As the regenerator/displacer get closer to bottom dead center, the gas enters the cylinder

much slower and further away from the thermocouple. Therefore, the measurements are less sensitive to temperature swing at that point.

6.3.1 HOT SIDE TEMPERATURE VS. TIME – N_2, 10 Hz

Figure 72 shows the temperature measurements for an experimental run with N_2, operating at 10 Hz with a temperature ratio of two. The temperature variation appears to be approximately 3 °C, which would indicate that the region near the top of the cylinder might be close to isothermal. This does not, however, imply that the entire hot space is necessarily nearly isotheral.

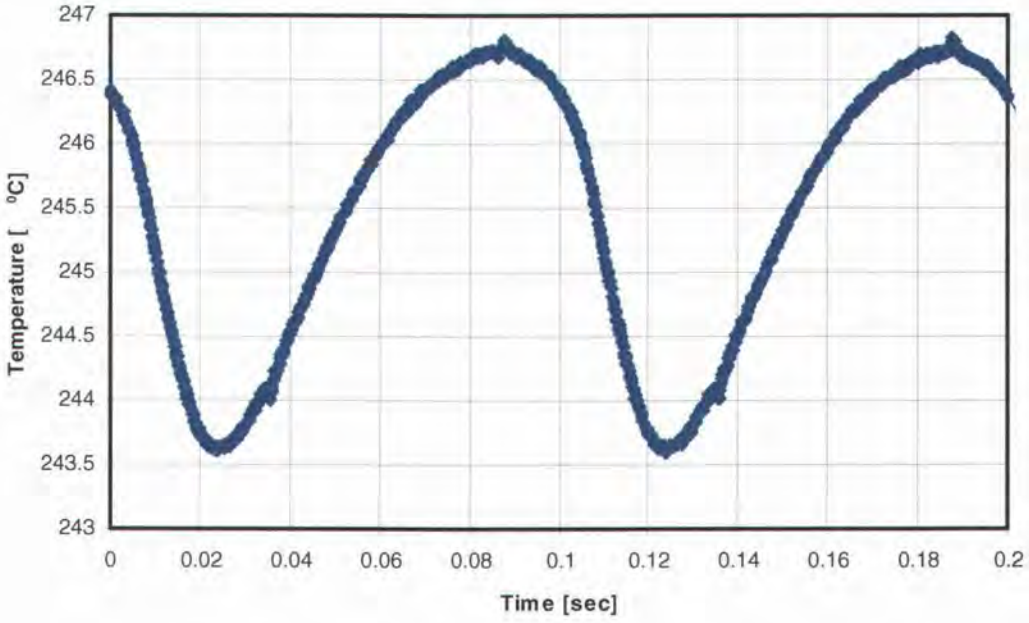

Figure 72 – Hot Side Temperature vs. Time – 10/28/04
Working Fluid = N_2, Speed = 10 [Hz], T_{RATIO} = 2.0

Temperature curves were measured for a range of temperature ratios from 1.2 to 2 for N_2 operating a 10 Hz. Those data sets were condensed into a summary plot as shown in Fig. 73. The thermocouple used (Omega, SCASS-10E-6) had a specified accuracy

of ±1.1 °C and, as shown in Appendix D, the maximum uncertainty for these temperature measurements is ±2.74 °C.

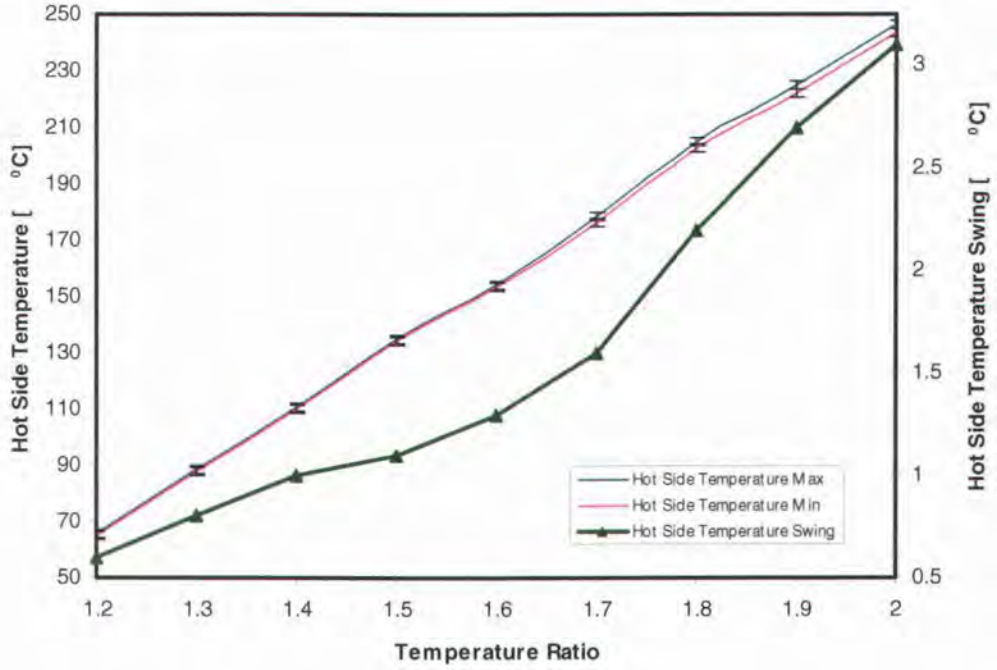

Figure 73 - Hot Side Temperature vs. Temperature Ratio – 10/28/04
Working Fluid = N_2, Speed = 10 [Hz]

6.3.2 HOT SIDE TEMPERATURE VS. TIME – He, 10 Hz

Figure 74 shows the temperature measurements for an experimental run with He, operating at 10 Hz with a temperature ratio of two. The temperature variation appears to be approximately 13.7 °C, which indicates that the temperature swing is higher for He than N_2, but still small.

Temperature curves were measured for a range of temperature ratios from 1.2 to 2 for He operating at 10 Hz. Those data sets were condensed into a summary plot as shown in Fig. 75. Again, the maximum uncertainty for these temperature measurements is ±2.74 °C.

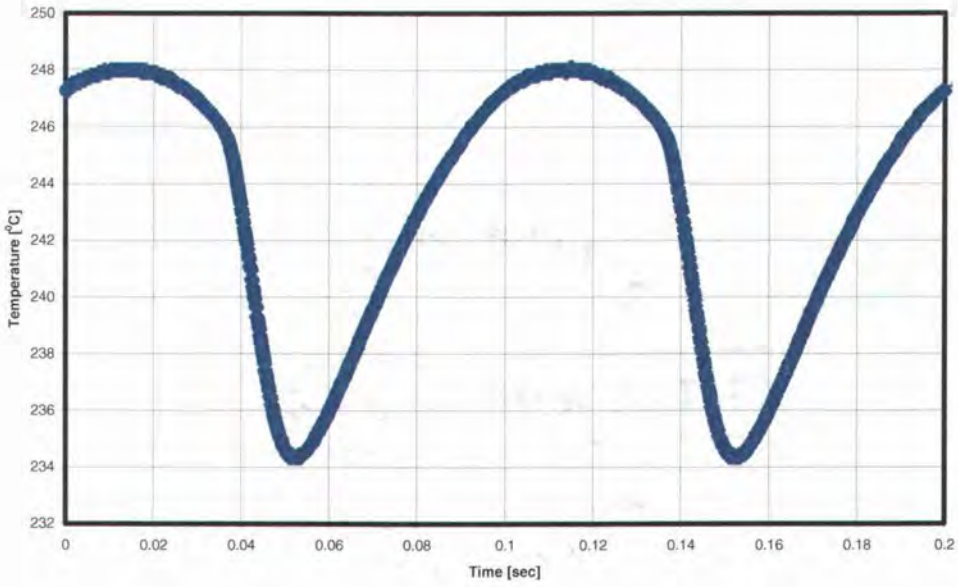

Figure 74 – Hot Side Temperature vs. Time – 11/02/04

Working Fluid = He, Speed = 10 [Hz], T_{RATIO} = 2.0

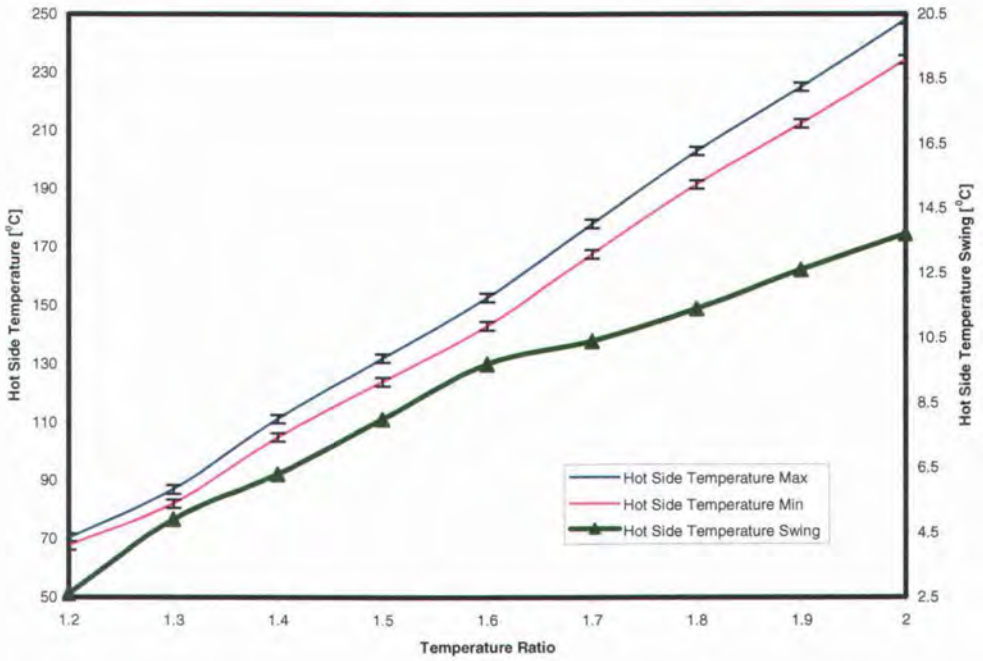

Figure 75 - Hot Side Temperature vs. Temperature Ratio – 11/02/04

Working Fluid = He, Speed = 10 [Hz]

Comparing Fig. 73 to Fig. 75 shows that the hot side temperature variation for He is larger than for N_2. This is surprising due to the higher thermal conductivity of He over N_2. However, He also has a higher specific heat than N_2, which may account for these results. Because the thermal conductivity of He is higher, the heat transfer rate to the gas is higher, but the higher specific heat requires more heat and consequently more time to raise the gas temperature.

7 CONCLUSIONS

An analytical model of the thermocompressor cycle has been developed, which incorporates dead volume in the cylinder, dead volume in the regenerator, and regenerator effectiveness. The model shows that the thermal efficiency of the device is highly sensitive to regenerator effectiveness. A regenerator optimization was presented, which indicated that the maximum predicted thermal efficiency for the device was 45-50% of Carnot efficiency with a regenerator effectiveness of approximately 96% and regenerator dead volume of approximately 26%. This model did not, however, take into account axial conduction along the regenerator, which would lower the thermal efficiency. This model, therefore, indicates that the thermocompressor must operate with very high regeneration to return approximately half of Carnot efficiency. This raises questions about the practicality of the device particularly of achieving regeneration high enough to make the concept advantageous. More detailed modeling work, which incorporates axial conduction and non-isothermal hot and cold spaces would be beneficial to further understanding this cycle.

A thermocompressor has been built and tested, which produces pressure ratios of approximately 75% of the temperature ratios. Nitrogen and Helium both appear to perform equally well despite the higher thermal conductivity and thermal diffusivity of Helium over Nitrogen. In addition, operating speed does not appear to significantly affect the pressure ratio. The temperature variation near the top of the hot side does not appear to fluctuate more than approximately 13.7 °C during operation. This indicates that the region near the top of the cylinder is close to isothermal. The experimental device demonstrates the feasibility and merits of magnetically coupling the regenerator/displacer to its drive system, which eliminates the need for a sliding seal. More experimental work would be helpful to investigate the practicality of achieving much higher regeneration, which would significantly improve system performance. In addition, designs incorporating increased heat transfer area to the hot and cold spaces could greatly improve performance by reducing temperature fluctuation in the cylinder during operation.

REFERENCES

1. Bush, V., Apparatus For Compressing Gases, U.S. Patent No. 2,157,229, 1939.

2. White, M. A., Miniature Stirling Engines for Artificial Heart Power, *Proc. 18th IECEC*, Paper No. 839112, pp. 694-701, 1983.

3. Gibson, B. M. et al., Bypass Gas Actuated Thermocompressor as an Implantable Artificial Heart Power Source, *Proc. 6th IECEC*, Paper No. 719043, pp. 310-316, 1971.

4. Martini, W. R. et al., Development of a Simplified Stirling Engine to Power Circulatory Assist Devices, *Proc. 3rd IECEC*, Paper No. 689102, pp. 733-749, 1968.

5. Martini, W. R., The Thermocompressor and its Application to Artificial Heart Power, *Proc. 4th IECEC*, Paper No. 699015, pp. 107-114, 1969.

6. Buck, K. E. et al., A Radioisotope-Power Stirling Engine for Circulatory Support, *Proc. 3rd IECEC*, Paper No. 689101, pp. 723-732, 1968.

7. Moise, J. C. et al., Development of a Thermocompressor Power System for Implantable Artificial Heart Application, *Proc. 8th IECEC*, Paper No. 739152, pp. 511-535, 1973.

8. Moise, J. C. et al., Status of a Thermocompressor-Powered Implantable Artificial Heart System, *Proc. 9th IECEC*, Paper No. 749118, pp. 799-804, 1974.

9. Moise, J. C. et al., Thermocompressor Powered Artificial Heart Assist System, *Proc. 10th IECEC*, Paper No. 759183, pp. 1242-1245, 1975.

10. Moise, J. C. et al., Thermocompressor Powered Artificial Heart Assist System, *Proc. 11th IECEC*, Paper No. 769024, pp. 150-156, 1976.

11. Moise, J. C. et al., Thermocompressor Powered Artificial Heart Assist System, *Proc. 12th IECEC*, Paper No. 779017, pp. 112-118, 1977.

12. Schneider, J. A. et al., A Miniature TES Powered Stirling-Cycle Engine, *Proc. 19th IECEC*, Paper No. 849118, pp. 1917-1922, 1984.

13. Arques, P., Piston Movement in Thermocompressor, *Proc. 32nd IECEC*, Paper No. 97324, pp. 1003-1008, 1997.

14. Karabulut, H., Thermodynamic Analysis of Bush Engine, *G.U. Journal of Science*, pp. 135-144, 2003.

15. Kornhauser, A., Analysis of an Idealized Stirling Thermocompressor, *Proc. 31st IECEC*, Paper No. 96422, pp. 1331-1336, 1996.

16. Peterson, R. B., Thermocompression Engine Cycle with Isothermal Expansion, *Energy Sources*, pp. 199-208, 1998.

17. Incropera, F. P.; DeWitt D. P., *Fundamentals of Heat and Mass Transfer*, 4th Edition, John Wiley & Sons, New York, 1996.

APPENDICES

APPENDIX A: EES THERMOCOMPRESSOR MODEL

An additional tool that was used in the analysis of the thermocompressor cycle was a software package called Engineering Equation Solver (EES). A model was built in EES which fully describes the operation and performance of the thermocompressor. The advantage of the EES model is that it uses an equation of state, which is built into EES, and therefore can be applied to a non-ideal gas working fluid. This model includes regenerator effectiveness, regenerator dead volume, and cylinder dead volume as parameters. Figure A1 is a screen shot of the EES diagram window for the model Figures A2 and A3 were produced with the EES model and are consistent with Figs. 11 and 12.

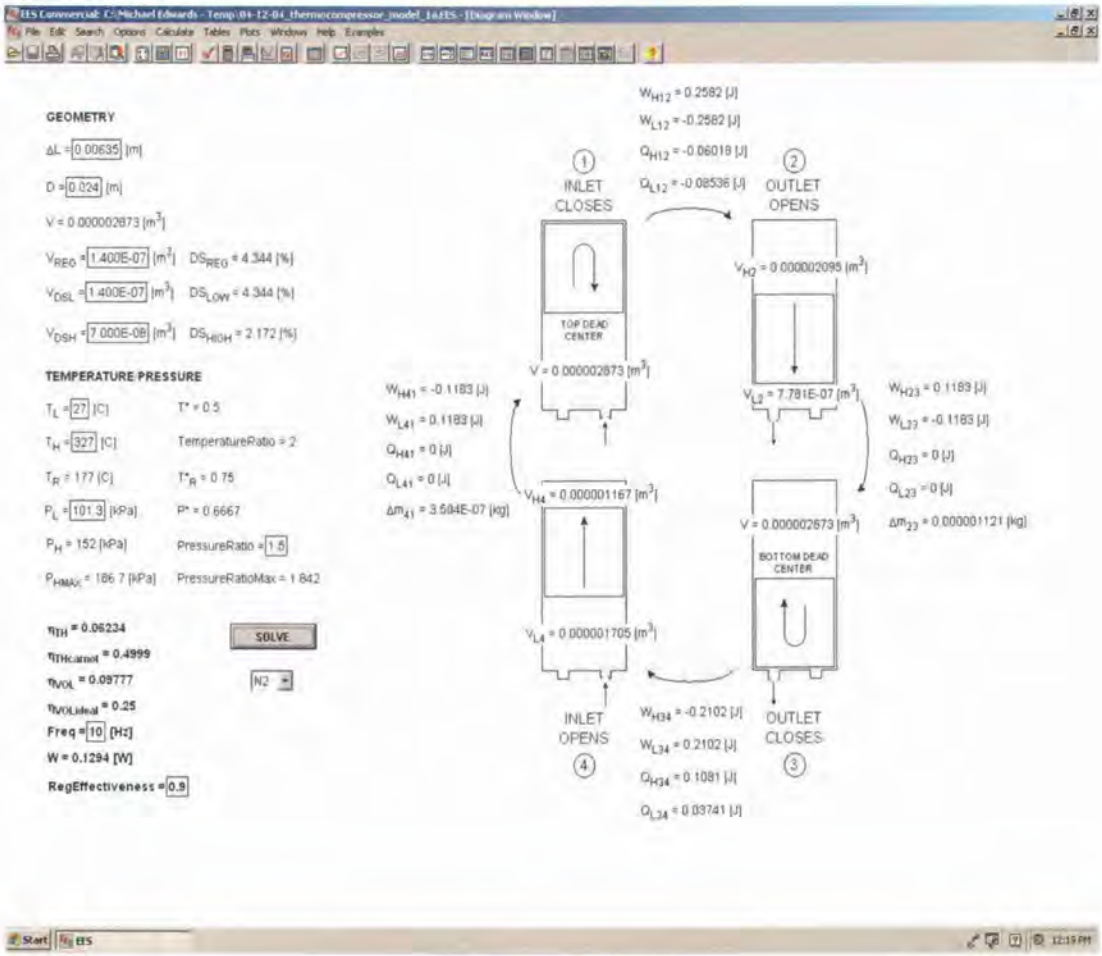

Figure A1 - EES Diagram Window

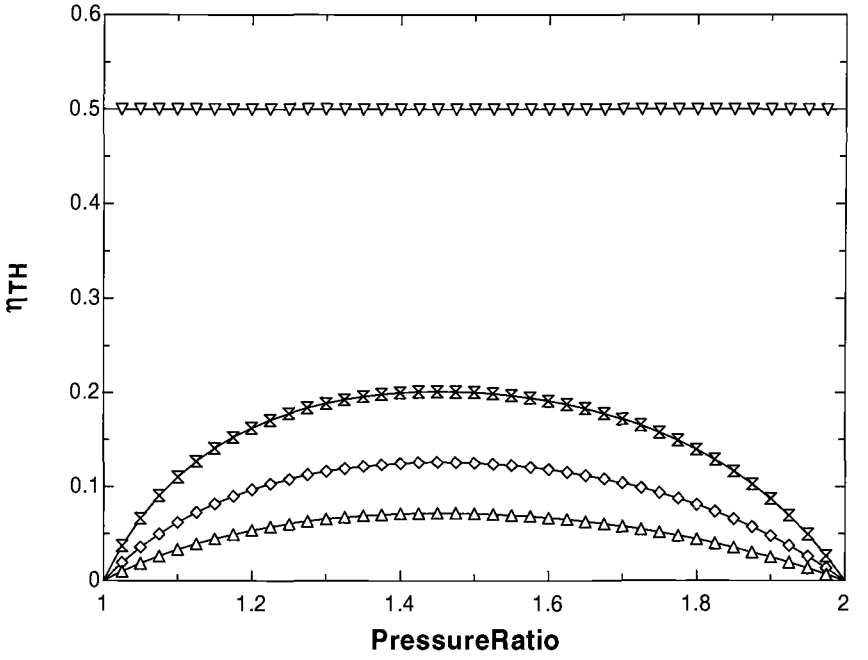

Figure A2 – Thermal Efficiency vs. Pressure Ratio

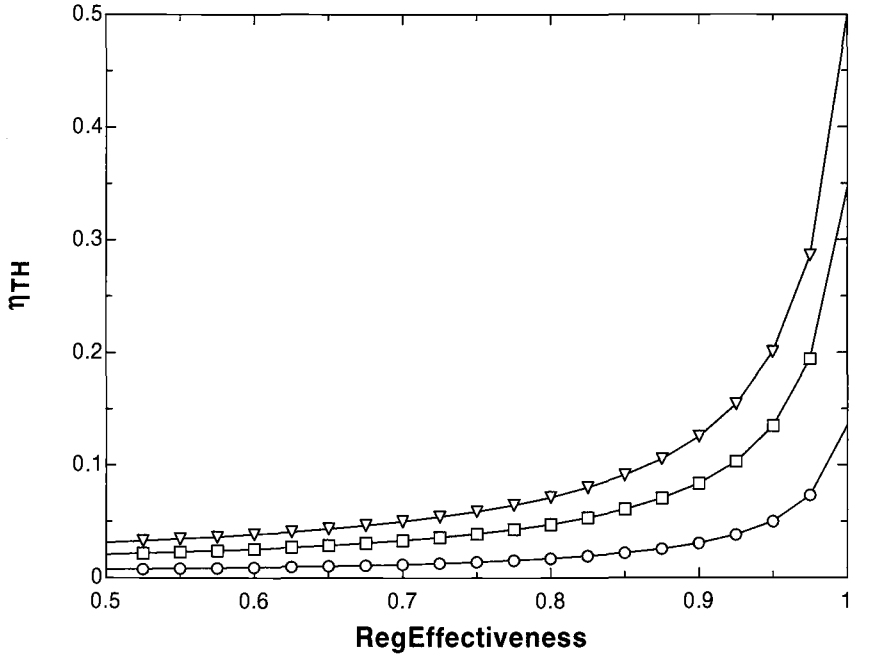

Figure A3 – Thermal Efficiency vs. Regenerator Effectiveness

The EES code is given below.

```
{THERMOCOMPRESSOR MODEL - VERSION 1

MICHAEL EDWARDS
RICH PETERSON

MECHANICAL ENGINEERING
OREGON STATE UNIVERSITY

SUMMER 2004}

{This EES program is used to model the performance of a thermocompressor using an ideal gas.
Regenerator volume and dead space are taken into accout in the model.}

{This SUBPROGRAM will find the pressure at any point X between State 1 and State 2.
These pressures will be used to numerically integrate the PV curve from State 1 to State 2.}
SUBPROGRAM P_1X2(workingFluid$,D,DELTAL,V_HX,V_REG,V_DSL,V_DSH,T_L,T_H,T_R,P_L,P_X)

{Volume of the thermocompressor.}
V=DELTAL*(PI*D^2)/4

{State 1}
m_L1=V/VOLUME(workingFluid$,T=T_L,P=P_L)
m_H1=0
m_REG1=V_REG/VOLUME(workingFluid$,T=T_R,P=P_L)
m_DSL1=V_DSL/VOLUME(workingFluid$,T=T_L,P=P_L)
m_DSH1=V_DSH/VOLUME(workingFluid$,T=T_H,P=P_L)
m_T1X=m_L1+m_H1+m_REG1+m_DSL1+m_DSH1

{State X}
m_LX=V_LX/VOLUME(workingFluid$,T=T_L,P=P_X)
m_HX=V_HX/VOLUME(workingFluid$,T=T_H,P=P_X)
m_REGX=V_REG/VOLUME(workingFluid$,T=T_R,P=P_X)
m_DSLX=V_DSL/VOLUME(workingFluid$,T=T_L,P=P_X)
m_DSHX=V_DSH/VOLUME(workingFluid$,T=T_H,P=P_X)
V=V_LX+V_HX
m_T1X=m_LX+m_HX+m_REGX+m_DSLX+m_DSHX

END

{This FUNCTION will numerically integrate the PV curve from State 1 to State 2 using the mid-point method.
The number of divisions from State 1 to State 2 is given by h.}
FUNCTION W_12(h,workingFluid$,D,DELTAL,V_H2,V_REG,V_DSL,V_DSH,T_L,T_H,T_R,P_L)

{First find dV:}
dV_H:=V_H2/h

work12:=0
n:=0
REPEAT

        {Find the pressure at point a:}
        V_HX:=n*dV_H
        CALL P_1X2(workingFluid$,D,DELTAL,V_HX,V_REG,V_DSL,V_DSH,T_L,T_H,T_R,P_L,P_X)
        P_1Xa:=P_X*1000

        {Move from point a to point b:}
        n:=n+1

        {Find the pressure at point b:}
        V_HX:=n*dV_H
        CALL P_1X2(workingFluid$,D,DELTAL,V_HX,V_REG,V_DSL,V_DSH,T_L,T_H,T_R,P_L,P_X)
        P_1Xb:=P_X*1000

        {Calculate the area under the curve from a to b and add to the current total area:}
        work12:=0.5*(P_1Xa+P_1Xb)*dV_H+work12
```

```
UNTIL (n=h)

{The work from State 1 to State 2 is given by the total area under the PV curve.}
W_12:=work12

END

{This FUNCTION will increase the number of divisions used to discretize the volume from State 1 to State 2.
The number of divisions from State 1 to State 2 will be increased until the error is below a stopping criteria.}
FUNCTION work_12(workingFluid$,D,DELTAL,V_H2,V_REG,V_DSL,V_DSH,T_L,T_H,T_R,P_L)

W_12b:=0

h:=1
REPEAT

        W_12a:=W_12b

        W_12b:=W_12(h,workingFluid$,D,DELTAL,V_H2,V_REG,V_DSL,V_DSH,T_L,T_H,T_R,P_L)

        h:=h+1

k:=W_12b-W_12a
UNTIL (k > -1E-6) AND (k < 1E-6)

work_12:=W_12b

END

{This SUBPROGRAM will find the pressure at any point X between State 3 and State 4.
These pressures will be used to numerically integrate the PV curve from State 3 to State 4.}
SUBPROGRAM P_3X4(workingFluid$,D,DELTAL,V_HX,V_REG,V_DSL,V_DSH,T_L,T_H,T_R,P_H,P_X)

{Volume of the thermocompressor.}
V=DELTAL*(PI*D^2)/4

{State 3}
m_L3=0
m_H3=V/VOLUME(workingFluid$,T=T_H,P=P_H)
m_REG3=V_REG/VOLUME(workingFluid$,T=T_R,P=P_H)
m_DSL3=V_DSL/VOLUME(workingFluid$,T=T_L,P=P_H)
m_DSH3=V_DSH/VOLUME(workingFluid$,T=T_H,P=P_H)
m_T3X=m_L3+m_H3+m_REG3+m_DSL3+m_DSH3

{State X}
m_LX=V_LX/VOLUME(workingFluid$,T=T_L,P=P_X)
m_HX=V_HX/VOLUME(workingFluid$,T=T_H,P=P_X)
m_REGX=V_REG/VOLUME(workingFluid$,T=T_R,P=P_X)
m_DSLX=V_DSL/VOLUME(workingFluid$,T=T_L,P=P_X)
m_DSHX=V_DSH/VOLUME(workingFluid$,T=T_H,P=P_X)
V=V_LX+V_HX
m_T3X=m_LX+m_HX+m_REGX+m_DSLX+m_DSHX

END

{This FUNCTION will numerically integrate the PV curve from State 3 to State 4 using the mid-point method.
The number of divisions from State 3 to State 4 is given by h.}
FUNCTION W_34(h,workingFluid$,D,DELTAL,V_H4,V_REG,V_DSL,V_DSH,T_L,T_H,T_R,P_H)

V:=DELTAL*(PI*D^2)/4
dV_H:=(V-V_H4)/h

work34:=0
n:=0
REPEAT

        V_HX:=V-n*dV_H
```

```
        CALL P_3X4(workingFluid$,D,DELTAL,V_HX,V_REG,V_DSL,V_DSH,T_L,T_H,T_R,P_H,P_X)
        P_3Xa:=P_X*1000

        n:=n+1

        V_HX:=V-n*dV_H
        CALL P_3X4(workingFluid$,D,DELTAL,V_HX,V_REG,V_DSL,V_DSH,T_L,T_H,T_R,P_H,P_X)
        P_3Xb:=P_X*1000

        work34:=0.5*(P_3Xa+P_3Xb)*dV_H+work34

UNTIL (n=h)

W_34:=-work34

END

{This FUNCTION will increase the number of divisions used to discretize the volume from State 3 to State 4.
The number of divisions from State 3 to State 4 will be increased until the error is below a stopping criteria.}
FUNCTION work_34(workingFluid$,D,DELTAL,V_H4,V_REG,V_DSL,V_DSH,T_L,T_H,T_R,P_H)

W_34b:=0

h:=1
REPEAT

        W_34a:=W_34b

        W_34b:=W_34(h,workingFluid$,D,DELTAL,V_H4,V_REG,V_DSL,V_DSH,T_L,T_H,T_R,P_H)

        h:=h+1

k:=W_34b-W_34a
UNTIL (k > -1E-6) AND (k < 1E-6)

work_34:=W_34b

END

{Thermocompressor Model}

{Volume of the thermocompressor.}
V=DELTAL*(PI*D^2)/4
DS_REG=100*V_REG/V_T
DS_LOW=100*V_DSL/V_T
DS_HIGH=100*V_DSH/V_T
V_T=V+V_REG+V_DSH+V_DSL

P_H=PressureRatio*P_L
PressureRatioMax=P_HMAX/P_L
P|star=P_L/P_H

T|star=(T_L+273)/(T_H+273)
TemperatureRatio=1/T|star
T|star_R=(T_R+273)/(T_H+273)
T_R=(T_H+T_L)/2

{First calculate the theoretical P_high_max from a mass balance.}

{State 1}
m_L1=V/VOLUME(workingFluid$,T=T_L,P=P_L)
m_H1=0
m_REG1=V_REG/VOLUME(workingFluid$,T=T_R,P=P_L)
m_DSL1=V_DSL/VOLUME(workingFluid$,T=T_L,P=P_L)
m_DSH1=V_DSH/VOLUME(workingFluid$,T=T_H,P=P_L)
m_T12=m_L1+m_H1+m_REG1+m_DSL1+m_DSH1

{State 2}
```

```
V_L2=m_L2*VOLUME(workingFluid$,T=T_L,P=P_H)
V_H2=m_H2*VOLUME(workingFluid$,T=T_H,P=P_H)
V=V_H2+V_L2

m_REG2=V_REG/VOLUME(workingFluid$,T=T_R,P=P_H)
m_DSL2=V_DSL/VOLUME(workingFluid$,T=T_L,P=P_H)
m_DSH2=V_DSH/VOLUME(workingFluid$,T=T_H,P=P_H)
m_T12=m_L2+m_H2+m_REG2+m_DSL2+m_DSH2

{State 3 w/o valves - this is the maximum P_H that can be reached}
m_L3MAX=0
m_H3MAX=V/VOLUME(workingFluid$,T=T_H,P=P_HMAX)
m_REG3MAX=V_REG/VOLUME(workingFluid$,T=T_R,P=P_HMAX)
m_DSL3MAX=V_DSL/VOLUME(workingFluid$,T=T_L,P=P_HMAX)
m_DSH3MAX=V_DSH/VOLUME(workingFluid$,T=T_H,P=P_HMAX)
m_T12=m_L3MAX+m_H3MAX+m_REG3MAX+m_DSL3MAX+m_DSH3MAX

{PROCESS 1-2}

{HOT SIDE}
W_H12=work_12(workingFluid$,D,DELTAL,V_H2,V_REG,V_DSL,V_DSH,T_L,T_H,T_R,P_L)

{Energy Balance}
(m_H2-m_H1)*u_H12*1000=Q_H12-W_H12+(m_H2-m_H1)*h_H12*1000

        u_H12=INTENERGY(workingFluid$,T=T_H)
        h_H12=ENTHALPY(workingFluid$,T=T_H)

{COLD SIDE}
W_L12=-W_H12

{Energy Balance}
(m_L2*u_L2*1000-m_L1*u_L1*1000)=Q_L12-W_L12+(m_L2*h_L2*1000-m_L1*h_L1*1000)

        u_L1=INTENERGY(workingFluid$,T=T_L)
        u_L2=INTENERGY(workingFluid$,T=T_L)
        h_L1=ENTHALPY(workingFluid$,T=T_L)
        h_L2=ENTHALPY(workingFluid$,T=T_L)

{PROCESS 2-3}

DELTAm_23=m_T12-m_H3

{HOT SIDE}
W_H23=P_H*(V-V_H2)*1000

Q_H23=0

{COLD SIDE}
W_L23=-W_H23

Q_L23=0

{PROCESS 3-4}

{State 3}
m_L3=0
m_H3=V/VOLUME(workingFluid$,T=T_H,P=P_H)
m_REG3=V_REG/VOLUME(workingFluid$,T=T_R,P=P_H)
m_DSL3=V_DSL/VOLUME(workingFluid$,T=T_L,P=P_H)
m_DSH3=V_DSH/VOLUME(workingFluid$,T=T_H,P=P_H)
m_T34=m_L3+m_H3+m_REG3+m_DSL3+m_DSH3

{State 4}
m_L4=V_L4/VOLUME(workingFluid$,T=T_L,P=P_L)
m_H4=V_H4/VOLUME(workingFluid$,T=T_H,P=P_L)
m_REG4=V_REG/VOLUME(workingFluid$,T=T_R,P=P_L)
m_DSL4=V_DSL/VOLUME(workingFluid$,T=T_L,P=P_L)
```

```
m_DSH4=V_DSH/VOLUME(workingFluid$,T=T_H,P=P_L)
V=V_H4+V_L4
m_T34=m_L4+m_H4+m_REG4+m_DSL4+m_DSH4

{HOT SIDE}
W_H34=work_34(workingFluid$,D,DELTAL,V_H4,V_REG,V_DSL,V_DSH,T_L,T_H,T_R,P_H)

{Energy Balance}
(m_H4-m_H3)*u_H34*1000=Q_H34-W_H34+(m_H4-m_H3)*h_H34*1000

        u_H34=INTENERGY(workingFluid$,T=T_H)
        h_H34=ENTHALPY(workingFluid$,T=T_H)

{COLD SIDE}
W_L34=-W_H34

{Energy Balance}
(m_L4*u_L4*1000-m_L3*u_L3*1000)=Q_L34-W_L34+(m_L4*h_L4*1000-m_L3*h_L3*1000)

        u_L3=INTENERGY(workingFluid$,T=T_L)
        u_L4=INTENERGY(workingFluid$,T=T_L)
        h_L3=ENTHALPY(workingFluid$,T=T_L)
        h_L4=ENTHALPY(workingFluid$,T=T_L)

{PROCESS 4-1}

DELTAm_41=m_L1-m_T34

{HOT SIDE}
W_H41=P_L*(0-V_H4)*1000

Q_H41=0

{COLD SIDE}
W_L41=-W_H41

Q_L41=0

{REGENERATOR EFFECTIVENESS}
gamma=CP(workingFluid$,T=T_R)/CV(workingFluid$,T=T_R)
Q_HHX12=((V_H2/V_T)+(1-P|star)*(V_DSL/V_T))*(gamma/(gamma-1))*(1-T|star)*(1-RegEffectiveness)
Q_HHX23=(1-(V_H2+V_DSH+V_REG+V_DSL)/V_T)*(gamma/(gamma-1))*(1-T|star)*(1-RegEffectiveness)

{THERMAL EFFICIENCY}
R=8314/M
M=MOLARMASS(workingFluid$)
eta_TH=(DELTAm_41*R*(T_L+273.15)*ln(P_H/P_L))/(Q_H12+Q_HHX12+Q_HHX23+Q_H34)
eta_THcarnot=1-(T_L+273.15)/(T_H+273.15)

{VOLUMETRIC EFFICIENCY}
rho_INLET=DENSITY(workingFluid$,T=T_L,P=P_L)
eta_VOL=DELTAm_41/(rho_INLET*V_T)
eta_VOLideal=1-(T|star/P|star)

{WORK OUTPUT}
W=Freq*(DELTAm_41*R*(T_L+273.15)*ln(P_H/P_L))
```

APPENDIX B: REGENERATOR OPTIMIZATION MATHCAD CODE

The following MathCAD code was used for the regenerator optimization, which was presented in Section 4.8.

THERMOCOMPRESSOR REGENERATOR OPTIMIZATION MODEL
SUMMER - WINTER 2004

MICHAEL EDWARDS

THERMOCOMPRESSOR CYCLE:

$$v_{H2}(P,T,T_R,v_{REG},v_{DSL},v_{DSH},\varepsilon,\gamma) := \left(\frac{1-P}{1-T}\right) - \left(\frac{1-P}{1-T}\right)\cdot\left(1-\frac{T}{T_R}\right)\cdot v_{REG} - (1-P)\cdot v_{DSH}$$

$$\Delta m_{H12}(P,T,T_R,v_{REG},v_{DSL},v_{DSH},\varepsilon,\gamma) := v_{H2}(P,T,T_R,v_{REG},v_{DSL},v_{DSH},\varepsilon,\gamma) + (1-P)\cdot v_{DSH}$$

$$w_{H12}(P,T,T_R,v_{REG},v_{DSL},v_{DSH},\varepsilon,\gamma) := -\left[\frac{1}{1-T} - \frac{1}{1-T}\cdot\left(1-\frac{T}{T_R}\right)\cdot v_{REG} - v_{DSH}\right]\cdot P\cdot\ln(P)$$

$$q_{H12}(P,T,T_R,v_{REG},v_{DSL},v_{DSH},\varepsilon,\gamma) := w_{H12}(P,T,T_R,v_{REG},v_{DSL},v_{DSH},\varepsilon,\gamma) - \Delta m_{H12}(P,T,T_R,v_{REG},v_{DSL},v_{DSH},\varepsilon,\gamma)$$

$$q_{HHX12}(P,T,T_R,v_{REG},v_{DSL},v_{DSH},\varepsilon,\gamma) := \Delta m_{H12}(P,T,T_R,v_{REG},v_{DSL},v_{DSH},\varepsilon,\gamma)\cdot\frac{\gamma}{\gamma-1}\cdot(1-T)\cdot(1-\varepsilon)$$

$$\Delta m_{H23}(P,T,T_R,v_{REG},v_{DSL},v_{DSH},\varepsilon,\gamma) := 1 - \left(v_{H2}(P,T,T_R,v_{REG},v_{DSL},v_{DSH},\varepsilon,\gamma) + v_{DSH} + v_{REG} + v_{DSL}\right)$$

$$q_{HHX23}(P,T,T_R,v_{REG},v_{DSL},v_{DSH},\varepsilon,\gamma) := \Delta m_{H23}(P,T,T_R,v_{REG},v_{DSL},v_{DSH},\varepsilon,\gamma)\cdot\frac{\gamma}{\gamma-1}\cdot(1-T)\cdot(1-\varepsilon)$$

$$v_{H4}(P,T,T_R,v_{REG},v_{DSL},v_{DSH},\varepsilon,\gamma) := \frac{P-T}{P\cdot(1-T)} - v_{DSH} - \frac{1-P}{P\cdot(1-T)}\cdot\frac{T}{T_R}\cdot v_{REG} - \frac{P-T}{P\cdot(1-T)}\cdot v_{REG} - \frac{1}{P}\cdot v_{DSL}$$

$$\Delta m_{H34}(P,T,T_R,v_{REG},v_{DSL},v_{DSH},\varepsilon,\gamma) := -\left(1-P\cdot v_{H4}(P,T,T_R,v_{REG},v_{DSL},v_{DSH},\varepsilon,\gamma) - P\cdot v_{DSH} - v_{REG} - v_{DSL}\right)$$

$$w_{H34}(P,T,T_R,v_{REG},v_{DSL},v_{DSH},\varepsilon,\gamma) := \left(\frac{T}{T-1} - \frac{1-T_R}{1-T}\cdot\frac{T}{T_R}\cdot v_{REG} - v_{DSL}\right)\cdot\ln\left(\frac{1}{P}\right)$$

$$q_{H34}(P,T,T_R,v_{REG},v_{DSL},v_{DSH},\varepsilon,\gamma) := w_{H34}(P,T,T_R,v_{REG},v_{DSL},v_{DSH},\varepsilon,\gamma) - \Delta m_{H34}(P,T,T_R,v_{REG},v_{DSL},v_{DSH},\varepsilon,\gamma)$$

$$\Delta m_{41}(P,T,T_R,v_{REG},v_{DSL},v_{DSH},\varepsilon,\gamma) := P\cdot\left(\frac{1}{T}-1\right)\cdot v_{H4}(P,T,T_R,v_{REG},v_{DSL},v_{DSH},\varepsilon,\gamma)$$

THERMAL EFFICIENCY:

$$w_{out}(P,T,T_R,v_{REG},v_{DSL},v_{DSH},\varepsilon,\gamma) := \Delta m_{41}(P,T,T_R,v_{REG},v_{DSL},v_{DSH},\varepsilon,\gamma)\cdot T\cdot\ln\left(\frac{1}{P}\right)$$

$$q_{in}(P,T,T_R,v_{REG},v_{DSL},v_{DSH},\varepsilon,\gamma) := q_{H12}(P,T,T_R,v_{REG},v_{DSL},v_{DSH},\varepsilon,\gamma) + q_{HHX12}(P,T,T_R,v_{REG},v_{DSL},v_{DSH},\varepsilon,\gamma) + q_{HHX23}(P,T,T_R,v_{REG},v_{DSL},v_{DSH},\varepsilon,\gamma) + q_{H34}(P,T,T_R,v_{REG},v_{DSL},v_{DSH},\varepsilon,\gamma)$$

$$\eta_{TH}(P,T,T_R,v_{REG},v_{DSL},v_{DSH},\varepsilon,\gamma) := \frac{w_{out}(P,T,T_R,v_{REG},v_{DSL},v_{DSH},\varepsilon,\gamma)}{q_{in}(P,T,T_R,v_{REG},v_{DSL},v_{DSH},\varepsilon,\gamma)}$$

ATMOSPHERIC CONDITIONS:

Atmospheric Pressure: $P_{atm} := 101325 Pa$

Room Temperature: $T_{atm} := 300 K$

MATERIAL PROPERTIES OF N2 @ 450 K:

$\rho := 0.7485 \frac{kg}{m^3}$ $\mu := 239.6 \cdot 10^{-7} \frac{N \cdot s}{m^2}$ $\mu_s := 200 \cdot 10^{-7} \frac{N \cdot s}{m^2}$ $v := \frac{\mu}{\rho}$

$c_p := 1050 \frac{J}{kg \cdot K}$ $k := 35.8 \cdot 10^{-3} \frac{W}{m \cdot K}$ $R := \frac{8314}{28.01} \frac{J}{kg \cdot K}$ $Pr := 0.703$ $\gamma := 1.4$

THERMOCOMPRESSOR GEOMETRY:

$$CylinderLength(AspectRatio, V, \lambda) := 2 \cdot AspectRatio \cdot \left[\frac{-1}{2} \cdot \frac{V}{(\pi \cdot (AspectRatio \cdot (-1 + \lambda)))} \right]^{\left(\frac{1}{3}\right)}$$

$$CylinderDiameter(AspectRatio, L) := \frac{L}{AspectRatio}$$

$$StrokeLength(L, \lambda) := L - \lambda \cdot L$$

$$CylinderArea(D) := \frac{\pi}{4} \cdot D^2$$

REGENERATOR GEOMETRY:

$$RegLength(L, \lambda) := \lambda \cdot L$$

$$RegArea(n, d) := n \frac{\pi}{4} \cdot (d)^2 \cdot in^2$$

$$RegPerimeter(n, d) := n \cdot \pi \cdot d$$

REGENERATOR SPEED: $f := 10 \cdot Hz$ $\Delta t := \frac{1}{2 \cdot f}$

MASS FLOW RATE: $mass(V) := \frac{P_{atm} \cdot V}{R \cdot T_{atm}}$ $m(V) := \frac{mass(V)}{\Delta t}$ $v_{AIR}(V, n, d) := \frac{m(V)}{\rho \cdot RegArea(n, d) \cdot \frac{1}{in^2}}$

REYNOLDS NUMBER: $Re(V, n, d) := \frac{v_{AIR}(V, n, d) \cdot d}{v}$

NUSSELT NUMBER:

$$Nu(V, L, \lambda, n, d) := \begin{cases} 3.66 & \text{if } \left(\frac{Re(V, n, d) \cdot Pr}{\frac{\lambda \cdot L}{d}} \right)^{\frac{1}{3}} \cdot \left(\frac{\mu}{\mu_s} \right)^{0.14} < 2 \\ 1.86 \left[\left(\frac{Re(V, n, d) \cdot Pr}{\frac{\lambda \cdot L}{d}} \right)^{\frac{1}{3}} \cdot \left(\frac{\mu}{\mu_s} \right)^{0.14} \right] & \text{if } \left(\frac{Re(V, n, d) \cdot Pr}{\frac{\lambda \cdot L}{d}} \right)^{\frac{1}{3}} \cdot \left(\frac{\mu}{\mu_s} \right)^{0.14} \geq 2 \end{cases}$$

FILM COEFFICIENT: $h(V,L,\lambda,n,d) := \frac{Nu(V,L,\lambda,n,d)\cdot k}{d}$

NUMBER OF TRANSFER UNITS: $NTU(V,L,\lambda,n,d) := \frac{h(V,L,\lambda,n,d)\cdot RegPerimeter(n,d)\cdot\lambda\cdot L}{c_p\cdot m(V)}$

REGENERATOR EFFECTIVENESS: $EPSILON(V,L,\lambda,n,d) := \frac{NTU(V,L,\lambda,n,d)}{1+NTU(V,L,\lambda,n,d)}$

FRICTION COEFFICIENT: $f(V,n,d) := \frac{64}{Re(V,n,d)}$

HEAD LOSS: $\Delta P(V,L,\lambda,n,d) := f(V,n,d)\frac{\rho\cdot v_{AIR}(V,n,d)^2}{2}\frac{\lambda\cdot L}{d}$

REGERENERATOR DEAD VOLUME: $REG\_VOL(V,L,\lambda,n,d) := \frac{RegArea(n,d)\cdot\lambda\cdot L}{V+RegArea(n,d)\cdot\lambda\cdot L}$

REGENERATOR SURFACE AREA: $REG\_AREA(D,n,d) := \frac{RegArea(n,d)}{CylinderArea(D)}$

SET OPERATING CONDITIONS:

TEMPERATURE RATIO: $T_{RATIO} := 2$ **PRESSURE RATIO:** $P_{RATIO} := \frac{T_{RATIO}+1}{2}$

$P_L := P_{atm}$ $P_H := P_{RATIO}\cdot P_{atm}$ $P_{AVG} := \frac{P_L+P_H}{2}$

$T_L := T_{atm}$ $T_H := T_{RATIO}\cdot T_{atm}$ $T_R := \frac{T_L+T_H}{2\cdot T_H}$

SET CYLINDER DIMENSIONS: $V := 0.175in^3$ $AspectRatio := 1$ $d := 0.020$ $V_{DSL} := 0$ $V_{DSH} := 0$

CALCULATE THERMAL EFFICIENCY:

$MaxLambda := 0.9$ $MinLambda := 0.5$ $i_{max} := 100$ $i := 0..i_{max}$ $\begin{bmatrix} A \\ B \end{bmatrix} := \begin{bmatrix} 0 & 1 \\ i_{max} & 1 \end{bmatrix}^{-1}\cdot\begin{bmatrix} MinLambda \\ MaxLambda \end{bmatrix}$ $\lambda_i := A\cdot i + B$

$MaxNumHoles := 360$ $MinNumHoles := 120$ $j_{max} := MaxNumHoles - MinNumHoles$

$j := 0..j_{max}$ $\begin{bmatrix} a \\ b \end{bmatrix} := \begin{bmatrix} 0 & 1 \\ j_{max} & 1 \end{bmatrix}^{-1}\cdot\begin{bmatrix} MinNumHoles \\ MaxNumHoles \end{bmatrix}$ $n_j := a\cdot j + b$

$$\eta_{i,j} := \eta_{TH}\left(\frac{1}{P_{RATIO}},\frac{1}{T_{RATIO}},T_R,REG\_VOL\left(V,CylinderLength\left(AspectRatio,V,\lambda_i\right),\lambda_i,n_j,d\right),V_{DSL},V_{DSH},EPSILON\left(V,CylinderLength\left(AspectRatio,V,\lambda_i\right),\lambda_i,n_j,d\right),\gamma\right)$$

$$EPSILON_{i,j} := EPSILON\left(V,CylinderLength\left(AspectRatio,V,\lambda_i\right),\lambda_i,n_j,d\right)$$

$$REG\_VOL_{i,j} := REG\_VOL\left(V,CylinderLength\left(AspectRatio,V,\lambda_i\right),\lambda_i,n_j,d\right)$$

LOCATE OPTIMUM VALUES FOR LAMBDA, EPSILON, AND REGENERATOR VOLUME:

RowIndex(C) :=
- N ← 100
- for h ∈ 0..N
  - $b_h \leftarrow 1$ if $\left(\eta_{h,C} = \max\left(\eta^{<C>}\right)\right) \cdot \left(\left|\max(\eta) - \max\left(\eta^{<C>}\right)\right| < 1 \cdot 10^{-5}\right)$
  - $b_h \leftarrow 0$ otherwise
- for h ∈ 0..N
  - $b_h \leftarrow b_h \cdot h$
- max(b)

Lambda :=
- N ← 240
- for h ∈ 0..N
  - R ← RowIndex(h)
  - $b_h \leftarrow \lambda_R$ if R>0
  - $b_h \leftarrow 0$ otherwise
- b

RegVolume :=
- N ← 240
- for h ∈ 0..N
  - R ← RowIndex(h)
  - $b_h \leftarrow REG\_VOL_{R,h}$ if R>
  - $b_h \leftarrow 0$ otherwise
- A ← 0
- B ← 0
- for h ∈ 0..N
  - $A \leftarrow A + b_h$ if $b_h > 0$
  - $B \leftarrow B + 1$ if $b_h > 0$
- $\frac{A}{B}$

RegEffectiveness :=
- N ← 240
- for h ∈ 0..N
  - R ← RowIndex(h)
  - $b_h \leftarrow EPSILON_{R,h}$ if R>0
  - $b_h \leftarrow 0$ otherwise
- A ← 0
- B ← 0
- for h ∈ 0..N
  - $A \leftarrow A + b_h$ if $b_h > 0$
  - $B \leftarrow B + 1$ if $b_h > 0$
- $\frac{A}{B}$

PROGRAM OUTPUTS:

SYSTEM OPERATING CONDITIONS: $T_{RATIO} = 2$ $P_{RATIO} = 1.5$ $V = 0.175\ in^3$ AspectRatio = 1 d = 0.02

MAXIMUM PREDICTED THERMAL EFFICIENCY: $\max(\eta) = 0.28$

OPTIMAL REGENERATOR DEAD SPACE: RegVolume = 0.27

OPTIMAL REGENERATOR EFFECTIVENESS: RegEffectiveness = 0.969

THERMAL EFFICIENCY VS. NUMBER OF HOLES AND LAMBDA:

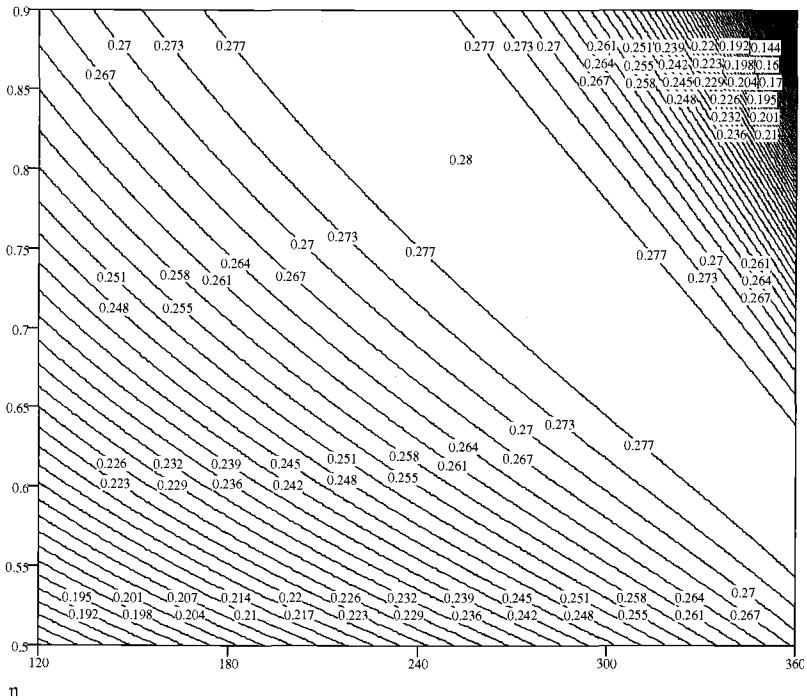

REGENERATOR VOLUME VS. NUMBER OF HOLES AND LAMBDA:

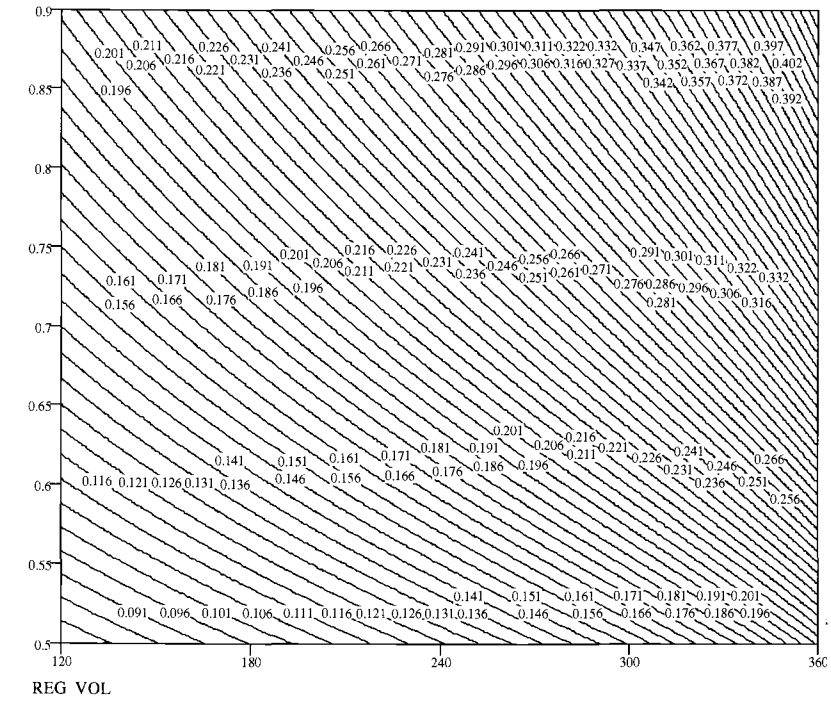

REGENERATOR VOLUME VS. NUMBER OF HOLES AND LAMBDA:

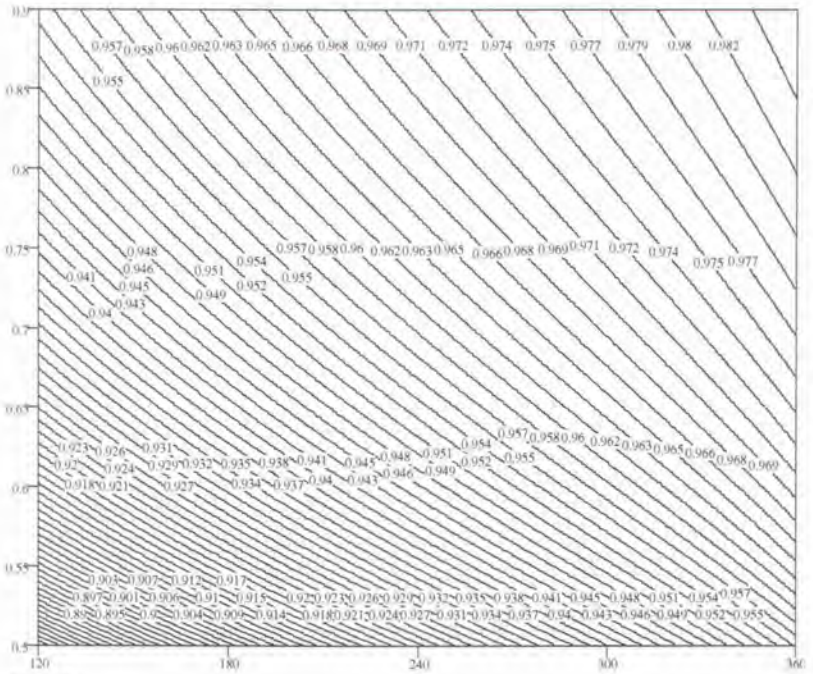

NUMBER OF HOLES VS. LAMBDA FOR OPTIMAL CONFIGURATION:

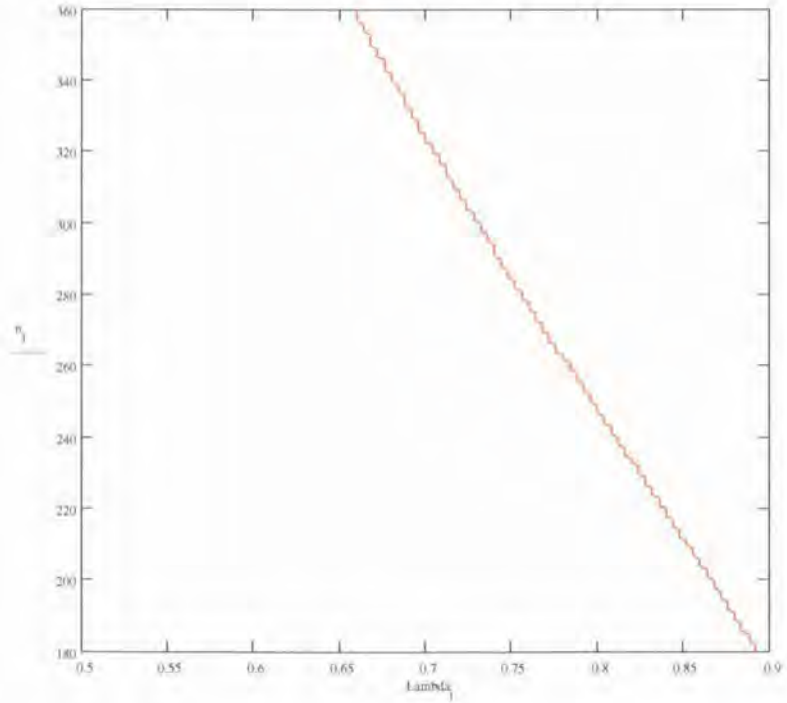

APPENDIX C: REGENERATOR EFFECTIVENESS MATHCAD CODE

The following MathCAD code was used to estimate the regenerator effectiveness of the regenerator, which was presented in Section 5.1.2.

REGENERATOR EFFECTIVENESS ESTIMATE
FALL 2004

MICHAEL EDWARDS

Atmospheric Pressure: $P_{atm} := 14.7 \cdot psi$

Room Temperature: $T_{atm} := 300 \cdot K$

Universal Gas Constant: $R := \frac{8314}{28.01} \cdot \frac{J}{kg \cdot K}$

Material Properties of N2 @ 450 K:

$\rho := 0.7485 \frac{kg}{m^3}$ $\mu := 239.6 \cdot 10^{-7} \cdot \frac{N \cdot s}{m^2}$ $\nu := \frac{\mu}{\rho}$ $\mu_s := 20$ $Pr := 0.703$

$c_p := 1050 \frac{J}{kg \cdot K}$ $k := 35.8 \cdot 10^{-3} \cdot \frac{W}{m \cdot K}$ $\alpha := 45.6 \cdot 10^{-6} \cdot \frac{m^2}{s}$

Regenerator Speed: $f := 10 \cdot Hz$ $\Delta t := \frac{1}{2 \cdot f}$

Regenerator Geometry:

$D := 0.025 \cdot in$ $N := 36$ $A := N \cdot \frac{\pi}{4} \cdot D^2$ $P := N \cdot \pi \cdot D$ $D_h := \frac{4 \cdot A}{P}$ $L := 0.69 \cdot in$

Thermocompressor Hot/Cold Volume: $\delta := 2 \cdot 0.125 \cdot in$ $V := \delta \cdot \frac{\pi}{4} \cdot (0.945 \cdot in)^2$

Fluid Flow Rate: $mass := \frac{P_{atm} \cdot V}{R \cdot T_{atm}}$ $m := \frac{mass}{\Delta t}$ $v_{AIR} := \frac{m}{\rho \cdot A}$

Reynold's Number: $Re := \frac{v_{AIR} \cdot D_h}{\nu}$

Nusselt Number: $Nu := 3.66$

Film Coefficient: $h := \frac{Nu \cdot k}{D_h}$

Number of Transfer Units: $NTU := \frac{h \cdot P \cdot L}{c_p \cdot m}$

Regenerator Effectiveness: $\varepsilon := \frac{NTU}{1 + NTU}$ $\varepsilon = 0.791$

APPENDIX D: EXPERIMENTAL UNCERTAINTY

The uncertainty for each of the measurements presented in the results section is given in this appendix. Because of the large number of data points in the measurements, only the uncertainty of the worst case will be shown for each measurement. Table D1 lists the specifications of each of the instruments used in the experimental setups.

Table D1: Instrument Specifications

Ruler

Resolution:	1/64 in

Strobe Light

Supplier:	Omega
Model number:	HHT41
Stated accuracy:	±0.1 FPM or ±0.1% of reading, whichever is greater
Trigger to flash delay:	<5 µsec

Digital Delay Generator

Supplier:	California Avionics Laboratories
Model number:	101BR
Stated accuracy:	0.0025% of delay or ±20 ns, whichever is greater

Type K Thermocouple

Supplier:	Omega
Model number:	KMQSS-062U-6
Stated accuracy:	0.4% of reading or 1.1^0 C, whichever is greater

Handheld Panel Temperature Meter

Supplier:	Omega
Model number:	DP470
Stated accuracy:	0.5^0 C
Resolution:	0.1^0 C

Handheld Temperature Meter

Supplier:	Omega
Model number:	HHM31
Stated accuracy:	±(0.3% of reading + 1^0 C)
Resolution:	0.1^0 C

Pressure Transducer

Supplier:	Endevco
Model number:	8530C-50
Stated accuracy:	0.22% of full scale
Accuracy:	0.11 psi
Sensitivity:	3.11 MV/psi

Barometer

Supplier:	Oakton
Model number:	03316-80
Stated accuracy:	1.0 mbar
Resolution:	1.0 mbar

Pressure Test Gauge

Supplier:	Dwyer
Model number:	7314D
Stated accuracy:	0.25 psi
Resolution:	0.01 psi

Type K Thermocouple

Supplier:	Omega
Model number:	SCASS-010E-6
Stated accuracy:	0.4% of reading or 1.1^0 C, whichever is greater

Signal Conditioner

Supplier:	Omega
Model number:	OM5-WMV-10A
Stated accuracy:	±(0.05% span + 10 μV RTI)

D.1 POSITION MEASUREMENT UNCERTAINTY

The uncertainty of the position measurement is half of the resolution of the ruler:

Maximum uncertainty of the position measurement: ±1/128 in

The uncertainty of the timing of the position measurement is the combined uncertainties of the digital delay generator and the strobe light flash delay:

- Digital Delay Generator: $u_{DDG} = (0.0025\%)(0.0999999) = 2.5 \cdot 10^{-6} s$
  (Maximum delay = 0.0999999 s.)
- Strobe Light: $u_{SL} = 5 \cdot 10^{-6} s$

$$\rightarrow \quad u_{PM} = \sqrt{u_{DDG}^{\ 2} + u_{SL}^{\ 2}}$$

Maximum uncertainty of the position measurement timing: $\boxed{\pm 5.6\ \mu s}$

D.2 TEMPERATURE MEASUREMENT UNCERTAINTY

The uncertainty of the hot temperature measurement is the combined uncertainties of the thermocouple and the handheld panel meter:

- Thermocouple: $u_{TCH} = (0.4\%)(340^0 C) = 1.36^0 C$
  (Maximum temperature measurement = 340^0 C.)
- Panel Meter: $u_{PM} = \sqrt{0.5^2 + 0.05^2}\,^\circ C$

$$\rightarrow \quad u_{TMH} = \sqrt{u_{TCH}{}^2 + u_{PM}{}^2}$$

Maximum uncertainty of the hot temperature measurement: $\boxed{\pm 1.45^0\ C}$

The uncertainty of the cold temperature measurement is the combined uncertainties of the thermocouple and the handheld panel meter:

- Thermocouple: $u_{TCC} = 1.1^0 C$
- Handheld Meter: $u_{HH} = (0.3\% \cdot 19 + 0.05)^0 C$
  (Maximum temperature measurement = 19^0 C.)

$$\rightarrow \quad u_{TMC} = \sqrt{u_{TCC}{}^2 + u_{HH}{}^2}$$

Maximum uncertainty of the cold temperature measurement: $\boxed{\pm 1.53^0\ C}$

D.3 CYLINDER PRESSURE MEASUREMENT UNCERTAINTY

The pressure transducer was calibrated with six data points. Although, there is some non-linearity in the oscilloscope, it is assumed to be negligible compared to the uncertainty of the calibration. The six data points are given in Table D2, and the calibration curve is shown in Fig. D1.

Table D2: Pressure Transducer Calibration Curve

Transducer Output [mV]	Pressure Reading [psia]	Calibration Instrument
-1.22	0	Vaccum Pump
43.9	14.71	Barometer
80.5	26.87	Test Gauge
112	37.19	Test Gauge
143	47.38	Test Gauge
43.1	14.71	Barometer

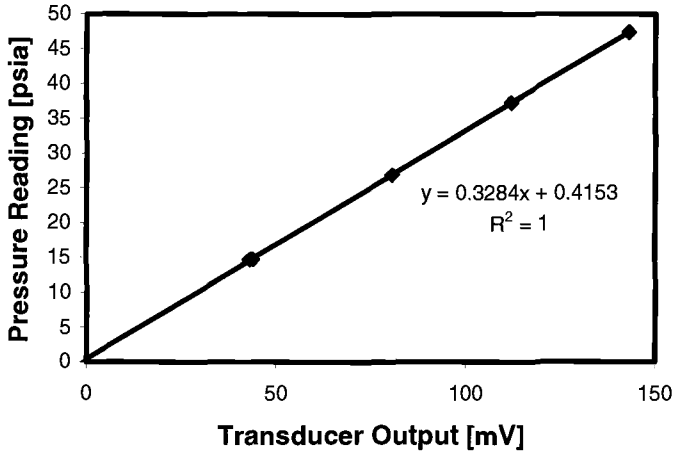

Figure D1 - Pressure Transducer Calibration Curve

The error of each of the calibration instruments propagates into the calibration curve. Unfortunately, because Microsoft Excel was used to curve fit the data points, the functional relationship between the calibration curve and the five data points is unknown. Therefore, the uncertainty analysis will be performed for the worst case scenario, which would include the maximum uncertainty for each of the calibration instruments and the uncertainty of the pressure transducer itself. It is assumed that the vacuum pump pulls a vacuum to at least 1.0 mbar.

- Vacuum Pump: $u_{VC} = 0.0145 psia$
- Barometer: $u_B = 0.0145 psia$
- Test Gauge: $u_{TG} = \sqrt{0.25^2 + 0.005^2}\, psia$
- Pressure Transducer: $u_{PT} = 0.11 psia$

$$\rightarrow \quad u_{PM} = \sqrt{u_{VC}^{\,2} + u_B^{\,2} + 3 \cdot u_{TG}^{\,2} + u_{PT}^{\,2}}$$

Maximum uncertainty of the pressure measurement: $\boxed{\pm 0.274 \text{ psia}}$

This uncertainty is 1.9% of the smallest pressure reading, which is 14.7 psia. It should be noted, however, that this is the maximum possible uncertainty. If the functional relationship between the calibration points and the calibration curve were known, a lower, more realistic uncertainty could be calculated.

D.4 DYNAMIC TEMPERATURE MEASUREMENT UNCERTAINTY

The thermocouple was calibrated with three data points. Ice water, room temperature, and boiling water. The room temperature was measured with another thermocouple and an Omega handheld. The three data points are given in Table A3, and the calibration curve is shown in Fig. D2.

Table D3: Thermocouple Calibration Curve

Voltage Output [V]	Temperature Reading [^{0}C]	Calibration Standards
0	0	Ice Water
0.42	22.8	Omega Handheld
2.1	100	Boiling Water

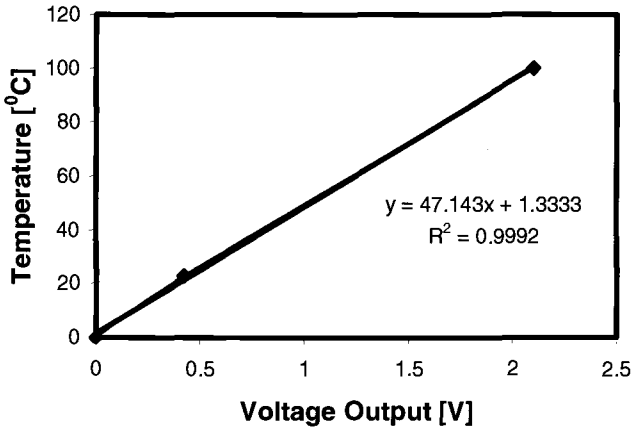

Figure D2 - Thermocouple Calibration Curve

The error of each of the calibration standards propagates into the calibration curve. Unfortunately, because Microsoft Excel was used to curve fit the data points, the functional relationship between the calibration curve and the three data points is unknown. Therefore, the uncertainty analysis will be performed for the worst case scenario, which would include the maximum uncertainty for each of the calibration standards, the uncertainty of the pressure transducer itself, and the uncertainty of the signal conditioner. It is assumed that the temperatures of the boiling and ice water are within $\pm 0.5^0$ C of 100 and 0 ^{0}C respectively, and the uncertainty of the Omega handheld is $\pm 1.53^0$ C as shown in Section D2.

- Boiling Water: $u_{BW} = 0.5°C$
- Ice Water: $u_{IW} = 0.5°C$
- Omega Handheld: $u_{HH} = 1.53°C$
- Thermocouple: $u_{TC} = (0.4\%)(340^0 C) = 1.36^0 C$
  (Maximum temperature measurement = 340^0 C.)
- Signal Conditioner: $u_{SC} = 500[(0.05\%)(10mV) + 10\mu V] = 7.5mV$
  $u_{SC} = 47.134(0.0075V) + 1.333 = 1.6865°C$
  $\rightarrow \quad u_{PM} = \sqrt{u_{BW}^2 + u_{IW}^2 + u_{HH}^2 + u_{TC}^2 + u_{SC}^2}$

  Maximum uncertainty of the temperature measurement: $\boxed{\pm 2.74^0 \text{ C}}$

This uncertainty is 3.6% of the smallest temperature reading, which is 75^0 C. It should be noted, however, that this is the maximum possible uncertainty. If the functional relationship between the calibration points and the calibration curve were known, a lower, more realistic uncertainty could be calculated.